ISTANBUL TECHNICAL UNIVERSITY ★ INSTITUTE OF SCIENCE AND TECHNOLOGY

SURFACE TAILORING OF MICRO AND NANO BEADS WITH FUNCTIONAL HAIRY GRAFTS

Ph. D. Thesis by
Bünyamin KARAGÖZ

Department : Polymer Science and Technology

Programme : Polymer Science and Technology

OCTOBER 2010

ISTANBUL TECHNICAL UNIVERSITY ★ INSTITUTE OF SCIENCE AND TECHNOLOGY

SURFACE TAILORING OF MICRO AND NANO BEADS WITH FUNCTIONAL HAIRY GRAFTS

Ph.D. Thesis by
Bünyamin KARAGÖZ
(515032003)

Date of submission : 26 August 2010
Date of defence examination: 20 October 2010

Thesis Supervisor : Prof. Dr. Niyazi BIÇAK (ITU)
Members of the Examining Committee : Prof. Dr. Yusuf Yağcı (ITU)
Prof. Dr. M. Ali Gürkaynak (IU)
Prof.Dr. A. Yakup Arıca (Gazi U)
Prof.Dr. Ahmet Kaşgöz (IU)

OCTOBER 2010

İSTANBUL TEKNİK ÜNİVERSİTESİ ★ FEN BİLİMLERİ ENSTİTÜSÜ

MİKRO VE NANO TANECİK YÜZEYLERİNİN FONKSİYONEL POLİMER SAÇAKLARIYLA DONATILMASI

DOKTORA TEZİ
Bünyamin KARAGÖZ
(515032003)

Tezin Enstitüye Verildiği Tarih : 26 Ağustos 2010
Tezin Savunulduğu Tarih : 20 Ekim 2010

Tez Danışmanı : Prof. Dr. Niyazi BIÇAK (İTÜ)
Diğer Jüri Üyeleri : Prof. Dr. Yusuf Yağcı (İTÜ)
Prof. Dr. M. Ali Gürkaynak (İÜ)
Prof.Dr. A. Yakup Arıca (Gazi Ü)
Prof.Dr. Ahmet Kaşgöz (İÜ)

EKİM 2010

FOREWORD

First of all, I would like to thank my thesis supervisor, Professor Niyazi Bıçak, for his kind guidance, brilliant comments, unlimited inspiration, valuable scientific support, recomendations throughout the thesis and his unique advises.

I wish to express my special thanks to the members of my thesis committee: Prof. Yusuf Yağcı and Prof. Mehmet Ali Gürkaynak for their valuable suggestions and guidance. I would also like to express my deep thanks Professor Yusuf Yağcı and Professor A. Yakup Arıca for improving the thesis by their knowledge and contributions.

I would like to thank my colleague, labmates and my friends, especially Dr. M. Atilla Taşdelen, Hakan Rıza Güngör, Selim Balıkçı, Serhat Çelik, S. Enis Kabasakal, Mustafa Gazi, Deniz Güneş, İpek Ösken, Yasemin Durmaz, Dr. Hakan Durmaz, Res. Asst. Abdullah Aydoğan, Aydan Dağ, Eda Güngör, Muhammet U. Kahveci.

Finally, I would like to dedicate this thesis to my family, my brother Zekeriya Karagöz and especially to the memory of my dear deceased elder brother İsmail KARAGÖZ.

This work is supported by ITU Institute of Science and Technology.

OCTOBER 2010 Bünyamin KARAGÖZ

TABLE OF CONTENTS

Page

FOREWORD ..... **v**
TABLE OF CONTENTS ..... **vii**
ABBREVIATIONS ..... **xi**
LIST OF TABLES ..... **xiii**
LIST OF FIGURES ..... **xv**
LIST OF SYMBOLS ..... **xix**
SUMMARY ..... **xxi**
ÖZET ..... **xxvii**
1. INTRODUCTION **1**
2. THEORETICAL PART **7**
2.1 Surface-Initiated Polymerization Techniques 7
2.2 Grafting from Methodology 7
2.2.1 Surface grafting by ionic polymerization 9
2.2.2 Surface grafting by ring opening polymerization 10
2.2.3 Surface grafting by ring opening metathesis polymerization 11
2.2.4 Surface grafting by controlled radical polymerization techniques 12
2.2.4.1 Surface-initiated atom transfer radical polymerization 12
2.2.4.2 Surface-initiated reversible-addition fragmentation chain transfer polymerization 15
2.2.4.3 Surface-initated nitroxide-mediated polymerization 17
2.2.4.4 Surface-initiated photoiniferter-mediated polymerization 18
2.2.5 Polymer brushes by grafting from metal oxide surfaces 19
2.2.6 Polymer brushes grafted from inert polymer surfaces 19
2.2.7 Direct radiation/plasma-mediated polymerization 20
2.3 Grafting onto Methodology 20
2.3.1 Click chemistry 21
2.3.1.1 Azide-alkyne cycloaddition reaction 21
2.3.1.2 Diels-Alder reaction 22
2.3.1.3 Catalysts for Diels-Alder reactions 23
2.3.1.4 Mercaptane addition to carbon-carbon double and triple bonds 23
2.4 Synthesis, Stabilization and Organic Modification of Nanoparticles 24
2.4.1 Synthesis of nanoparticles 24
2.4.1.1 Spray pyrolysis methods 24
2.4.1.2 Sol-Gel process 25
2.4.1.3 The Pechini method 25
2.4.1.4 Chemical vapor deposition 26
2.4.1.5 Physical vapor deposition 26
2.4.1.6 Synthesis of nanoparticles in microemulsions 26
2.4.1.7 The Germ-Growth method 26
2.4.1.8 The precipitation methods 27

2.4.1.9 Hydrothermal methods 27
2.4.2 Organic modification and stabilization of nanoparticle surfaces 28
2.4.2.1 Stabilization of nanoparticles in synthesis conditions 28
2.4.2.2 Stabilization with polymer ligands 29
2.4.3 Tailoring of nanoparticle surfaces with polymer brushes 30
2.4.3.1 Grafting from nanoparticle surfaces by ring opening polymerization 32
3. EXPERIMENTAL WORK 33
3.1 Materials and Chemicals 33
3.1.1 Monomers 33
3.1.2 Solvents 34
3.1.3 Other chemicals 35
3.2 Instrumentation 37
3.2.1 Nuclear magnetic resonance spectroscopy (NMR) 37
3.2.2 Infrared spectrophotometer (FT-IR) 37
3.2.3 UV-Visible spectrophotometer 37
3.2.4 Thermogravimetric analyses (TGA) 37
3.2.5 Scanning electron microscopy (SEM) 37
3.2.6 X ray diffraction (XRD) 37
3.2.7 Transmission electron microscopy (TEM) 38
3.2.8 Dynamic light scattering (DLS) 38
3.2.9 Optical photography 38
3.2.10 Gel permeation chromatography (GPC) 38
3.2.11 Fluorescence spectrophotometer 38
3.2.12 Transmitted-reflected light microscope 38
3.2.13 X-ray photoelectron spectra (XPS) 39
3.2.14 Environmental scanning electron microscopy (ESEM) 39
3.3 Preperation Methods 39
3.3.1 Synthesis of 2-bromoethyl methacrylate (BEMA) monomer 39
3.3.1.1 Synthesis of bromoethyl methacrylate based microspheres by suspension polymerization 40
3.3.1.2 Determination of bromide content of the microspheres 40
3.3.1.3 Surface initiated atom transfer radical polymerization of GMA from the bromoethyl groups 41
3.3.1.4 Synthesis of model initiator, bromoethyl acetate 41
3.3.1.5 The use of bromoethyl acetate as initiator for atrp of mma 42
3.3.1.6 Surface initiated ring-opening polymerization of 2-methyl 2-oxazoline from the bromoethyl groups 43
3.3.1.7 Hydrolysis of polyoxazoline brushes 43
3.3.1.8 Determination of amine content of the hydrolysis product 43
3.3.2 Synthesis of P(S-DVB) micro-beads by suspension polymerization 43
3.3.2.1 Acetoxy mercuration of P(S–DVB) beads 44
3.3.2.2 Chlorine exchange reaction 44
3.3.2.3 Reaction with 2-bromoacetyl bromide 44
3.3.2.4 Determination of the bromine content 44
3.3.2.5 Graft copolymerization of styrene from the supported P(S-DVB) microspheres 45
3.3.2.6 ATRP of GMA from the active chain ends of polystyrene brushes 45
3.3.2.7 Amino functionalization of grafted P(S-SVB) microspheres 45
3.3.2.8 Immobilization of lipase on microspheres 46

3.3.2.9 Activity assays of lipase 46
3.3.2.10 Determination of the kinetic parameters of the enzyme preparations 47
3.3.2.11 Thermal and storage stability of the immobilized lipases 47
3.3.2.12 Enzymatic synthesis of banana flavor esters 47
3.3.2.13 Operational stability of immobilized lipase in ester synthesis 48
3.3.3 Synthesis of PDVB microspheres via precipitation polymerization 48
3.3.3.1 Hydrobromination of PDVB microspheres 48
3.3.3.2 Azidation of PDVB microspheres 49
3.3.3.3 Synthesis of alkyne functional ATRP initiator 49
3.3.3.4 Preparation of alkyne functional poly(ethylene glycol) 50
3.3.3.5 Preparation of alkyne functional poly(methyl methacrylate) 50
3.3.3.6 Synthesis of alkyne functional poly(*tert*-butyl acrylate) 50
3.3.3.7 PEG grafted PDVB microspheres via Click reaction 51
3.3.3.8 PEG and PMMA grafted PDVB microspheres via Click reaction 51
3.3.3.9 PEG and P*t*BA grafted PDVB microspheres via Click reaction 51
3.3.3.10 Enzyme adsorption and desorption experiments 52
3.3.4 Surface adsorption of poly(2-hydroxypropylene maleate) on SiO_2 and TiO_2 nanoparticle and its thermal curing 53
3.3.4.1 Adsorption and thermal crosslinking of the polyester on the microparticle surfaces 53
3.3.4.2 Estimation of polyester adsorption on the microparticles by Langmuir isotherm approach 54
3.3.4.3 Surface initiated polymerization of ε-caprolactone from the nanoparticle surfaces 54
3.3.4.4 Preparation of polymer nanocomposite films 54
3.3.5 Synthesis of $Zn(NH_3)_4(OH)_2$ solution 55
3.3.5.1 Preparation of zinc oxide nanoparticles 55
3.3.5.2 Preparation of poly(methyl methacrylate-*b*-glycidyl methacrylate) 55
3.3.5.3 Encapsulation of zinc oxide nanoparticle with the block copolymer 56
3.3.5.4 Preparation of polymer nanocomposite films 56
4. RESULTS AND DISCUSSION 59
4.1 Bromo Ethyl Methacrylate Based Hairy Functional Polymers 59
4.1.1 A new method for preparing bromoethyl methacrylate monomer 59
4.1.2 A suspension polymerization recipe for synthesis of bromo ethyl functional micro-beads 60
4.1.3 Surface initiated ATRP from the bromoethyl groups 62
4.1.4 Surface initiated ROP from the bromoethyl groups 66
4.2 Synthesis of P(S-DVB) microbeads with epoxy functional brushes as enzyme carrier 69
4.2.1 Properties of the functionalized microspheres 70
4.2.2 Immobilization of lipase on the P(S-DVB)-*g*-P(S-GMA) based microspheres 73
4.2.3 Effect of pH and temperature on the free and immobilized lipase activity 77
4.2.4 Kinetic parameters of the free and immobilized lipases 79
4.2.5 Thermal stability of the free and immobilized lipase 80
4.2.6 Enzymatic activity in banana esters synthesis 81
4.2.7 Operational stability in esters synthesis 83

4.3 Modification of poly(divinylbenzene) microspheres by hydrobromination-Click chemistry protocol and their protein adsorption properties 84
4.3.1 Synthesis of PDVB microbeads by precipitation polymerization method and its azide functionalization 85
4.3.2 Preperation of alkyne terminal polymers 87
4.3.3 Grafting of the polymers onto surface via Click chemistry 87
4.3.4 Protein adsorption 89
4.4 A General Method for Organic Modification of Inorganic Nanoparticles 94
4.4.1 Surface adsorption of poly(2-hydroxypropylene maleate) 94
4.4.2 Encapsulation of the nanoparticles by thermal crosslinking of the surface adsorbed polyester 96
4.4.3 Cationic ring opening polymerization of ε-caprolactone from the residual hydroxy groups 99
4.4.4 Nanocomposite films 104
4.5 Size Controlled Synthesis of Zinc Oxide Nanocrystallites and Generation of Core-Sell Structures by Post Treatment with Glycidylmethacrylate Block Copolymers 105
4.5.1 Size-controlled synthesis of ZnO nanoparticles 105
4.5.2 Encapsulation of the nanoparticles 111
4.5.3 Film formation of ZnO core-shell nanocrystals 113
5. CONCLUSION 115
REFERENCES 119
CURRICULUM VITA 137

ABBREVIATIONS

BEMA : 2-Bromoethyl methacrylate
PBEMA : Poly(2-bromoethyl methacrylate)
DVB : Divinyl benzene
PDVB : Poly(divinyl benzene)
P(S-DVB) : Poly(styrene-divinyl benzene)
GMA : Glycidyl methacrylate
PGMA : Poly(glycidyl methacrylate)
MeOX : 2-Methyl 2-oxazoline
MMA : Methyl Methacrylate
PMMA : Poly(methyl metacrylate)
***t*BA** : *tert*-Butyl acrylate
P*t*BA : Poly(*tert*-butyl acrylate)
St : Styrene
PS : Poly(styrene)
ε-CL : ε-caprolactone
PCL : Poly(ε-caprolactone)
PEG : Poly(ethylene glycol)
EGDMA : Ethylene glycol dimethacrylate
SIP : Surface Initiated Polymerization
ATRP : Atom Transfer Radical Polymerization
RAFT : Reversible Addition Fragmentation Chain Transfer
NMP : Nitroxide Mediated Polymerization
TGA : Thermogravimetric analyses
ROP : Ring Opening polymerization
XPS : X-ray Photoelectron Spectra
^{1}H NMR : Hydrogen Nuclear Magnetic Resonance Spectroscopy
FT-IR : Fourier Transform Infrared Spectrophotometer
UV : Ultra Violet
GPC : Gel Permeation Chromatography
DSC : Differential Scanning Calorimetry
XRD : X ray diffraction
TEM : Transmission Electron Microscopy
DLS : Dynamic Light Scattering
MWD : Molecular Weight Distribution
PDI : Polydispersity Index
DMF : *N*,*N*-dimehthylformamide
H-TETA : 1, 1, 4, 7, 10, 10-hexakis [hexyl 1, 4, 7, 10-tetraazadecane]
PMDETA : *N, N, N',N'', N''*-Pentamethyldiethylenetriamine
CH_2Cl_2 : Dichloromethane
THF : Tetrahydrofuran
CuAAC : Copper catalyzed azide-alkyne cycloaddition
1,3-DPCA : 1,3-dipolar cycloaddition

LIST OF TABLES

Page

Table 4.1: The recipe for suspension copolymerization of BEMA yielding transparent microspheres. 61
Table 4.2: Preparation of alkyne functional polymers. 87
Table 4.3: Effect of enzyme loading on the biocatalytic activity of immobilized enzymes. 92
Table 4.4: Zeta potential and electrokinetic charge densities for the microspheres before and after enzyme loading and desorption in the presence of PEG and $(NH_4)_2SO_4$. 93
Table 4.5: Adsorption of the polyester on microparticle surfaces. 95
Table 4.6: Some characteristics of the nanoparticles prior and after grafting with PCL. 104
Table 4.7: Composition and size characteristics of the ZnO nanoparticles inferred from TGA and DLS measurements..... 108

LIST OF FIGURES

Page

Figure 2.1: Schematic illustration of grafting from approach on solid support 8
Figure 2.2: Poly(styrene) brushes grown by living cationic polymerization. 9
Figure 2.3: Poly(styrene) brushes grown by living anionic polymerization. 9
Figure 2.4: Surface-initiated ring opening polymerization of ε-caprolactone on gold surfaces 10
Figure 2.5: Surface-initiated ring opening polymerization of L-lactide on solid support 10
Figure 2.6: Surface-initiated ring opening polymerization of *N*-carboxy anhydrides of L-glutamates on solid substrate 11
Figure 2.7: Transition metal tethered on the surface of silica nanoparticle 11
Figure 2.8: ROMP initiator used for immobilization on silica nanoparticles and the first generation of Grubbs catalyst 12
Figure 2.9: Immobilization of ATRP initiator sites on WANG resin 13
Figure 2.10: Introducing ATRP initiator groups on P(S-DVB) resin beads. 14
Figure 2.11: Poly(glycidyl methacrylate) brushes on P(S-DVB) microspheres 14
Figure 2.12: Immobilization of AIBN like azo-initiator onto silica surfaces and SI-RAFT polymerization of methyl methacrylate from the initiation sites. 15
Figure 2.13: Surface initiated-RAFT polymerization of butyl acrylate from dithiobenzoate modified silica nanoparticles 16
Figure 2.14: Surface initiated-RAFT polymerization of methyl acrylate from trithiocarbonate modified silica particles 16
Figure 2.15: Immobilization of TEMPO derivative NMP agent on silica surface and surface initiated-NMP of styrene. 17
Figure 2.16: Block copolymerization of styrene-methyl methacrylate by irradiation on dithiocarbamate immobilized silica nanoparticle. 18
Figure 2.17: Schematic illustration of surface functionalization of inert polymer surfaces 20
Figure 2.18: Schematic illustration of grafting onto approach 21
Figure 2.19: Schematic illustration of nanoparticle stabilization by polymer ligands 29
Figure 4.1: ^{1}H-NMR spectrum of the monomer, bromoethyl methacrylate (BEMA) in $CDCl_3$. 60
Figure 4.2: Optical photoimage of cross-linked PBEMA microparticles prepared by suspension polymerization using PNVP (1 %) as stabilizer. 62
Figure 4.3: FT-IR spectrum of PBEMA microspheres before (a) and after surface grafting with GMA (b) 64
Figure 4.4: First order kinetic plot for the surface initiated graft copolymerization of GMA on PBEMA microspheres by ATRP. 65

Figure 4.5: Full scale XPS of PBEMA microspheres before (a), and after surface initiated grafting with GMA(b). The window shows 3p and 3d core levels of the bromide on the PBEMA microspheres. 65
Figure 4.6: FT-IR spectrum of PBEMA microspheres before (a), after surface grafting with MeOx (b), and its hydrolysis product with poly(ethyleneimine) brushes(c). 67
Figure 4.7: First order kinetic plot for the surface initiated ring opening polymerization of MeOx at 110 ^{o}C. 67
Figure 4.8: Full scale XPS of PBEMA microspheres before (a), and after grafting with PMeOx and hydrolysis product of the later (c). N 1s core level centered at 402 eV is given (inset). 68
Figure 4.9: SEM images of the bare PBEMA microspheres (a), and their surface grafted counterparts with PGMA (b), and PMeOx (c) 69
Figure 4.10: (a) P(S-DVB)-Br (the product Step 1; P(S-DVB)-Br); (b) polystyrene grafted (S-DVB) (the product Step 2; P(S-DVB-*g*-(PS)-Br); (b) the second block P(GMA) grafted on to the first styrene block (the product of Step 3; P(S-DVB)-*g*-P(S-GMA) and (d) Spacer-arm attached P(S-DVB)-*g*-P(S-GMA)-HMDA. 72
Figure 4.11: Scanning electron micrograph images of P(S-DVB)-*g*-P(S-GMA) microspheres. 73
Figure 4.12: Effect coupling duration time on the immobilization efficiency of the lipase on the P(S-DVB)-*g*-P(S-GMA)-HMDA-GA microspheres. 76
Figure 4.13: Effect of pH on the activity of free and immobilized lipase on the P(S-DVB)-*g*-P(S-GMA)-HMDA-GA microspheres; the relative activities at the optimum pH were taken as 100% for free and immobilized lipase, respectively. 77
Figure 4.14: Effect of temperature on the activity of the free and immobilized lipase on the P(S-DVB)-*g*-P(S-GMA)-HMDA-GA microspheres; the relative activities at the optimum temperature were taken as 100% for free and immobilized lipase, respectively. 78
Figure 4.15: Thermal stability of the free and immobilized lipase at two different temperatures. 81
Figure 4.16: Effect of temperature on the enzymatic production of ethyl acetate and iso-amyl acetate using immobilized lipase on the P(S-DVB)-*g*-P(S-GMA)-HMDA-GA microspheres. 82
Figure 4.17: Effect of acid: alcohol ratio on the ester synthesis activity of the immobilized lipase. 82
Figure 4.18: Operational stability of immobilized lipase during ethyl acetate and iso-amyl acetate synthesis. The same enzyme microspheres were used for each batch during repeated use. 84
Figure 4.19: Optical microscope image of PDVB (a), brominated PDVB (b), azide functionalized PDVB microspheres (c). 86
Figure 4.20: FT-IR spectra of bare PDVB, hydrobrominated PDVB and azido functional PDVB spherical beads. 86

Figure 4.21: FT-IR spectra of azidated PDVB microsphere (PDVB-N_3) (a), poly(ethylene glycol) and poly(*tert*-butyl acrylate) grafted PDVB microsphere (PDVB-*g*-PEG/P*t*BA) (b), poly(ethylene glycol) and poly(methyl methacrylate) grafted PDVB microsphere (PDVB-*g*-PEG/PMMA) (c) and poly(ethylene glycol) grafted PDVB microsphere (PDVB-*g*-PEG) (d). 88
Figure 4.22: TGA traces of PDVB microspheres (a), azidated PDVB microsphere (PDVB-N_3) (b), poly(ethylene glycol) grafted PDVB microsphere (PDVB-*g*-PEG) (c), poly(ethylene glycol) and poly(tert-butyl acrylate) grafted PDVB microsphere (PDVB-*g*-PEG/P*t*BA) (d), and poly(ethylene glycol) and poly(methyl methacrylate) grafted PDVB microsphere (PDVB-*g*-PEG/PMMA) (e). 89
Figure 4.23: Effect of pH on the adsorptive amount of microspheres (Adsorption buffer; pH 4.0, 50 mM acetate buffer; adsorption time: 2 h; T: 25 ^{o}C; ■ (PDVB-g-PEG), • (PDVB-g-PEG/P*t*BA), ▲ (PDVB-g-PEG/ PMMA)). 90
Figure 4.24: Effect of enzyme concentration on the adsorptive amount of microspheres (Adsorption buffer; pH 4.0, 50 mM acetate buffer; adsorption time: 2 h; T: 25 ^{o}C; ■ (PDVB-g-PEG), • (PDVB-g-PEG/P*t*BA), ▲ (PDVB-g-PEG/ PMMA)). 91
Figure 4.25: FT-IR spectra of the fumed silica (a), the SiO_2 nanopowder with adsorbed Poly(2-hydroxypropylene maleate) (PHPM) (b), the SiO_2 nanopowder with cured PHPM capsules (c) and encapsulated SiO_2 nanopowder with Poly(ε-Caprolactone) surface grafts (d) in 1600-1800 cm^{-1} range. 96
Figure 4.26: FT-IR spectra of TiO_2 nanoparticles, naked (a), with adsorbed polyester (b) with cured polyester capsules (c) and with Poly(ε-Caprolactone) surface grafts (d) in 1600–1800 cm^{-1} range. 97
Figure 4.27: TGA of the SiO_2 nanopowders with crosslinked polyester capsules and with Poly(ε-Caprolactone) surface grafts. 98
Figure 4.28: TGA curves of the TiO_2 nanoparticles with crosslinked polyester capsules (upper curve) and with Poly(ε-Caprolactone) surface grafts (lower curve). 98
Figure 4.29: XRD spectra of virgin silica nanopowder (left) and silica nanoparticle with cured polyester capsule. 99
Figure 4.30: XRD spectra of the commercial TiO_2 nanopowders showing rutile and anatase crystalline structures, before (left part) and after curing of the adsorbed polyester (right part). 99
Figure 4.31: TEM micrographs of the Poly(ε-Caprolactone)-shelled SiO_2 nanopowders. 100
Figure 4.32: TEM micrographs of the Poly(ε-Caprolactone)-shelled TiO_2 nanopowders. 101
Figure 4.33: DLS profiles of the SiO_2 nanoparticles after PHPM adsorption (A), cured at 180 $^{\circ}$C (B) and surface grafted with PCL (C). 101
Figure 4.34: DLS profiles of the TiO_2 nanoparticles after PHPM adsorption (A), after curing at 180 $^{\circ}$C (B) and after surface grafting with PCL (C). 102
Figure 4.35: SEM pictures of free-standing poly (methyl metacrylate-*stat*-butyl acrylate) composite films with SiO_2 (a) and TiO_2 (b) nanopowders. . 104

Figure 4.36: Schematic representation of size controlled ZnO nanoparticle formation in aqueous alcohol solution by simultaneous ligand exchange with DDA..... 106
Figure 4.37: FT-IR spectrum of ZnO nanoparticles bearing coordinating DDA ligands before (a) and after encapsulation with PMMA-*b*-PGM (b).. 107
Figure 4.38: TGA of the ZnO nanoparticles stabilized with coordinating DDA ligands. 107
Figure 4.39: A plot of ZnO particle dimension versus metal/ligand molar ratio 109
Figure 4.40: XRD difractogram of ZnO nanoparticles prepared (L/M :0.44) by the ligand exchange method at room temperature. 110
Figure 4.41: ESEM image of ZnO nanoparticle with L/M:0.44 before (A) and after reacting with PMMA-*b*-PGMA (B) taken from acetone dispersions..... 110
Figure 4.42: Encapsulation of ZnO nanoparticles by reaction of coordinated amino groups with epoxy groups of PMMA-PGMA block copolymer in toluene..... 111
Figure 4.43: DLS of ZnO nanoparticle sample (with L/M:0.44) showing size increment after reacting with PMMA-*b*-PGMA..... 112
Figure 4.44: SEM picture of the cast film obtained from acetone dispersions of encapsulated ZnO nanoparticles (L/M:0.44) in the presence of PMMA-*stat*-PBA as matrix polymer. 113

LIST OF SYMBOLS

$\mathbf{I_{eff}}$	: Initiator efficiency
$\mathbf{M_{th}}$	: Theoritical molecular weight
$\boldsymbol{M_n}$	: The number average molecular weight
$\boldsymbol{M_w}$	: The weight average molecular weight
$\boldsymbol{M_w/M_n}$	: The molecular weight distribution
$\mathbf{^oC}$	: Celsius
M	: Molarity
nm	: Nanometer
µm	: Micrometer
$\mathbf{K_m}$	: Michaels constant
$\boldsymbol{V_{max}}$	: Maximum rate of reaction
$\mathbf{q_E}$	: Equilibrium adsorption
C	: Concentration
$\mathbf{C_E}$	: Equilibrium concentration
λ	: Wavelength
$\boldsymbol{\eta}$	: efficiency factor
$\boldsymbol{v_{immobilized}}$	: reaction rate of the immobilized enzyme
$\boldsymbol{v_{free}}$	: reaction rate of free enzyme
A	: Absorbance
d	: Density
r	: Diameter

SURFACE TAILORING OF MICRO AND NANO BEADS WITH FUNCTIONAL HAIRY GRAFTS

SUMMARY

Tailoring of solid particles in micron or nano-sizes with functional hairy grafts has been one of the most popular area of research in recent years. Interest is due to widespread application of these materials in various fields such as designing of drug delivery systems, biological assays, compotibilizing with different materials and preparing efficient catalyst carrying systems. This dissertation focuses on surface modification of nano and micron size organic and inorganic particles with polymers. The whole content of the thesis can be classified into five sections.

In the first section a new synthesis method is described for the preparation of functional monomer, 2-bromoethyl methacrylate (BEMA). This monomer was then employed for synthesis of bromoethyl functional microspheres by suspension copolymerization methodology using ethyleneglycol dimethacylate as crosslinker and methyl methacrylate as diluting comonomer (Figure 1). The bromo ethyl surface groups were then used for surface initiated polymerization of glycidyl methacrylate and 2-methyl 2- oxazoline by atom transfer radical polymerization and ring opening polymerizations, respectively.

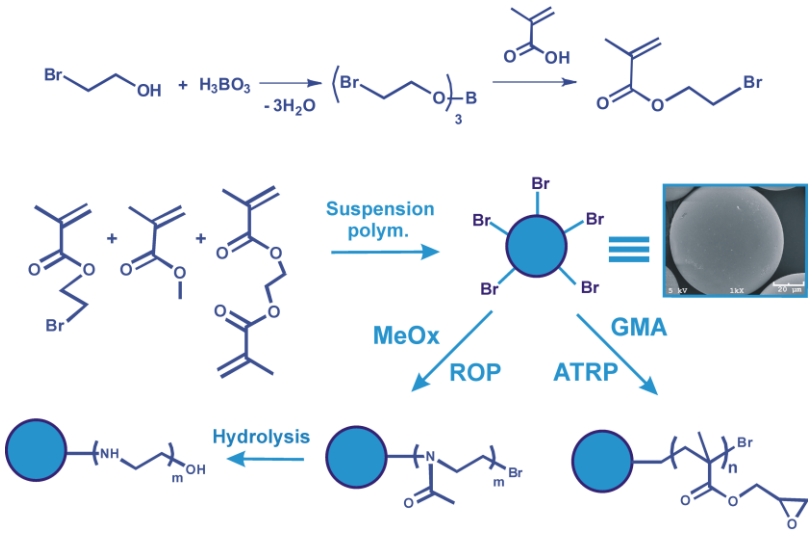

Figure 1: Synthesis of 2-bromo ethyl methacrylate monomer and its suspension polymerization and graft copolymerization of glycidyl methacrylate and 2-methyl 2- oxazoline.

Both procedures yielded dense surface grafts with reasonably high number of repeating units. The oxazoline brushes on the microspheres were successfully transformed into poly(ethylene imines) quantitatively, as inferred from FT-IR spectra, XPS and standart analytical procedures. Although, the surface grafting methodology have been described few times in the literature previously, the structure

presented in this work differs from their counterparts in that, the brushes in the present case tethered to the surfaces by non-hydrolysible linkages. Having non-hydrolysible linkages, these structures are very useful as catalyst or reagent carrier which recyclable many times.

In the second part of the study poly(styrene)-poly(gylcidyl methacrylate) block grafts were created on bromo acetyl fuctionalized poly(styrene-divinyl benzene) microspheres by ATRP technique. The resulting material was demonstrated to be useful for lipase immobilization via epoxy groups of the PGMA block (Figure 2). The results showed that ester hydrolysis ability of the attached lipase enzyme is reasonably fast due to partial mobility of the graft chains. Obviously, distance from P(S-DVB) core by linear PS spacer chains makes the enzymatic reaction faster.

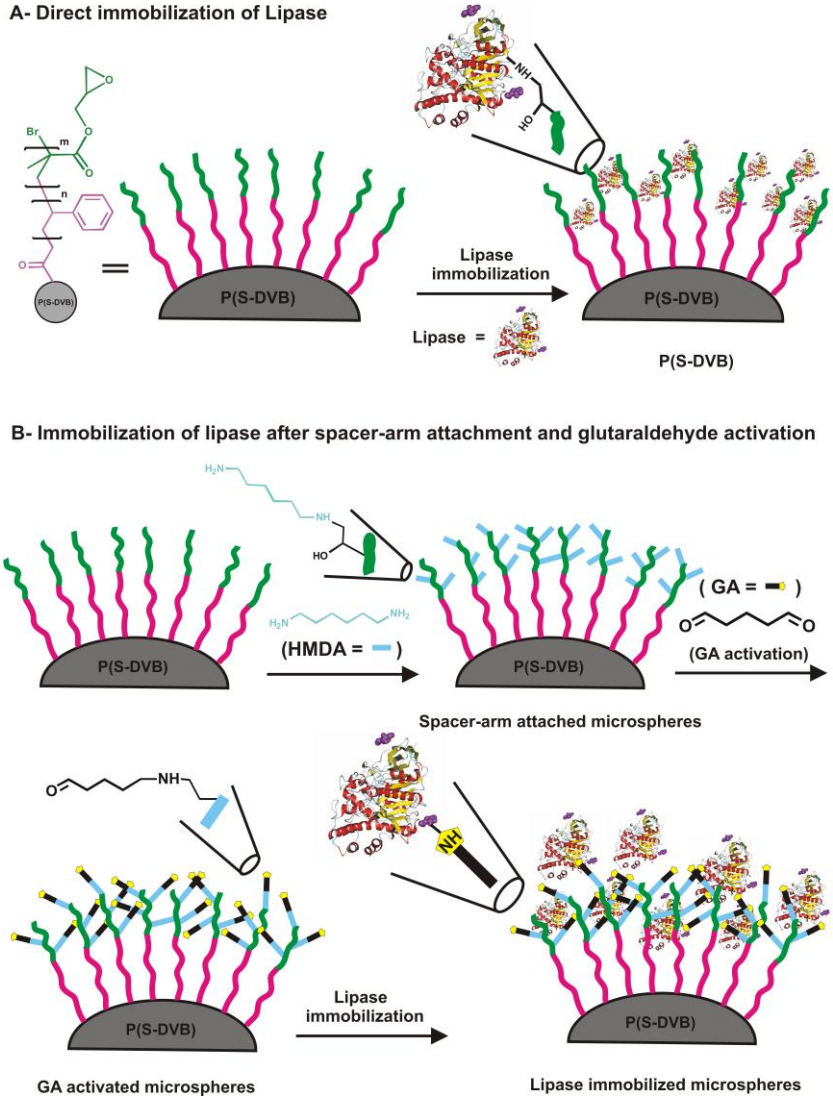

Figure 2: Chemistries used for the covalent immobilization of lipase on the P(S-DVB)-*g*-P(S-GMA) and P(S-DVB)-*g*-P(S-GMA)-HMDA microspheres.

In the third section commercial divinyl benzene (with 55 % DVB) was polymerized by precipitation polymerization methodology in acetonitrile solution to give 1-3 micron size of particles. The residual double bonds of the microspheres were subjected to hydrobromination and subsequent condensation with NaN_3 in DMF. The

azide functions so generated on the microspheres were used for clicking with the alkyne terminated polymers namely, poly(methyl methacrylate), poly(*tert*-butyl acrylate) and poly(ethylene glycol) in the presence of copper catalyst (Figure 3).

In the study alkyne terminated poly(methyl methacrylate) and poly(*tert*-butyl acrylate) were seperately prepared by copper madiated ATRP methodology using alkyne functional ATRP initiator derived from 2-bromoisobutyryl bromide and propargyl alcohol. Whereas, alkyne terminated PEG (PEG-2000 or PEG-5000) were obtained by esterification of PEG with 4-pentynoic acid using DCC as water scavanger at room temperature. In the study only PEG and binary mixture of poly(methyl methacrylate) and poly(ethylene glycol) or poly(*tert*-butyl acrylate) and poly(ethylene glycol) were anchored to the surface of the microspheres by copper catalyzed azide-alkyne click reactions.

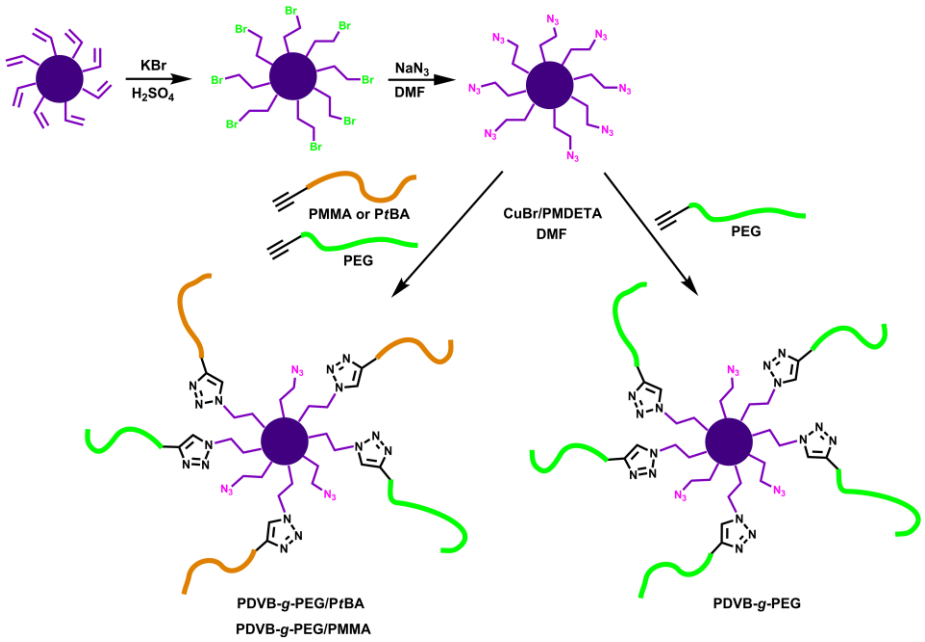

Figure 3: Preparation of microspheres containing hydrophilic and/or hydrophobic polymer chains by hydrobromination and click reactions.

Protein adsorbtion and desorption abilities of those structures were compared with each other. The results showed that PDVB-g-PEG exhibits long term enzyme activity whereas the microspheres bearing PEG/PMMA mixed grafts shows high enzyme loading capacity and better reversibility probably due to good balance of the hydrophilicity with hydrophobicity. Most probably high activity of the enzyme supported on PEG surface grafts **(**1.14 Unit mg^{-1} protein/g support**)** is due to hydrophilicy of the substrate, 2,2-azinobis-(3-ethylbenzothiazoline-6-sulphonic acid).

In the fourth section, we have presented a new procedure for organic modification of preprepared SiO_2 and TiO_2 nanoparticle surfaces. This was achieved by physical adsorbtion of poly(2-hydroxypropylene maleate) (PHPM) on the nanoparticle surfaces. Self-curing ability of this polyester allowed encapsulation of the nanoparticles within the crosslinked polyester. Crosslinking of the polyester takes place by addition of hydroxyl groups to the maleate double bonds above 180 ^{o}C. The residual hydroxy groups on the nanoparticle surfaces were employed as initiaiton sites for ring opening polymerization of ε-Caprolactone (Figure 4). High grafting

degrees (22.2-71.4 %) were attained within reasonable times (6-8h). And resulting materials were determined to be dispersible in acetone solution of poly(methyl methacrylate-*stat*-butyl acrylate). The resulting dispersion gave nearly transparent and homogenous free-standing films on the glass slides.

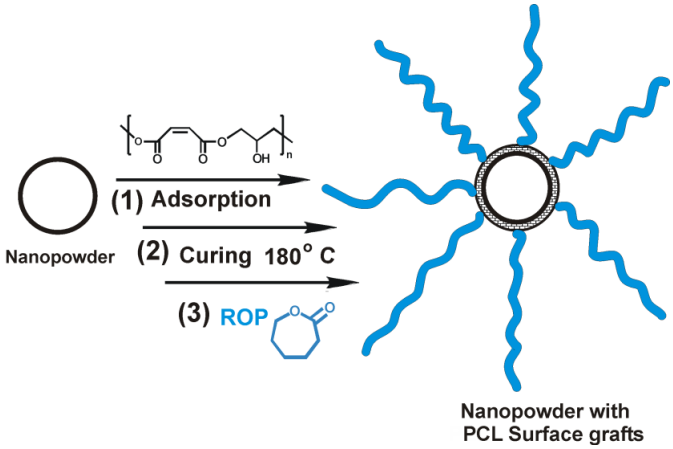

Figure 4: Schematic illustration of SiO_2 and TiO_2 nanoparticle encapsulation with poly(2-hydroxypropylene maleate) and ring opening polymerization of ε-Caprolactone from the residual hydroxy groups on the nanoparticle surfaces.

In the last section of the thesis, we present a method, "ligand exchange method", for size-controlled synthesis of zinc oxide nanoparticles (Figure 5). Controlled-nucleation growth and the use of amphiphilic block copolymers are the most common routes for size control of nanoparticles in the chemical synthesis methods. These approaches have limited success for precise control of the particle sizes. In this part of the study zinc oxide nanoparticles were synthesized using zinc tetramine complex as precursor in the presence of dodecylamine.

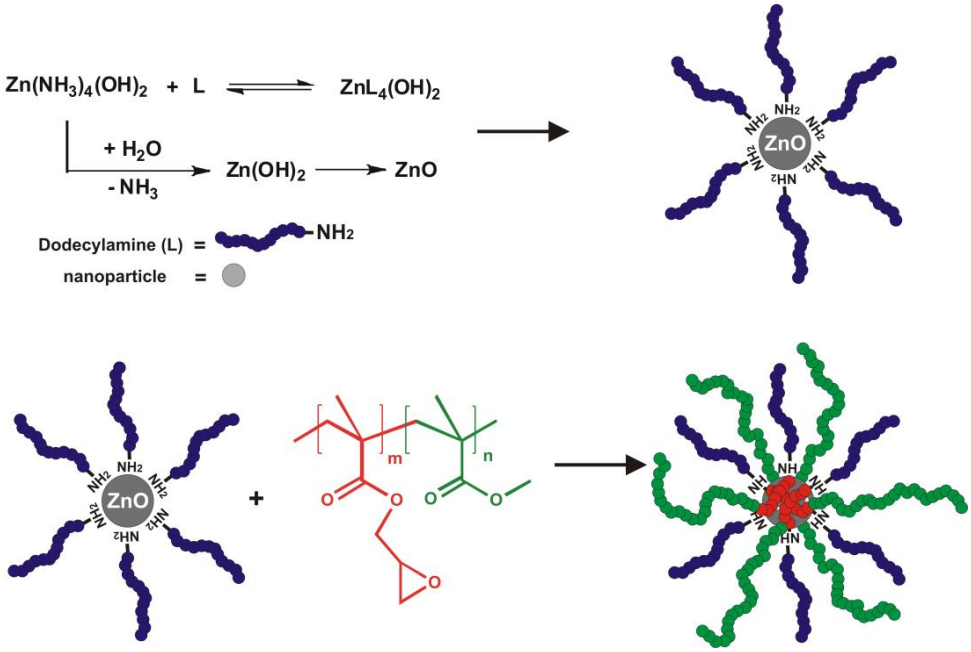

Figure 5: ZnO nanoparticle synthesis with ligand exchange method and encapsulation with Poly(GMA-*b*-MMA).

Gradual removal of ammonia in alcohol-water mixture was demonstrated to give nanoparticles (60-210 nm) bearing dodecylamine molecules at their surfaces. In conjuction with this, a simple theoritical model providing a relationship between the size and L/M ratio was proposed. Characterizations of the resulting material with FT-IR, TGA, DLS, ESEM revealed that the particle sizes of zinc oxide is controlled by stoichiometrical ratio of amine ligand to the zinc metal.The results showed that L/M molar ratio is inversely proportional to the particle size and the key parameter in the size control.

Those nanoparticles were readily encapsulated by reaction of epoxy groups of block copolymer of glycidyl methacrylate with coordinated amino groups. This process yields core-crosslinked zinc oxide nanoparticles with linear PMMA shells. The resulting core-shell particles were utilized to produce free-standing films by casting from aceton solution of poly(methyl methacrylate-*stat*-butyl acrylate).

MİKRO VE NANO TANECİK YÜZEYLERİNİN FONKSİYONEL POLİMERLER SAÇAKLARIYLA DONATILMASI

ÖZET

Mikron veya nano boyutlu katı tanecik yüzeylerine fonksiyonel saçaklı polimer aşılamak son yılların en popüler çalışma alanlarındandır. Bu ilginin sebebi bu malzemelerin yeni ilaç taşıma sistemlerinin dizaynı, biyolojik maddeleri tanıyan moleküler yapıların oluşturulması, başka maddelerle uyumluluk sağlama ve daha etkin kataliz taşıyıcı yapıların dizaynı gibi bir çok dalda çok geniş kullanım alanları bulmalarıdır. Bu sebeplerden dolayı bu tez, nano ve mikron boyutundaki organik ve inorganik tanecik yüzeylerinin polimerlerle modifiye edilmesine odaklanılmıştır. Tezin bütünü beş ana başlık altında sınıflandırılmıştır.

İlk bölümde bir fonksiyonlu monomer olan 2-bromoetil metakrilatın (BEMA) sentezlenmesi için yeni bir yöntem ortaya konmuştur. Daha sonra bu monomerin, çapraz bağlayıcı olarak etilen glikol dimetakrilat ve seyrelitici monomer olarak metil metakrilat kullanılarak süspansiyon kopolimerleştirilmesiyle ile bromo etil fonksiyonlu mikroküreler elde edilmiştir. Daha sonra yüzeydeki bromo etil grupları üzerinden sırasıyla glisidil metakrilat ve 2-metil 2-oksazolinin yüzeyden başlayan atom transfer radikal polimerleşmesi ve halka açılma polimerleşmesi ile yüzeye aşılanmaları gerçekleştirilmiştir (Şekil 1).

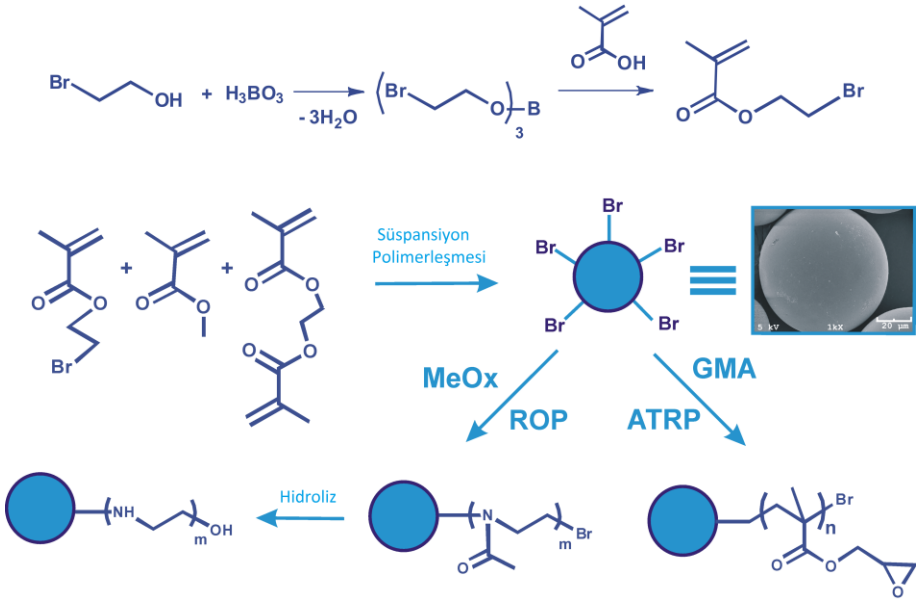

Şekil 1: 2-bromo etil metakrilat monomer sentezi ve bu monomerin süspansiyon polimerleşmesi ve glicidil metakrilat ve 2-metil 2-oksazolin aşı kopolimerleşmesi.

Her iki prosedürde de yüzeyde oldukça yüksek sayıda tekrarlanan üniteli yoğun aşı polimerleri elde edilmiştir.Mikrokürelerin yüzeyindeki oksazolin saçaklarının tamamının başarıyla poli(etilen imin)'lere dönüştürüldüğü FT-IR spektrumları, XPS ve standart analitik prosedürler kullanılarak kanıtlanmıştır. Bu tür yüzeyden aşılama yöntemi önceki literatürde de birçok kez gösterilmiş olmakla beraber, bu çalışmada sunulan yöntemin yüzeye bağlanan saçakların kıralamayan bağlarla bağlı oluşu nedeniyle literatürdeki benzerlerinden farklıdır. Hidroliz olmayan bağlara sahip olan bu yapılar bir çok defa kullanılabilen kataliz ve reaktif grup taşıyıcı olarak kullanılmaya oldukça elverişlidir.

İkinci kısımda yapılan çalışmada, bromo asetil fonksiyonlu poli(stiren-divinil benzen) mikro kürelerin yüzeyine poli(stiren)-poli(glisidil metakrilat) blokları ATRP tekniği kullanılarak aşılanmıştır. Elde edilen ürünün PGMA bloğunda bulunan epoksi gruplarının yüzeye lipaz tutturulması için kullanışlı olduğu gösterilmiştir. Sonuçlar saçaklara tutturulan lipasın yüzeydeki aşı zincirlerinin saçakların kısmi hareketliliği nedeniyle ester hidroliz yeteneğinin oldukça yüksek olduğu göstermiştir (Şekil 2). Açıktır ki burada , enzimin çaprazbağlı P(S-DVB) küre yüzeyinden lineer PS aşı zincirleri vasıtasıyla uzaklaştırılması nedeniyle enzim reaksiyonunun hızlanmaktadır.

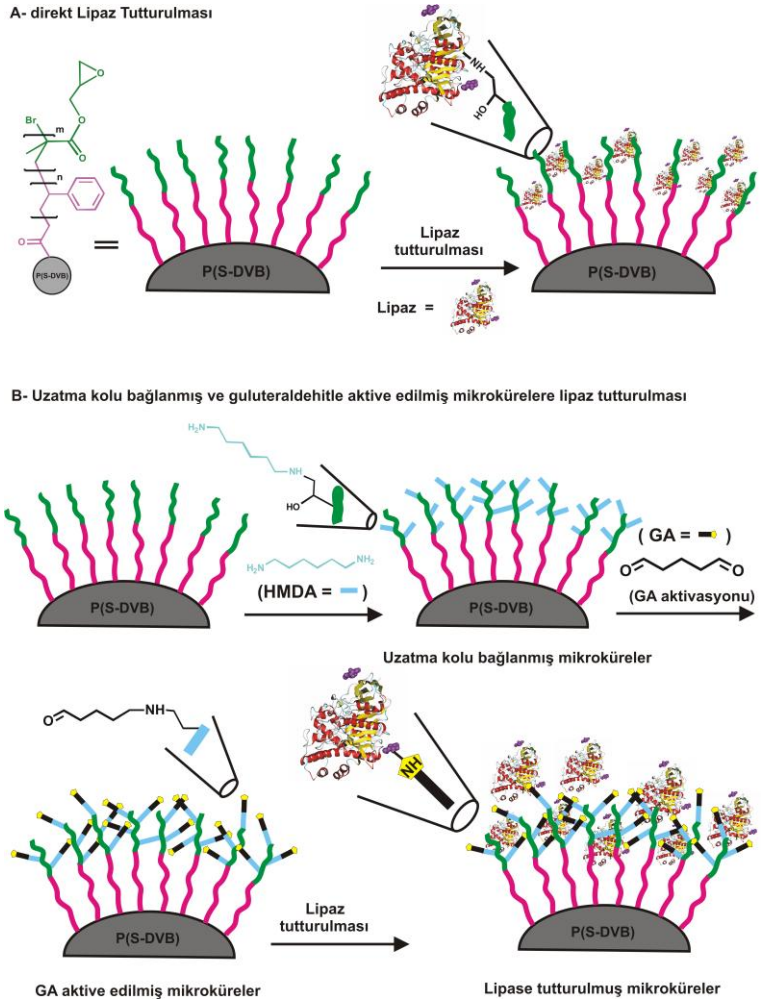

Şekil 2: P(S-DVB)-*g*-P(S-GMA) ve P(S-DVB)-*g*-P(S-GMA)-HMDA mikro-kürelerine kovalent bağla enzim bağlanması için kullanılan kimyasal yöntemler.

Üçüncü kısımda asetonitril çözeltisinde çökelme polimerizasyonu yöntemi kullanılarak ticari divinil benzen (%55 DVB) polimerleştirilmiş ve 1-3 mikron boyutunda microküreler elde edilmiştir. Microküreler üzerindeki reaksiyona girmeden arta kalan çifte bağlar önce hidrobromlanmış daha sonra NaN_3 ile DMF çözücüde reaksiyona uğratılarak azid fonksiyonuna dönüştürülmüştür. Daha sonra bu azidlenmiş mikroküreler alkin sonlu polimerlerle, poli(metil metakrilat), poli(*ters*-bütil akrilat) ve poli(etilen glikol) , bakır(I) kataliz varlığında etkileştirilerek azid alkin birleşmesi gerçekleştirilmiştir.

Bu çalışmada kullanılan alkin sonlu poli(metil metakrilat) ve poli(*ters*-bütil akrilat) ayrı ayrı 2-bromo isobutil bromür ve propargil alkolden türetilmiş alkin fonksiyonlu ATRP başlatıcı ile bakır katalizli ATRP metodu kullanılarak hazırlanmıştır. Alkin sonlu PEG (PEG-2000 veya PEG-5000) ise su tutucu ajan olarak DCC kullanılarak 4-pentinoik asit ile PEG'un oda sıcaklığındaki esterleşme reaksiyonu ile elde edilmiştir. Bu çalışmada tamamı alkin uç grubu taşıyan PEG, PEG-PMMA karışımı ve PEG-P(*ters*-BA) karışımı ayrı ayrı bakır katalizörlü azid-alkin klik reaksiyonu ile azid fonksiyonlu mikroküre yüzeylerine ile bağlanmıştır (Şekil 3).

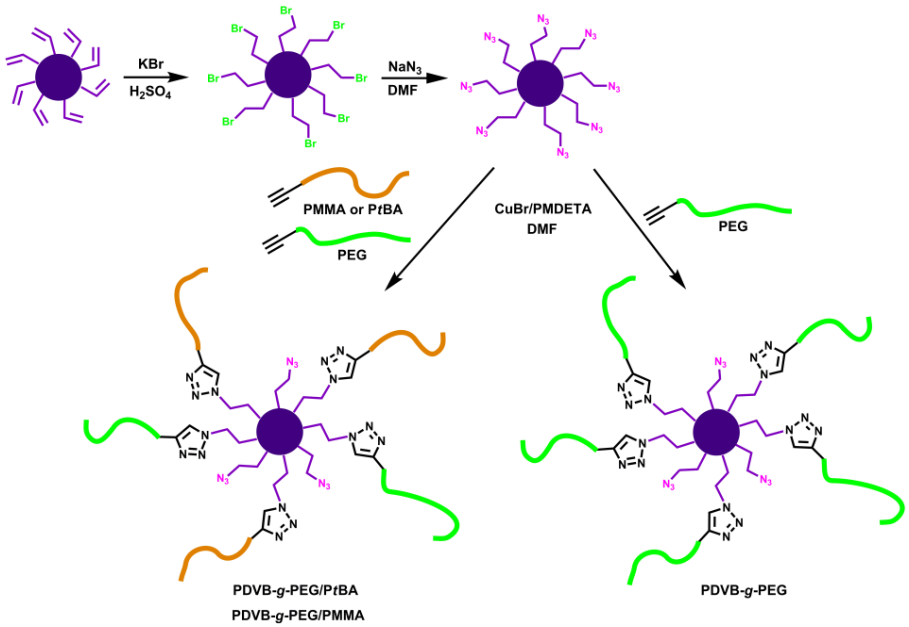

Şekil 3: Hidrobromlama ve klik reaksiyonları ile hem hidrofilik hem de hidrofobik polymer zincirleri taşıyan mikrokürelerin elde edilmesi.

Elde edilen bu yapıların protein adsorpsiyon ve desorpsiyon özellikleri birbirleri ile kıyaslandı. Sonuçlar gösterdi ki PDVB-g-PEG mikroküreleri takdirinde enzim aktivitesi en uzun süre korunurken yüzeyinde PEG/PMMA karışımı aşıları taşıyan mikroküreler daha yüksek enzim bağlama kapasitesi ve daha iyi geridönüşüm özelliğine sahitirler ki bunun muhtemel sebebi yapıdaki hidrofiliklik ile hidrofobiklik dengenin iyi sağlanmış olmasıdır. Pek muhtemeldir ki PEG aşılanmış mikrokürenin yüksek enzim aktiviteli(1.14 Unit mg^{-1} protein/g destek malzemesi) oluşu etkileşen maddenin de, 2,2-azinobis-(3-etilbenzotiazolin-6-sulfonik asit) hidrofillik olmasıdır.

Dördüncü kısımda, önceden hazırlanmış SiO_2 ve TiO_2 nanotanecik yüzeylerinin organik modifikasyonu için yeni bir prosedür ortaya konmuştur. Bu işlem ilk basamakta poli(2-hidroksipropilen maleat)'ın (PHPM) nanotanecik yüzeylerine fiziksel adsorbsiyonu ile gerçekleştirilmiştirç. Adsorbe edilen poliesterin kendi

kendine çapraz bağlanabilme özelliği nanotanecik yüzeylerinin çapraz bağlanmış poliester ile bohçalanmasına imkan vermiştir. Çapraz bağlanma 180 ^{o}C'de hidroksi gruplarının maleat çifte bağlarına katılması ile sağlanmıştır. Nanotanecik yüzeyinde çapraz bağlanmadan arta kalan hidroksi grupları ε-Kaprolakton halka açılma polimerizasyonu ile yüzeye aşılanmasında başlatma noktaları olarak kullanılmıştır. Böylece kabul edilebilir zaman dilimlerinde (6-8 saat) oldukça yüksek aşılanma dereceleri (22.2-71.4 %)) elde edilmiştir. Elde edilen ürünlerin poli(metil metakrilat-*stat*-butil akrilat)'ın aseton çözeltesinde iyi dispers olduğu gösterilmiştir. Ayrıca bu dispersiyonların oldukça seffaf ve homojen film oluştudukları görülmüştür (Şekil 4).

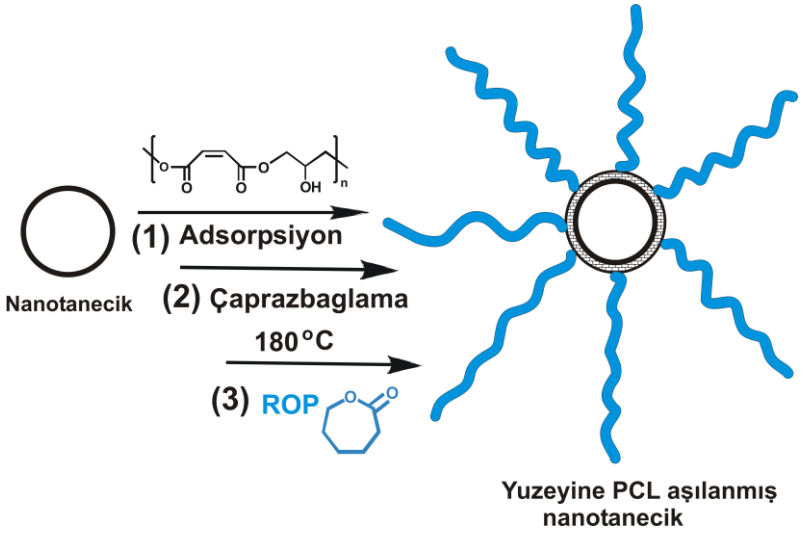

Şekil 4: SiO_2 ve TiO_2 nanotanecilerinin poli(2-hidroksipropilen maleat) ile bohçalanması ve nanotanecil yüzeyinde arta kalan hidroksi grupları ile halka açılması polimerizasyonu ε-kaprolakton aşılanmasının şematik gösterimi.

Tezin son kısmında sunduğumuz "ligand değişim methodu" ile boyutları ayarlanabilir çinko oksit nanotaneciklerinin sentezlenebileceği gösterilmiştir. Kimyasal yolla nanotanecik sentezilerinde kontrollü-çekirdek büyümesi prensibi uygulanarak veya amfifilik blok kopolimerler kullanarak sağlanabilmektedir. Ancak bu yaklaşımların tanecik boyutlarını kontrol etmedeki başarısı sınırlıdır Çalışmanın bu kısmında dodecilamin varlığında çinkotetramin kompeksi kullanılarak çinko oksit nanotanecikleri sentezlenmiştir (Şekil 5).

Bu aşamada su-alkol karışımından amonyağın yavaş yavaş uzaklaşmasıyla yüzeyinde dodesilamin bulunan nanotanecikler (60-210 nm) sentezlenmiştir. Burada ayrıca, nanotanecik boyutuyla L/M oranını ilişklendiren basit bir teorik model ortaya konmuştur. Elde edilen malzemenin FT-IR, TGA, DLS, ESEM ile karekterizasyonları çinko oksit nanotanecik boyutlarının çinko / amin ligantı arasındaki sitokiyometrik oranla kontrol edildiğini göstermiştir. Sonuçlar nanotanecik boyutunun L/M oranı ile ters orantılı olduğunu ve bunun boyut kontrolünde anahtar parametre olduğunu göstermiştir.

Elde edilen nanotanecikler yüzeyindeki koordine olmuş amino gruplarının glisidil metakrilat blok kopolimerinin yapısındaki epoksi grupları arasındaki reaksiyonuyla kolayca bohçalanmıştır. Bu işlem çekirdekte çapraz bağlı matrix içinde çinko oksit nanotanecikleri ile kabukta PMMA lineer zincirleri içeren bir yapı verir.

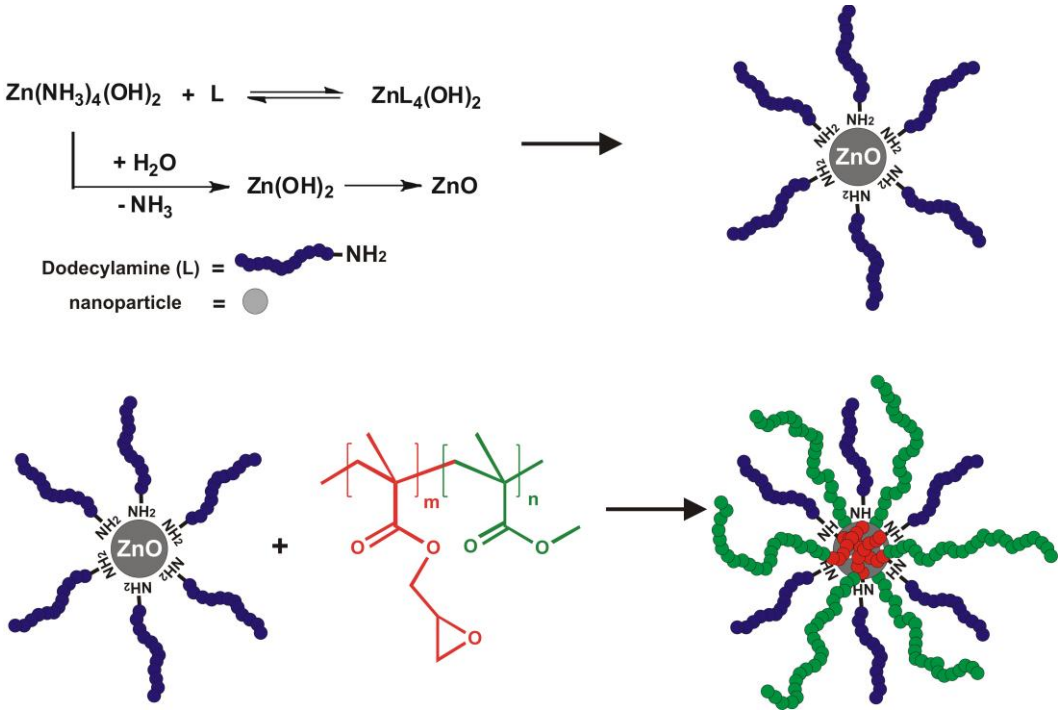

Şekil 5: Ligand değişim metodu kullanılarak ZnO nanotaneciklerinin sentezi ve poli(GMA-*b*-MMA) blok kopolimeri ile bohçalanması.

Bu şekilde ele geçen çekirdek-kabuk tipli nanotaneciklerin ile aseton poli(metil metakrilat-*stat*-butil akrilat) kopolimeri çözeltileriyle karıştırılmasıyla oluşturulan dispersiyonları sağlam filmler elde etmede kullanılmıştır.

1. INTRODUCTION

Tailoring of nano or micron size solid surfaces with polymers has been one of the most attractive areas of research in last two decades. Such a surface modification opens up new application possibilities ranging from medicine to microelectronics [1, 2]. The surface modification simply provides compatibility with organic matrixes. Due to this reason those materials find extensive use as the main ingredient of the composites. Surface modification of insoluble inorganic or organic solids, on the other hand, allows preparing materials having diverse applications. For instances poly(styrene-divinyl benzene) resin beads with poly(ethylene oxide) surface grafts has been commercialized and sold under trade name of "Wang Resin" which is useful as stationary phase for chromatographic separation of proteins[3]. Perhaps most attractive exploitation of these materials is their use as enzyme or catalyst carrier [4]. Since those supported catalysis can be recycled many times, these find in large-scale industrial processes as well. Inorganic pigment nanoparticles when organically modified can be used for the manufacturing of inorganic-organic hybrid nanocomposites [5]. These nanostructures find extensive use in design of enzyme linked imino sorbent assay (ELISA) and micro-electronic devices etc [6].

Polymer supported catalysts have many advantages over the conventional-catalysis. For instance, main problem of the metal catalysts is their rapid deactivation by poisoning with exposure to the air. The polymeric structure selected herein will provide protection of the catalyst. There appear many publications dealing with polymer supported catalysts [7]. Main purpose is recovery of the catalysts. Attachment of catalyst species onto insoluble polymer particles is an important art for recovery of the catalysts in large scale processes. Perhaps only disadvantage of those materials is slow reactions due to heterogeneity of their processes.

We thought that applications of the solid particles with surface grafts are not limited to the uses described above. Decoration of solid supports with functional hairy grafts opens up new avenue to generate more efficient functional materials [8]. The use of

the hairy grafts as carrier for reagents or catalyst provides faster reactions due to partial mobility of the graft chains [9]. Comparing with the common beaded polymers possessing directly attached functional groups to the surfaces, the hairy structures ensure quasi homogenous reaction conditions [10]. Considering insolubility of the bead core and miscibility of the graft chains in the solvents, the hairy graft structures comprise easy isolation facility and fast reaction abilities.

Creating surface tethered graft polymer chains on solid substrate is difficult task in practice. Various techniques; *grafting-onto, grafting-through and grafting-from* approaches have been studied to produce such structures [11]. The "*grafting onto*" technique has limited success owing to steric hindrances of the polymer chains approaching the surface. This technique does not allow good control over chain density on the surface [12]. However, this technique has gained renewed interest in recent years by using so called "*click chemistry*" approach in which prepolymers bearing easily reacting terminal groups are coupled with suitable surface functionalities generated on the solid surface. Diels-Alder reaction and azide-alkyne coupling reactions are most common routes in the click chemistry. The "*grafting from*" technique, on the other hand, provides better control of the chain densities and assembled polymer chains on the surface without homopolymer formation [13, 14]. Polymerization from the initiator groups on solid surfaces is also termed as "*surface initiated polymerization*" (SIP). In the SIP method anionic, cationic and radical initiating techniques can be employed in principle. However, controlled living radical techniques are most common approaches to generate polymer brushes due to their tolerance against trace water and protic solvents [15]. Moreover, the living end groups allow forming di or multi-block graft structures.

Among controlled living polymerization techniques, ATRP is especially fruitful process which is applicable in grafting even from solid particle surfaces [16]. However covalent linking of the initiating sites to any solid surface is the crucial task. This can be achieved either by surface modification with suitable reagents possessing haloalkyl functionality or by preparation of the solid support using appropriate functional comonomer. The linkage between solid core and initiator group is also important. Non-hydrolysibility of this linkage is preferable when the resulting functional material is to be processed under harsh conditions. Attachment of the initiator groups by ester linkage is common approach and has been widely

employed by many authors [17, 18]. However, hydrolysis of this bond chemically or enzymatic means deters the use of this approach when the hairy grafts are considered as reusable catalyst carrier for large scale and continuous processes.

ATRP has been employed also for graft copolymerization of acrylate monomers from solid planar[19] or spherical [20] surfaces. A common approach for graft copolymerization from solid surfaces by ATRP involves two main steps: introduction of ATRP initiators onto the surface and subsequent initiation of the polymerization from surface-bound initiation sites. The first step is crucial for the success of surface initiated graft copolymerization by ATRP. Yu et al demonstrated controlled grafting of poly (GMA) from 2-bromoester functional surfaces on hydrogen terminated silica substrates [21]. Haddleton's group [3] described the use of Wang resin with benzyl alcohol functionality as solid substrate. Reaction of the methylol groups with 2-bromoisobutyryl bromide followed by grafting from bromoisobutyrate functions was demonstrated to be efficient in graft copolymerization of methacrylate monomers. Stöver's group described two methods for incorporation of initiator groups on densely crosslinked polystyrenes possessing vinyl residues. In the first method, the vinyl residues were transformed into chloroethyl functionalities by hydrochlorination [22]. In the second approach the vinyl residues were converted to hydroxyethyl groups. In either case the following reaction with 2-bromoisobutyryl bromide created the initiator groups on the spherical surface [23].

Recently Stover et.al. described a method so called "precipitation polymerization" method for preparing densely crosslinked divinyl benzene microspheres with residual double bond at the surfaces. This report has found great attention since it is unique process for obtaining microspheres with uniform size (1-5 μm) and shape, which can lead to narrow disperse microspheres free of any added surfactant or stabilizer [24]. In this technique, homogenous reaction mixture (monomer, radical initiator and solvent) become opaque during the polymerization and subsequently phase separation occurs between polymer and continuous medium.

Organic-inorganic hybrids consisting of nano-size inorganic fillers and polymer as binder are of increasing interest due to their unusual optical, electrical and mechanical properties originating from large surface area to volume ratio and finite size effects [25]. Surface modification of inorganic nanoparticles is essential for the

attachment of the organics or polymers. Attachment of polymers onto surfaces of nanoparticles is mostly preferred way of their surface modification. Beside traditional sol-gel technique [26], *in situ*-polymerization [27, 28], grafting onto [29], grafting from [30]and grafting through [31]polymerization techniques have been widely applied for surface modification of nano-size particles. The "grafting from" technique is also versatile tool for creating polymer brushes on solid nanoparticle surfaces.

Controlled radical polymerization processes, namely atom transfer radical polymerization (ATRP) [32], nitroxide mediated radical polymerization (NMP) [33] and reversible addition-fragmentation chain transfer (RAFT) [34] processes have been employed successfully in the SIP of various monomers from metal, pigment and semiconductor nanoparticles. An alternative approach for decoration of nanoparticle surfaces with polymers is ring opening polymerization (ROP) of some cyclic esters, e.g. ε-caprolactone. ROP of ε-caprolactone has been reported by Dubois and his coworkers in which the cyclic ester monomer was polymerized in living fashion through amine-terminated silane coupling agent on the surfaces of silica nanoparticles using trialkyl aluminum as initiator [35].

One key issue in SIP strategy is immobilization of initiator groups onto the particle surfaces for application of the "grafting from" technique. However, there is yet no general recipe applicable to every particle surface for immobilization of the initiating groups and modification of each surface essentially needs different individual chemical processes. For instance a common way of introducing initiator groups onto silica surface is modification with silane coupling agents. Numerous silane coupling agents with amine, halogen or vinyl residues have been developed for modification of silica surfaces [36]. However, the silane coupling agents are almost limited to silica surfaces and they cannot be used for incorporation of the initiating sites onto a wider selection of other particle surfaces.

One critical issue in nano-structured materials is size of the particle. The size of the particle greatly influences optical and electrical properties of the final materials. For instance 1-5 nm size of nanoparticles has diverse optical properties such as transparency and tunable dielectricity in electrical field. There appears two significant way of size control of the nanoparticles in preparing by wet chemical

methods. Control of particle size by using micellar core as template is the most common route for preparing nanoparticles in desired size range. The process however greatly influenced by many reaction parameters such as solvent, temperature and salt. Success of this method over the size control is limited in most cases. The second approach is so called "controlled nucleation growth" which is based on generation of highest number of nucleation centers in the beginning at high temperatures [37]. This strategy has also been combined with surfactant stabilization methodology. Although this strategy is useful for obtaining smallest sizes, it is not successful in attaining any fixed particle size.

This thesis is aimed at generation of functional hairy graft polymers linked to the surfaces of micron or nano-sized supports with non-hydrolysable bonds. These macromolecular structures were designed by using various polymerization techniques such as classical radical polymerization, ATRP, CROP and click chemistry techniques. The resulting materials were considered as support for more efficient enzyme carrier, protein separating medium, macromolecular chelating ligand for metal ion separations etc. These works have been presented under five subtitles:

1. Preparation of cross-linked poly(2-bromoethyl methacrylate) microspheres and decoration of their surfaces with functional polymer brushes.
2. Poly(glycidylmethacrylate)-polystyrene copolymer grafted nano-composite P(S-DVB) microspheres from surface initiated-atom transfer radical polymerization: Immobilization of lipase and application in esters synthesis.
3. Modification of Poly(divinylbenzene) Microspheres by Hydrobromination-Click Chemistry Protocol and Their Protein Adsorption Properties.
4. Novel strategy for tailoring of SiO_2 and TiO_2 nanoparticle surfaces with poly(ε-Caprolactone).
5. Ligand Exchange Method for Size-Controlled Synthesis of ZnO Nanoparticles in Solution.

2. THEORETICAL PART

2.1 Surface-Initiated Polymerization Techniques

Surface-initiated polymerization (SIP) has been widely used for tailoring of solid surfaces to impart wettability, further chemical modification capability, biocompatibility and corrosion resistance. Organic modification of surfaces by direct immersion coating by and spraying are some of the traditional methods. This method however is based on physisorption and do not give permenantly linked organic layers. Attachment of the organic layer to the insoluble supports by covalent linkages is most desirable to attain stable surface layers.

Three main strategies: (i) the *grafting to*, (ii) the *grafting from* and (iii) *grafting through* strategies have been employed to create graft layers on the solid surfaces. The *grafting to* strategy involves linking of the prepolymers to the surfaces via suitable linkers such as activated double bond, epoxy or amino groups etc. Although the experimental work up is simple and straightforward, the grafting yield of this strategy is generally low and it is difficult to attain thick and dense graft layers. The method however may provide satisfactory polymer brushes when low molecular weight polymers are grafted onto the surfaces.

Grafting through approach on the other hand has limited use for grafting of micron size particles. The method however is fruitful for preparing nanocomposite materials from nanopowders. For instance Ford et al. described polymerization of acrylic monomers in the presence of trimethoxysilyl propylmethacrylate (MEMO) coupled colloidal silica to obtain stable and homogenous dispersion[38].

2.2 Grafting from Methodology

The *grafting from* method involves initiation of the polymerization from the the surface bond initiator groups. The grafting from solid surfaces has also been termed as surface initiated polymerization (SIP). This technique is superior to the other methods in that, it provides dense surface brushes and if the initiation is performed

by one of the controlled polymerization techniques, bilayer block graft layers can also be generated with negligible free polymer formation (Figure 2.1).

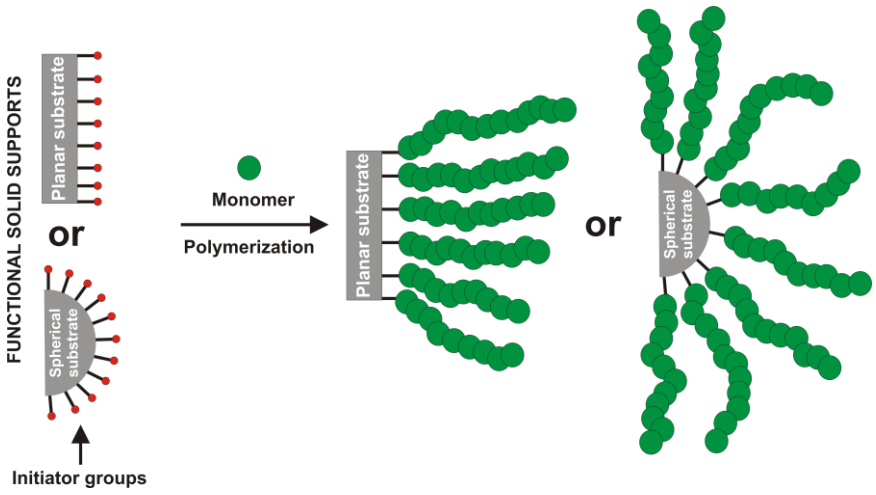

Figure 2.1: Schematic illustration of grafting from approach on solid support.

A number of methods has been reported for generation of graft layers on the solid surfaces. Traditional radical polymerization methods, controlled free radical polymerization (CRP) techniques, ionic polymerization techniques, photopolymerization techniques and metatetesis polymerization techniques have been widely employed for obtaining surface brushes.

Traditional radical polymerization techniques are of only historical importance and seem to be largely replaced with the living polymerization techniques nowadays. There appear some examples of the use of traditional radical polymerization teqniques in the literature. The method involves chemical pre-treatment such as ozonation, diazotization and xanthation of the surfaces and following polymerization of the monomers[39].

Logically direct use of unbound radical source may also provide grafting onto solid surfaces. In this case the radical fragment formed in solution may generate a new radical on the solid support by hydrogen abstraction and polymerization takes place on the surface. In this respect many redox couples such as Fenton reagent and permanganate-oxalate and cerium(IV)-alcohol redox couples have been used for grafting [40-42]. Obviously main drawback of this approach is formation of waste amounts of unbound free homopolymer.

2.2.1 Surface grafting by ionic polymerization

Application of ionic polymerization methods for grafting from solid surfaces is relatively rare. Perhaps the most widely studied ionic polymerization for grafting is the use of triflate surface initiating groups. Jordan and Ulman presented trifluoromethane sulfonate (triflate) groups generated on 11-hydroxyundecanethiol groups attached to gold coated surface for initiation of the living cationic ROP of 2-ethyl-2-oxazoline to produce linear poly(*N*-propionylethyleneimine) (PPEI) surface brushes [43].

In another study, Zhao and Brittain introduced a method providing self-assembled monolayer of polystyrene on glass surfaces via cumyl methyl ether moieties deposited on silicon wafer. Activation with $TiCl_4$ in the presence of di-*tert*-butylpyridine as proton scavenger was demonstrated to yield polystyrene brushes up to 30 nm of thickness (Figure 2.2) [44].

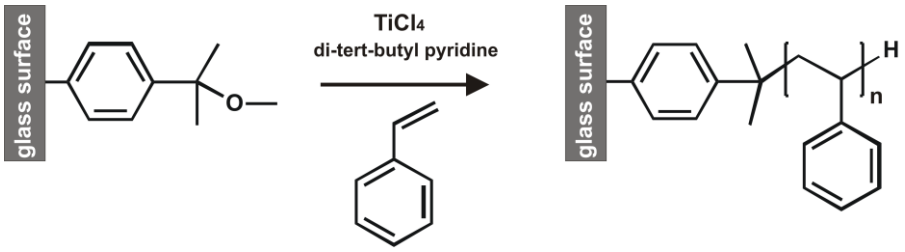

Figure 2.2: Poly(styrene) brushes grown by living cationic polymerization.

Since anionic polymerization is a living process its use for the surface grafting is attractive. However, the process needs extremly dry conditions and low temperatures. These drawbacks deter its extensive use in the grafting processes.

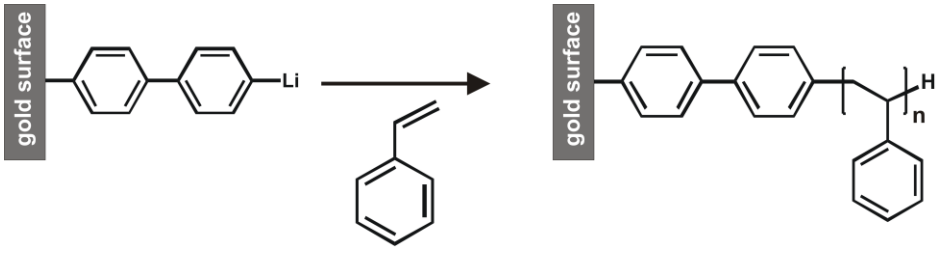

Figure 2.3: Poly(styrene) brushes grown by living anionic polymerization.

There appear few important controbutions on its use for the grafting from the solid surfaces. One successful example is the anionic polymerization of styrene on gold

substrates initiated by biphenyllithium groups to give very uniform films with a thickness of 18 nm (Figure 2.3) [45].

2.2.2 Surface grafting by ring opening polymerization

Surface-initiated ring opening polymerization (ROP) is an attractive route to attain surfaces coated with thin polymer films. Husseman *et al.* have reported for generation of poly(ε-caprolactone) (PCL) brushes on gold surfaces using *insitu* generated aluminium alkoxide catalyst (Figure 2.4) [46].

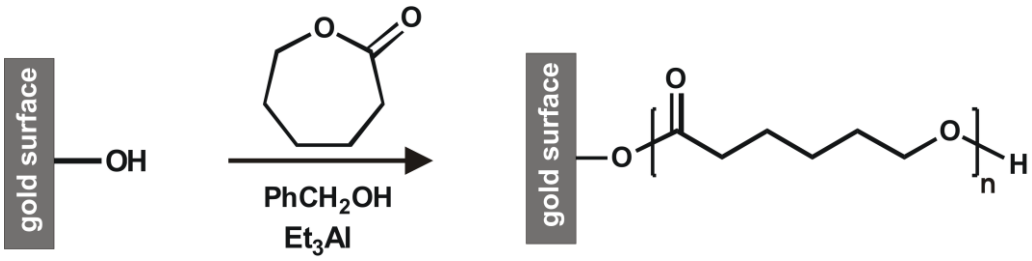

Figure 2.4: Surface-initiated ring opening polymerization of ε-caprolactone on gold surfaces.

In a similar study reported by Choi and Langer, tin(II) octoate catalyst have been employed for producing chiral poly(lactic acid) brushes on gold and silicon substrates by ROP of L-lactide. The resulting biodegradable polymer with controlled releasing ability has also been interest for chiral separation and molecular recognition applications (Figure 2.5) [47].

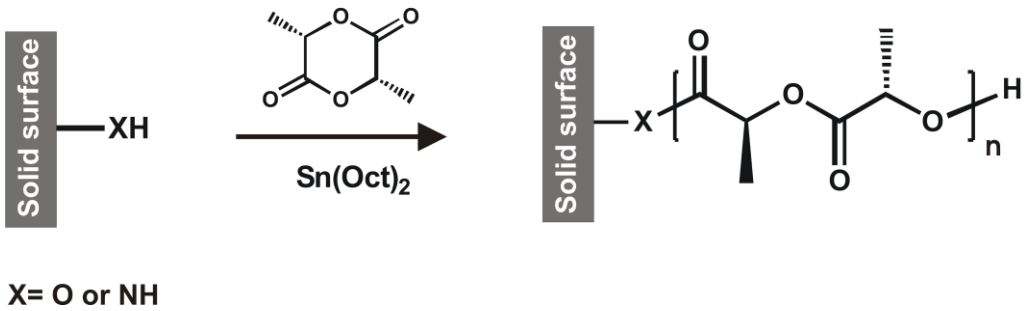

Figure 2.5: Surface-initiated ring opening polymerization of L-lactide on solid support.

There are many reports dealing with generation of polypeptide brushes on amine-functionalised silicon wafers and glass slides. Schouten and co-workers reported poly(L-glutamate) brushes by ROP of *N*-carboxy anhydrides (NCA) of L-glutamates (Figure 2.6) [48].

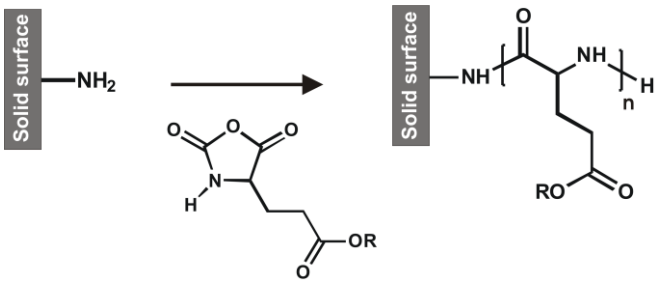

Figure 2.6: Surface-initiated ring opening polymerization of *N*-carboxy anhydrides of L-glutamates on solid substrate.

The detailed study revealed that the polypeptide brushes adopt an a-helix conformation on the Surface. Moreover, the "living" nature of the polymerization was demonstrated by the re-initiation yielding diblock copolymer brushes.

2.2.3 Surface grafting by ring opening metathesis polymerization

Little work has been published on the use of ROMP for surface grafting Mingotaud et al. described a ruthenium catalyst immobilized on 200 nm of silica nanoparticles for ROMP of Norbornene (Figure 2.7).

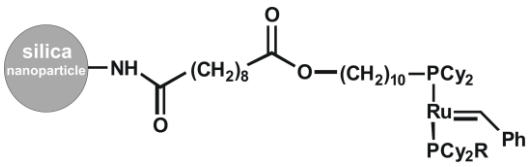

Figure 2.7: Transition metal tethered on the surface of silica nanoparticle.

The ruthenium catalyst was generated by reaction of acyl chloride functionalized silica surface with ruthenium catalyst bearing hydroxyl groups. This catalyst was demonstrated to give satisfactory graft densities as high as 7 μmol m^{-2} [49].

In a similiar study [50] a metathesis catalyst has been anchored on silica nanoparticles by reaction with 5-norbornene-2-yl(ethyl)ethoxydimethylsilane and 5-(bicycloheptenyl) triethoxysilane and following reaction with Grubbs first generation catalyst. The supported catalyst was then used for polymerization of norbornene to give a graft thickness of 15-30 nm (Figure 2.8).

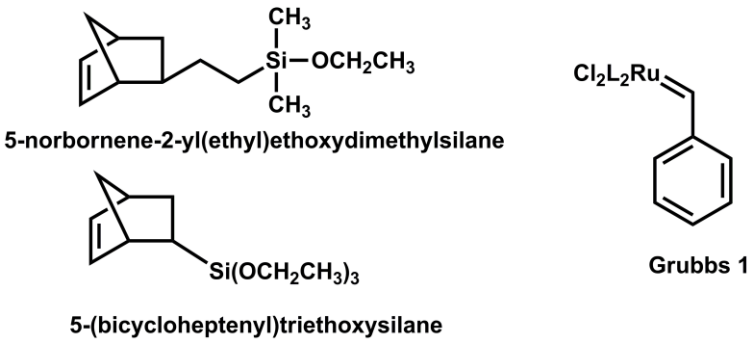

Figure 2.8: ROMP initiator used for immobilization on silica nanoparticles and the first generation of Grubbs catalyst.

Recently, Moon and Swager described polymerization of norbornene-capped poly(*p*-phenylene ethynylene) macromonomer by ROMP to give brushes with poly(*p*-phenylene ethynylene) "molecular wire" side chains [51]. The metathesis technique is expected to find wider application for grafting from solid surfaces in the near future.

2.2.4 Surface grafting by controlled radical polymerization techniques

Among various polymerization techniques radical-based controlled/"living" strategies are most frequently used in comparison to the other controlled/"living" polymerization methods. Since radical polymerization reactions have a high tolerance toward a wide range of functional groups and water, it is superior to the ionic polymerization methods.

2.2.4.1 Surface-initiated atom transfer radical polymerization

SI-ATRP was first reported by Huang and Wirth in 1997. They successfully grafted poly(acrylamide) (PAM) brushes from benzylchloride-derivatized silica particles [52]. Comparing with the other controlled living polymerization techniques ATRP is unique, because it avoids homopolymer formation and provides better control of the chain growth in graft copolymerization [53]. This method can be used for grafting from solid planar and spherical surfaces [54].

Surface grafting by ATRP simply involves immobilization of ATRP initiator to solid surface and following polymerization from the surface. Therefore, incorparation of the initiator to the surface is of prime importance in practice. Modification of the silica surface has been widely studied for incorporation of ATRP initiation sites.

Common approach is the use of a silane-coupling agent and subsequent reaction with appropriate molecule possessing ATRP initiators [55].

Yu et al. described controlled grafting of poly(glycidyl methacrylate) by initiation with 2-bromoester functions on the surfaces on hydrogen terminated silica substrates [21]. Haddleton's group [3] reported the use of Wang resin with benzyl alcohol functionality as solid substrate. The reaction with 2-bromoisobutyryl bromide and followed by grafting from bromoisobutyrate functions was demonstrated to give graft copolymers derived from methacrylate monomers (Figure 2.9).

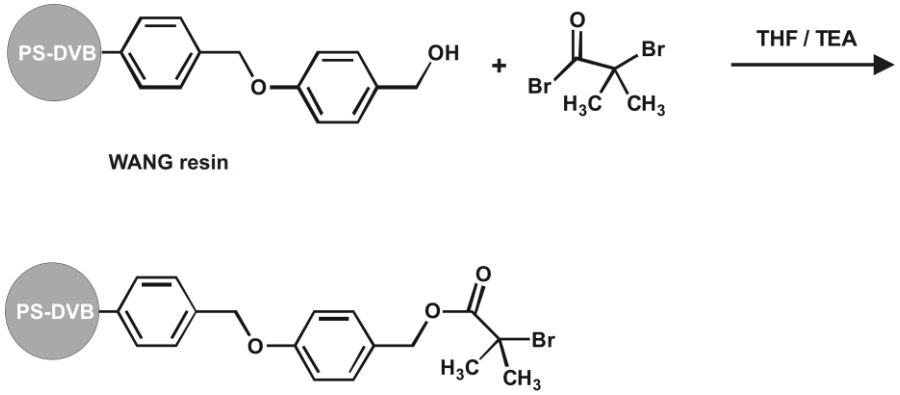

Figure 2.9: Immobilization of ATRP initiator sites on WANG resin.

Stöver's group described two routes to incorporate ATRP initiator groups starting from densely crosslinked polystyrenes possessing vinyl residues. In the first route, the vinyl residues were transformed into chloroethyl functionalities by hydrochlorination [22]. In the second route the vinyl residues were converted to hydroxyethyl groups. These were employed for generation of isobutyryl bromide groups on the spherical surface [23]. Both methods were demonstrated to give densely graft surface constituting with methacrylate polymers including PGMA. This group also demonstrated that modification of lightly crosslinked poly(DVB-*co*-HEMA) with 2-bromoisobutyryl bromide allows generation of diblock grafts including poly(MMA-*co*-GMA) poly(MMA-*co*-dimethylaminoethyl methacrylate) on the crosslinked solid support [56].

It is important to note that ATRP initiation is not only confined to haloalkyl functionality. Also solid supported *N*-halosulfonamides were demonstrated to initiate ATRP efficiently (Figure 2.10) [57].

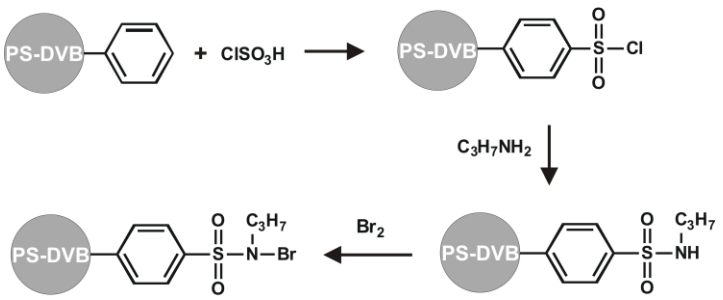

Figure 2.10: Introducing ATRP initiator groups on P(S-DVB) resin beads.

N-halosulfonamides tethered to crosslinked P(S-DVB) resin have been used for generating dangling poly(glycidyl methacrylate) chains which are useful for easy functionalization to impart different functionalities (Figure 2.11) [8].

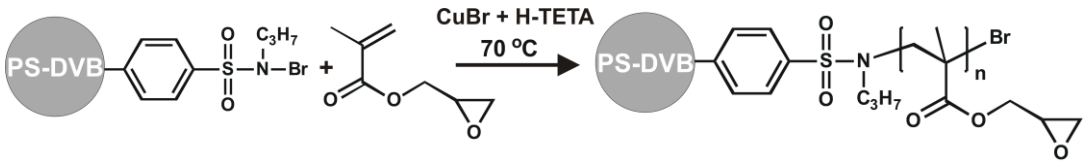

Figure 2.11: Poly(glycidyl methacrylate) brushes on P(S-DVB) microspheres.

Advantage of *N*-halosulfonamide initiation site is its hydrolytic stability which allows further use and recycling of dangling chains as catalyst or reagent carrier.

Since ATRP is a heterogenous process in nature, the chain-growth control can not be achieved as efficiently as in the case for the solution polymerization. Matyjaszewski et al. described addition of Cu(II) as deactivator to attain better control of the chain growth of polystyrene (PS) brushes on bromoisobutyrate-functionalized silicon wafers [58].

Reverse ATRP process in which Cu(I) species are *insitu* generated by reaction of Cu(II) with a conventional radical source has also been employed for the SI-ATRP of various acrylic and styrenic monomers. Sedjo et al. reported preparation of PS and PS-*b*-PMMA brushes from a conventional radical azo-functionalized silica substrate using $Cu^{II}Br_2$/bpy complex [59]. Those studies revealed that, SI-ATRP is an excellent technique to prepare polymer brushes on solid surfaces.

2.2.4.2 Surface-initiated reversible-addition fragmentation chain transfer polymerization

Another controlled living polymerization technique, reversible termination, reversible-addition fragmentation chain transfer (RAFT) polymerization is based on is based on reversible chain transfer. This process needs the use of additional radical source, which is different from typical ATRP process. Compounds possessing dithioester, dithiocarbamate, or trithiocarbonate groups have been used as chain transfer agents. Extention of this technique to the grafting from solid surfaces can be achieved either by using supported RAFT agent or by surface-immobilized conventional free radical initiators.

Baum and Brittain described immobilized an AIBN like azo-initiator onto silica surfaces for polymerization of methyl methacrylate, *N*,*N*-dimethylacrylamide, styrene monomers (PS) in the presence of 2-phenylprop-2-yl dithiobenzoate as chain transfer agent [60]. The process was demonstrated to be poor and slow for the chain growth and addition of untethered radical initiator (AIBN) was essential to attain reasonable grafting degrees (Figure 2.12).

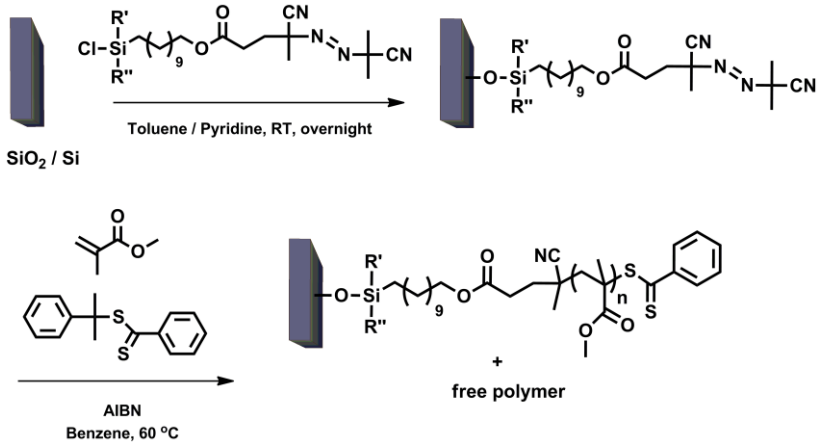

Figure 2.12: Immobilization of AIBN like azo-initiator onto silica surfaces and SI-RAFT polymerization of methyl methacrylate from the initiation sites.

In addition to the use of free radical initiator-modified substrates, SI-RAFT can also be carried out using surface-immobilized RAFT agents. The RAFT agent can be immobilized in two different ways, which are referred to as the R-group and Z-group approaches (Figure 2.13) [61, 62].

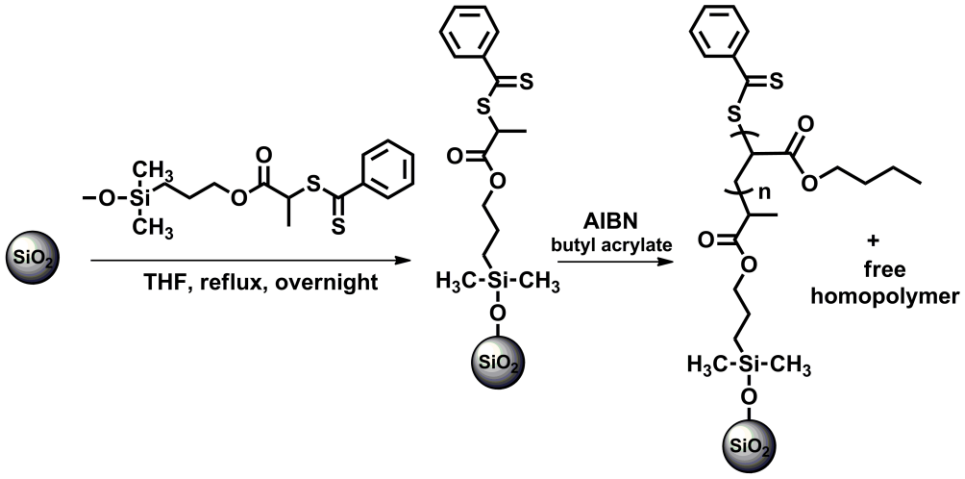

Figure 2.13: Surface initiated-RAFT polymerization of butyl acrylate from dithiobenzoate modified silica nanoparticles.

A number of ways has been described for anchoring the RAFT agents to the solid supports such as silica and crosslinked polymeric substrates. For instance, dithiobenzoate- or trithiocarbonate-derivatized silicon wafers [61], silica(nano) particles have been used to prepare a variety of methacrylic, acrylic, styrenic, and acrylamide-based brushes (Figure 2.14).

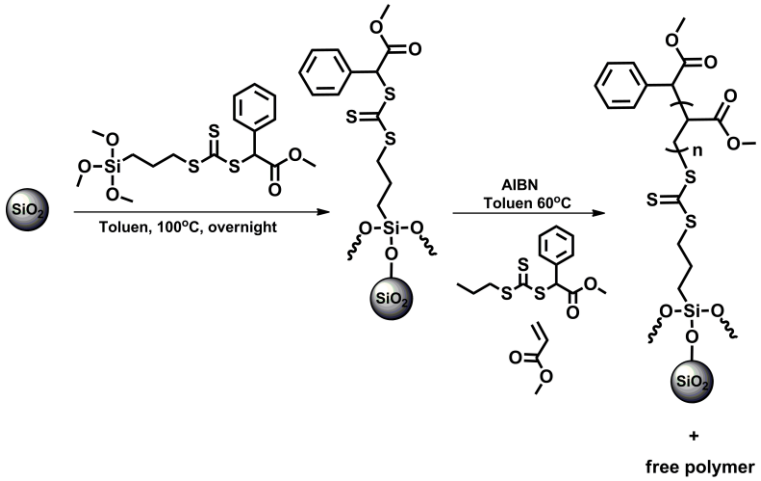

Figure 2.14: Surface initiated-RAFT polymerization of methyl acrylate from trithiocarbonate modified silica particles.

Advantages of RAFT polymerization is that it tolerates to wide range of (sensitive) monomers bearing different functional groups. Common drawbacks of RAFT are unavaliability of the RAFT agents and low brush densities due to detachment of grafted chains during the process. Moreover, formation of unbound homopolymer in solution is another important limitation of the process while grafting from solid surfaces. In fact the use of RAFT for grafting of solid surfaces can not be considered

as a true *grafting from* process, since the chains grown in the solution are linked to the solid surface.

2.2.4.3 Surface-initated nitroxide-mediated polymerization

Nitroxide-mediated polymerization on the other hand resembles mechanistically to RAFT process and is simply based upon reversible activation/deactivation of growing polymer chains by a nitroxide radical. The first report on surface-initiated nitroxide-mediated polymerization (SI-NMP) was published by Husseman et al.(Figure 2.15) [33]. This group demonstrated functionalization of silicon wafer with nitroxide group and polymerization of styrene monomer yielding a graft thickness up to 120 nm.

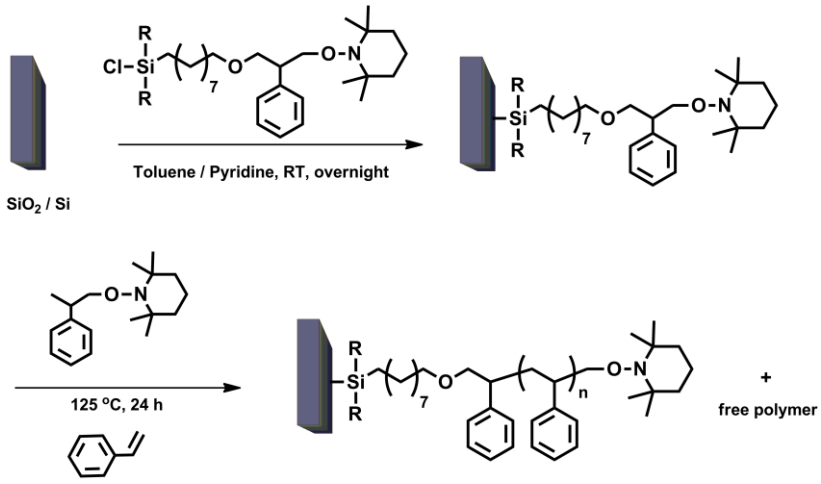

Figure 2.15: Immobilization of TEMPO derivative NMP agent on silica surface and surface initiated-NMP of styrene.

Nitroxide-mediated polymerization (NMP) was also employed by several other groups for the generation of PS brushes on TEMPO-functionalized Merrifield resins [63], magnetite [64] or titanium nanoparticles [65]. In addition, several other polymer brushes, such as poly(4-vinylpyridine) (P4VP) [66], Poly(styrene sulfonate sodium salt) [67] and poly(4-(poly(ethyleneglycol) methyl ether) styrene) (PSPEG) brushes [68] have been prepared via surface initiated-NMP from TEMPO-modified substrates. One important drawback of TEMPO-mediated polymerization is that its utility is almost confined to styrenic monomers. With acrylic monomers NMP gives relatively high polydispersities and low *M*n values due to reversible deactivation with β-H elimination of the growing polymer chains. Also a waste amount of homopolymer formation is another drawback of the process similar to those of the

RAFT process. Another drawback of NMP is that the process needs relatively high temperatures which limits its use for polymerization of temperature sensitive monomers.

2.2.4.4 Surface-initiated photoiniferter-mediated polymerization

Iniferters are substances simultaneously acting as *ini*tiators, trans*fer* agents, and *ter*minators. Irradiation of these substances result in dissosiation yielding a reactive carbon-centered radical and a relatively stable dithiocarbamyl radical which was first described by Otsu et al. in 1982 [69]. The polymerization starts from carbon-centered radical and it is reversibly deactivated by termination with dithiocarbamyl radical and this provides control of the polymerization.

The rate of polymerization, is directly related to the intensity and duration of irradiation. Matsuda and co-workers reported preparing benzyl-*N*,*N*-diethyldithiocarbamate- functionalized substrates for polymerization of a wide variety of monomers to generate brushes therefrom [70]. This strategy has been employed for producing thick brushes of poly(acrylic acid), poly(*N*-isopropyl acrylamide), poly(poly(ethylene glycol) methacrylate), poly(sodium methacrylate), and poly(methacrylic acid) [71-73]. De Boer et al. described an efficient procedure involved coupling of silicon substrates with trimethoxysilane functional benzyl-*N*,*N*-diethyldithiocarbamate derivative and grafting with styrene and styrene-methyl methacrylate block copolymers (Figure 2.16) [74].

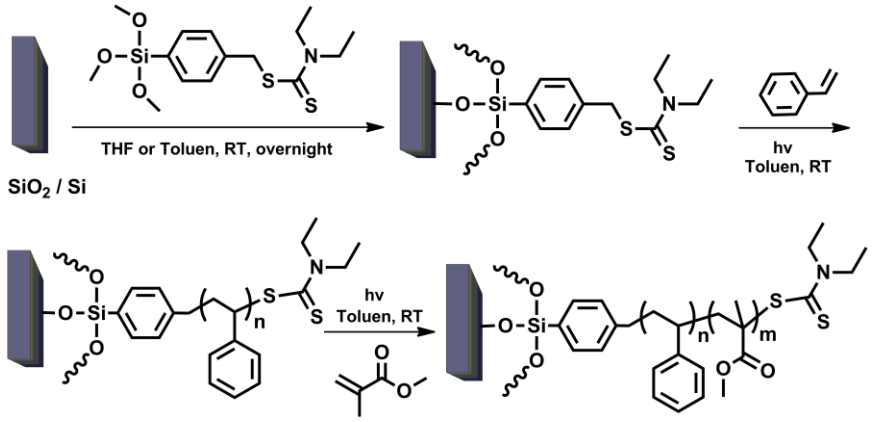

Figure 2.16: Block copolymerization of styrene-methyl methacrylate by irradiation on dithiocarbamate immobilized silica nanoparticle.

Since photoiniferter process do not need neither free radical source nor radical captures for the deactivation, it is attractive. Perhaps only limitation of this process

is that it is not applicable to light sensitive surfaces. Furthermore, surface initiated-PIMP does not need to remove the catalyst and is therefore especially suitable for the preparation of biomedical materials.

2.2.5 Polymer brushes by grafting from metal oxide surfaces

Grafting of metal and metal oxide surfaces with polymers is of special importance due to their extensive use in various fields. However, most of examples for CRP are related to silica [16], aluminum [75], titanium [76], or iron oxide [77] substrates. Generally premodification of these substrates to introduce initiation sites involves the use of silane coupling agents. The literature relevant to grafting from other metal oxide surfaces is scarce.

The most tedious task for grafting from metal oxide surfaces is incorparation of ATRP initiating groups. Various procedures have been reported for generation of ATRP initiators on inorganic particles. Hatton and co-workers [78] reported ATRP of acrylic monomers from oleic acid-coated magnetic nanoparticles in which the surfactant is partially replaced with ricinoleic acid for further functionalization with an ATRP initiator.

In a similar study nanoparticles of Fe_2O_3 or magnetite stabilized with oleic acid were ligand exchanged with 3-chloropropionic acid or 2-bromoisobutyric acid to allow surface initiated-ATRP [79]. Premodification other metal oxide surfaces for introducing ATRP initiator groups generally needs different chemical processes depending on the nature of the surfaces.

2.2.6 Polymer brushes grafted from inert polymer surfaces

Incorporation of initiator groups into non-functional polymer substrates needs different processes (Figure 2.17).

For instance, polypropylene and poly(tetrafluoroethylene) substrates requires ozonization or plasma pretreatment for generation of hydroxyl or carboxylic acid groups, which can be further modified with 2-bromoisobutyryl bromide to initiate ATRP [80, 81].

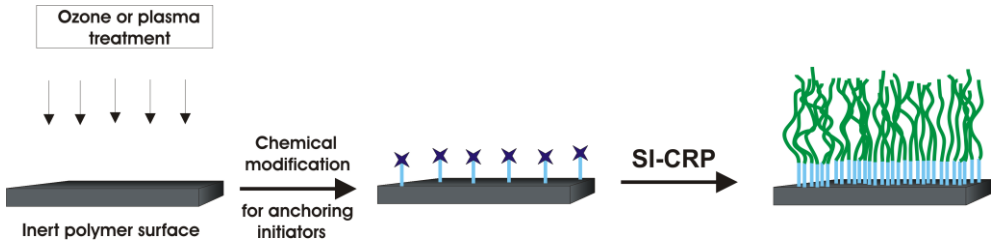

Figure 2.17: Schematic illustration of surface functionalization of inert polymer surfaces.

2.2.7 Direct radiation/plasma-mediated polymerization

It should be also mentioned that direct initiation from surfaces of inert polymers by γ-irradiation is a fruitful process allows generation of surface grafts without using special initiators. Recent studies involves the use of RAFT agent such as cumyl phenyldithioacetate to speed up of the polymerization and increase grafting efficiencies of styrene on polypropylene surfaces [82].

Similarly, the surface of polyethylene-*co*-polypropylene (PE*co*-PP) sheets have been grafted by means of γ-irradiation in the presence of RAFT agent, 1-phenylethyl phenyldithioacetate to generate radicals both on the polymer surface and in the monomer solution [83].

2.3 Grafting onto Methodology

In the "grafting onto" solid surfaces the polymers bearing a reactive end group prepared separately and linked chemically to the solid surfaces (Figure 2.18). Although the process proceed with low grafting yields especially in the case for high molecular weight prepolymers, it is being used for surface grafting with some functional monomers which cannot be polymerize by ATRP or relating methods. Of course, success of the grafting strickly depends on chemical reactivity of the polymer end groups with the linkers on the solid surfaces. In this respect, quickly reacting groups are essential to attain reasonable graft yields. The process termed as "*click chemistry*" provides nearly quantitative yields of the reaction between the groups on the mobile and stationary phases.

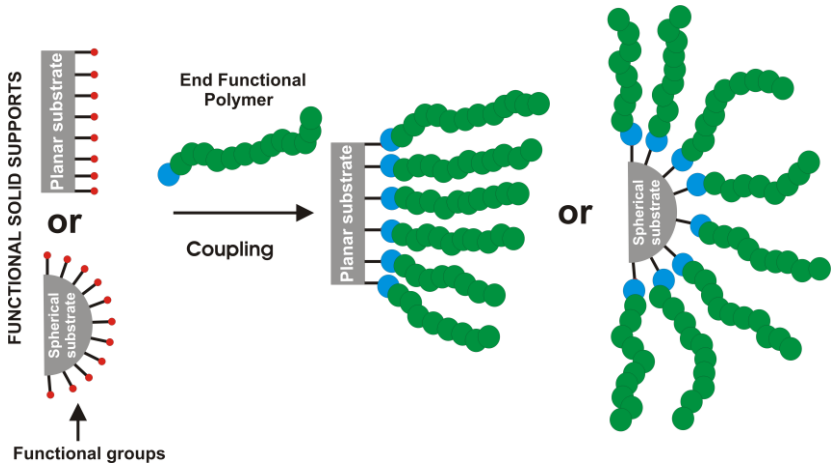

Figure 2.18: Schematic illustration of grafting onto approach.

2.3.1 Click chemistry

The term "Click chemistry" has been coined by Sharpless [84] in 2001 in order to describe quick connection of two different molecules. Generally, every fast and quantitative reaction can be considered in terms of the click chemistry. Beside this, the click chemistry reactions are expected to give no by-products. There are several reactions which have been considered fulfilling this criteria such as additions of mercaptanes to carbon-carbon double or triple bonds, the cycloaddition reactions involving Diels-Alder (DA) reactions and copper(I)-catalyzed azide-alkyne (CuAAC) couplings.

2.3.1.1 Azide-alkyne cycloaddition reaction

The reaction of azides with terminal alkynes yield 1,2,3 triazoles in the presence of copper catalyst. The reaction is almost quantitative in appropriate conditions. The reaction is believed to occur 1-3 dipolar addition mechanism (reaction (2.1)). The azide anion is analogue to propargyl anion. Thanks to Huisgen, our current knowledge on triazole chemistry is mainly based on his pioneering works on the subject [85]. He described synthesis of various five-membered heterocyclic rings such as triazole, triazoline, isoxazole, 4-isoxazoline etc. It was demonstrated that, good regioselectivity is attained by cycloaddition of highly electron-deficient terminal alkynes even without any catalyst. However, the other alkynes usually afford mixtures of the 1,4- and 1,5-regioisomers [86].

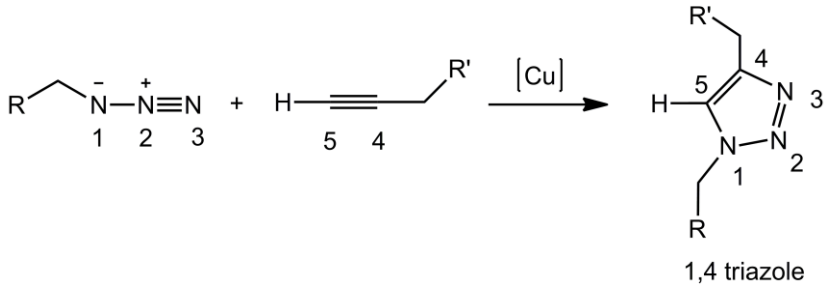

(2.1)

Further contributions by the Sharpless [87] and Meldal [88] groups revealed that, Cu(I) is exceptional catalyst which improves not only regioselectivity yielding exclusively 1,4-regioisomer, but also increase the reaction rates up to 10^7 times. Main advantage of the process is that, it eliminates the needs for heating at elevated temperatures [89]. Absence of the side reactions of the copper catalyst is its additional benefit.

2.3.1.2 Diels-Alder reaction

The Diels-Alder (DA) reaction is also known as [4π+2π] cycloaddition reaction, which takes place between diene and a dienophile (Reaction (2.2)). The reaction has been well studied in organic chemistry. Although many catalysts have been presented for DA reaction, it is common reaction of diens and proceeds even without catalyst. The reaction tolerates various functional groups such as electron donating groups (like -OR, $-NR_2$, etc) or electron-withdrawing groups (like $-NO_2$, -CN, -COR, etc). Mechanistic investigation revealed that DA cycloaddition reaction proceeds via cis-isomer of the diene component.

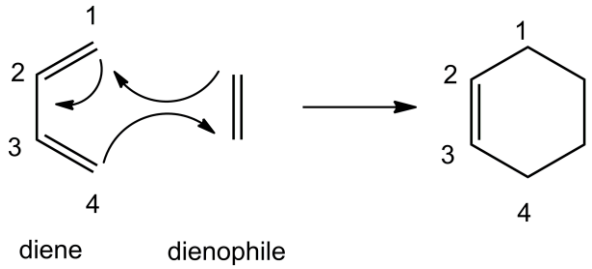

(2.2)

Obviously the diene structures enabling fast cis-trans isomerization yields faster DA adducts. Since cyclic dienes possess *trans*- conformer they are extremely fast in DA reactions. For instance, cyclopentadiene reacts with maleic anhydride to give the *endo* isomer rather than the *exo* isomer in high yields [90].

2.3.1.3 Catalysts for Diels-Alder reactions

Many Lewis acids including $SnCl_4$, $ZnCl_2$, $AlCl_3$, and derivatives of $AlCl_3$ such as $(CH_3)_2AlCl$ and $(C_2H_5)_2AlCl$ has been demonstrated to be good catalysts for DA reactions [91]. It has been demonstrated that dienophiles bearing electron-withdrawing groups such as carbonyls are much prone to DA reactions in the presence of Lewis acids as given in reaction (2.3). Lewis acids are considered to form complexes at the carbonyl oxygen and this facilitates the reaction [92] .

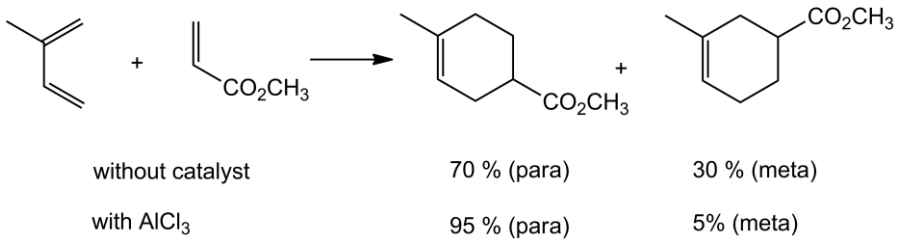

(2.3)

Common solvents for DA reactions are non-polar and aprotic solvents such as aliphatic and aromatic hydrocarbons. Nevertheless, many other solvents such as water, ethylene glycol and formamide have also been used successfully in a number of DA reactions [93, 94].

2.3.1.4 Mercaptane addition to carbon-carbon double and triple bonds

Addition of thiols to C=C bonds is principally Michael type addition which is favor when the double bond is activated by electron-withdrawing neighboring groups such as carbonyl or nitrile groups. The reaction has been well documented in organic chemistry for over 100 years [95].

Generally, the thiol-ene reaction can be performed in radical conditions and accelerated thermally or photochemical means [96, 97]. In the presence of radicals a thiyl radical, $RS^{\cdot}$, forms immediately and this adds to the double bonds. The intermediate carbon-centered radical undergoes chain transfer by transferring its radical to another thiol molecule and generates a second thiyl radical as shown reaction (2.4) [98].

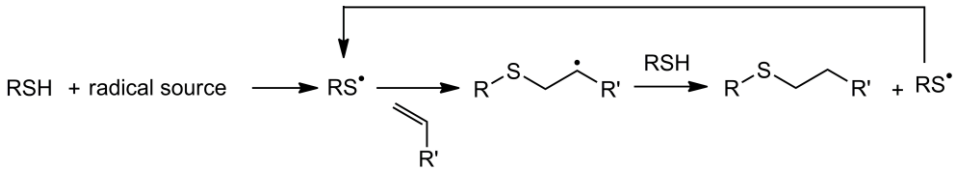

(2.4)

Thiol addition to a number of activated alkenes in the presence of nucleophilic catalysts (NEt_3, primary/secondary amines or certain phosphines) has been reported in the literature as given in reaction (2.5) [99].

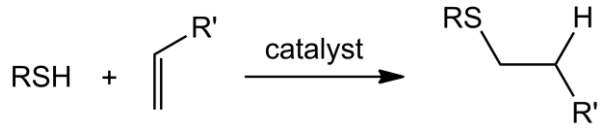

(2.5)

R'= ester, amide, cyano

2.4 Synthesis, Stabilization and Organic Modification of Nanoparticles

Design of new inorganic/organic nanostructured materials has been one of the fundamental researches in recent years. Increasing interest in these materials is due to their unusual electrical and optical behaviors different from those of their bulk counterparts. High surface to volume ratio and quantum confinement effects of the nanosize particles induce transparency and high chemical sensitivity towards trace reagents in gaseous or liquid states. Tremendous papers and review articles have been devoted to their synthesis in spherical, road-like and nanowire forms. Moreover, their compounding with polymers and organics has found considerable attention for fabrication of so called “nanohybrid materials” or nanocomposites.

2.4.1 Synthesis of nanoparticles

A number of physical and chemical methods have been reported for the synthesis of nanoparticles. Although it is difficult to make a discrete borderline between the synthetic procedures, we wish to follow commonly accepted classification for their synthesis.

2.4.1.1 Spray pyrolysis methods

The spray pyrolysis method simply involves spraying of an aqueous or organic solution of the nanoparticle precursor into a hot zone in which it decompose to give nanopowders. In this process, the undesired wastes are evaporated away. Although a wide particle size distribution is obtained, this method is already being used for large-scale production of metal or metal oxides [37]. Metal alkoxides and metal salts of glycolic and citric acids are common precursors used in the presence of stabilizers such as poly(vinyl alcohol). The spray pyrolysis method has been employed to

prepare different kinds of nanoparticles, including metals, metal oxides, such as Ag [100], Ni [101] and ZnS [102]. In another variant of this method, the nanoparticle procurser is decomposed in an inert solvent.

2.4.1.2 Sol-Gel process

Traditional sol-gel process is based on hydrolysis and condensation of an alkoxide-based precursor such as tetraethyl orthosilicate ($Si(OEt)_4$, TEOS) as shown in reaction (2.6). The first example of this process dates back to Ebelmen's work in 1846 [103]. The reaction takes place by exchanging alcohols with hydroxides and full exchange results in gelation.

$$Si(OR)_4 + nH_2O \rightarrow Si(OR)_4\text{-}n(OH)_n + n\text{ROH} \quad \textbf{(2.6)}$$

Drying of gel by slow evaporation gives a porous mass so called "*xerogel*". Drying by supercritical solvent extraction gives somewhat different mass naming "*aerogel*". The final step of this process is calcinations at 400-800 ^oC. Without the calcinations step, the process however, yields amorphous nanoparticle aggregates. The calcinations was demonstrated to be essential to obtain crystalline nanoparticles. This method has been widely utilized in preparing various nanoparticles of TiO_2 [104] and ZrO_2 [105].

In an interesting variation of the sol-gel process developed by Neiderberger et al, [106] a nonhydrolytic sol-gel reaction of a metal chloride with benzyl alcohol was demonstrated to give nanocrystalline products in 4-8 nm diameters without a calcination step.

2.4.1.3 The Pechini method

Another important variation of the sol-gel process is Pechini method developed 1967 [107]. This method relies on formation of complexes or complex salts between bi- and tridentate ligands such citric acid or EDTA with transition metal ions or alkaline earths and polymerization of the residual acids with a polyalcohol such as ethylene glycol to establish gelation of the mixture. After drying, the gel is pyrolysed to burn up of the organic portion and gives agglomerated submicron oxide particles.

Poly(vinyl alcohol) has been demonstrated to give rapid gelation in Pechini type syntheses [108]. This type of reactions is referred to as "*polymer combustion*

synthesis". Various metal oxide nanoparticles have been prepared by this technique [109] .

2.4.1.4 Chemical vapor deposition

In this technique, the vaporized precursors are introduced into a furnace. The substance adsorbed onto hot walls of the furnace, thermally decompose or react with another gas to give nanoparticles. This process has been used for preparing nanoparticles of Fe_2O_3 [110], TiO_2 [111] and SiC [112]. This method allows also preparing nanorods by gradual and seeded deposition of the nanocrystals. For instance introducing of acetylene-ammonia mixture (1/2-1/10 volume ratio) yields carbon nanotubes in desired lengths depending on the reaction time [113].

2.4.1.5 Physical vapor deposition

This method is based evaporation or sublimation of the material and it is transferred into a chamber in which nanoparticle or nanorod forms by nucleation growth on a substrate. Various examples of the process have been described for the synthesis of nanorods or nanowires of metal oxides, such as Ga_2O_3 nanowires [114] and ZnO nanorods [115].

2.4.1.6 Synthesis of nanoparticles in microemulsions

Microemulsions are thermodynamically stable and homogenous dispersions surfactant micelles [116]. Formation of the metal oxides or metals in these microemulsions yields nanoparticles. In such system, the micellar cores behave as nanoreactors to form nanoparticles in confined sizes.

Common surfactants studied are cetyl trimethylammonium bromide (CTAB), pentaethylene glycol dodecyl ether (Triton-X), sodium bis(2-ethylhexyl) sulfosuccinate (trade name, Aerosol OT or AOT). The later is also useful for reverse micelle systems. The method is especially useful for preparing metal nanoparticles such as Cu [117] and Pt nanoparticles [118] using hydrazine or hydrogen as reducing agents.

2.4.1.7 The Germ-Growth method

This method is a variation of the microemulsion process in which, first some seed crystals are generated in the micellar cores and then, they are subjected to grow by

following addition of the precursor and reactant [119]. One interesting example of this process is preparation of Co_2B nanoparticles by sequential addition of Co(II) and $NaBH_4$ to the micellar solutions containing Co seeds [120].

2.4.1.8 The precipitation methods

The precipitation method involves precipitation of metal or metal oxide nanoparticles in aqueous or organic solutions containing capping and/or stabilizing agents. This method is particularly useful for preparing metal nanoparticles or bimetallic alloys. In fact, thermal decomposition of a suitable metal precursor in the presence of a polymer is one of the oldest methods of preparing colloidal metals.

For instance, decomposition of $Co_2(CO)_8$ under inert atmosphere at 130-170 °C in ethylene glycol containng poly(4-vinylpyridine) as capping agent has been demonstrated to give 45 nm of Co particles [121]. Decomposition of cobalt carbonyl occurs according to the reaction (2.7) .

$$Co_2(CO)_8 \rightarrow 2Co(s) + 8CO \qquad \textbf{(2.7)}$$

Various metal carbonyls have been used as precursor for preparing metal nanoparticles. Since CO provides a reducing medium, metal carbonyls are preferred to obtain metal particles with high catalytic activities. Smith and Wychick reported that, the use of nitrogen-containing polymers such as copoly(styrene-4-vinylpyridine) and copoly(styrene-*N* vinylpyrolidone) lead to formation of metal-clusters [122].

High-boiling mixture of trioctylphosphine and trioctylphosphine oxide has been used as the reaction medium. This mixture was demonstrated to act also as passivating agent and stabilizer for metal nanoparticles. Moreover, efficacy of this method has been improved by using microwave assisted reaction system.

The precipitation process has also been utilized for preparing various metal oxides and pigments in nanometer particle sizes [123].

2.4.1.9 Hydrothermal methods

Supercritical fluids exhibit almost zero surface tensions and have high solvating abilities. For instance, the critical point of water is 374 °C (218 atm). Above this point water (supercritical) becomes a powerful solvent and able to dissolve many substances which are insoluble under ambient conditions. The reactions are

performed under high-pressure in bombs or autoclaves and referred to as "*solvothermal processing*".

Advantage of the process is that, the resulting products are completely crystalline and do not require post-annealing processes.

The process has been successfully employed for synthesis of nanocrystalline TiO_2, which is an efficient photocatalyst for the oxidative decomposition of toxic chemicals. Recently Cheng et al. developed a hydrothermal process for preparing pure rutile and anatase crystallites from aqueous $TiCl_4$ [124]. They reported that, rutile formation is favor in acidic conditions, while basic media favor anatase crystals and NaCl reduces the average particle sizes.

This method generally yields nanocrystalline structures with high catalytic activities. For instance, Gautam et al. described a solvothermal process using trioctyl phosphine oxide as a capping agent for peparing monodisperse CdSe particles in 1-3 nm size range [125].

2.4.2 Organic modification and stabilization of nanoparticle surfaces

Modification of nanoparticle surfaces with low molecular organic compounds or with polymers is main goal for manufacturing of nanostructured composite materials. Although classical surfactant stabilization methods of colloid chemistry is still being used to some extend, modern material science technology needs more stable and narrow size distribution of colloidal dispersions with permanent stabilities. This is generally achieved mostly by attachment of organic molecules or polymers via formation of covalent, ionic or coordinative bonds.

The term "core-shell" nanoparticle is generally used to describe bilayer nanoparticles bearing polymers or organics tethered to surface covalently. The shell layer provides compatibility of the nanoparticle substance with polymer matrixes, which is useful for designing of high performance coatings [126].

2.4.2.1 Stabilization of nanoparticles in synthesis conditions

Stabilization of nanoparticles during their synthesis by wet chemical processes is crucial not only for the stabilization but also for control of size distributions. This control is based on steric stabilization induced by surface linked surfactant molecules. The role and application of low molecular weight surfactants in the

synthesis of the nanoparticles have already been discussed in the section of nanoparticle syntheses.

2.4.2.2 Stabilization with polymer ligands

Coating of nanoparticle surfaces with polymers may induce compatibility and much different functionality. For instance, fluorinated polymer coatings give "*non-stick*" surfaces, due to low surface tension of this type of polymers [127]. Surface coatings with poly(ethylene oxide) impart water-solubility and biocompatibility which are of interest for delivery of therapeutic agents and lowering the cytotoxicity of the nanoparticles [128]. Polymers have been used as ligands for stabilization of inorganic nanoparticles for many years [129].

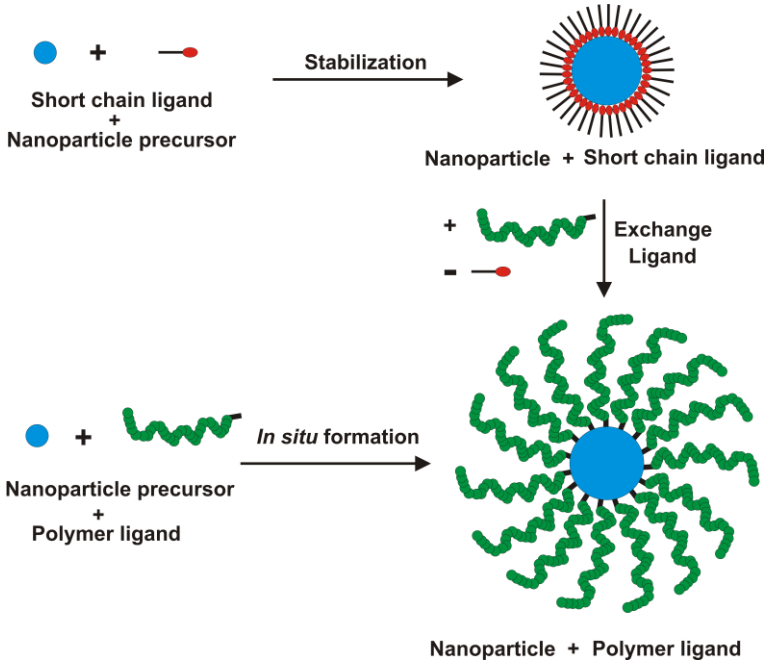

Figure 2.19: Schematic illustration of nanoparticle stabilization by polymer ligands.

There appear two common routes for stabilization of nanoparticles by backbone-functional and end-functional polymer ligands. In the first route, nanoparticles are *insitu* generated in the micellar solution of the polymer ligands (Figure 2.19). In the second route, surfactant stabilized nanoparticles mixed with the solution of polymer ligands. In this case, preoccupied surfactants or low molecular weight ligands are gradually replaced with the polymer ligands.

Finke and coworkers reported that, poly(4-vinyl pyridine) ligands with average molecular weights, M_n :3500-55000 have little effect on stabilization of iridium nanoclusters [130]. Polymer ligands with lower molecular weights, however provide faster nanoparticle formation and better stabilization. Kinetic control of the particle size and shape is best controlled by oligomers. Amphyphilic block copolymers are especially useful for preparing nanoparticles. One block having affinity to the nanoparticle surface localizes it and the other block affords solubility and steric stabilization.

Generally, polymer-coated metallic nanoparticles are consired to be less reactive as catalysis due to the polymer barrier. However, palladium nanoparticles prepared in poly(styrene)-*block*-poly (4-vinylpyridine) copolymer micelles have been demonstrated to show comparable activities with those of naked palladium in the Heck reaction [131]. This methodology has been largely used for preparing different metal or metal oxide nanoparticles. Platonova et al. prepared Co nanoparticles (1 nm) by decomposition of cobalt octacarbonyl in a polystyrene-poly(4-vinyl pyridine) copolymer solution [132]. Synthesis of $CoFe_2O_4$ [133] and Fe_3O_4 [134] nanoparticles have been achieved using similar block copolymers.

2.4.3 Tailoring of nanoparticle surfaces with polymer brushes

Generation of polymer brushes on inorganic nanoparticle surfaces has been a key issue in preparing nanocomposites and other nanostructured materials. This is essential for the compatabilization of inorganics with organic matrixes. In principle, common grafting protocols, *grafting- onto*, *grafting-from* and *grafting-through* can be employed to generate surface grafts on nanoparticles. All of those need to create linker or initiator groups covalently attached to the particle surfaces prior to connect with prepolymers or to initiate graft copolymerization from the surfaces. Creating a linker or initiator groups on preexisting nanoparticles is achieved by premodification of the surfaces with suitable coupling agents. This is usually carried out by pretreatment with silane coupling agents possessing trichlorosilane or trialkoxysilane connecting with alkyl or aryl group with a suitable functional group. Although silane coupling agents have been developed originally for surface modification of silica surfaces, these agents have been demonstrated to be useful for

also coupling of many other metal oxides such as TiO_2, Al_2O_3, Fe_2O_3,Fe_3O_4 etc [135].

Among those approaches, the *grafting-from* is mostly preferred method for generation of dense grafts and controlled chain growths on the surfaces. General experimental procedure of this approach involves immobilization of the initiator molecule on the silica particle followed by surface initiated ATRP [15]. Grafting of various styrene and acrylic monomers has been performed from the initiator-grafted silica particle by ATRP. Incorporation of the initiator groups is crucial issue for decoration of nanoparticle by SI-ATRP methodology. This is performed by reaction with specially designed silane coupling agents bearing halo-alkyl groups as initiator for ATRP.

(2-(4-Chloromethylphenyl) ethyl)dimethylethoxysilane (CPDS), (3-(2-bromo isobutryl)propyl) dimethylethoxysilane (BPDS), and (3-(2-bromopropionyl) propyl)dimethylethoxysilane (BIDS) are common monosiloxane type coupling agents possessing ATRP initiator groups as given in reaction (2.8).

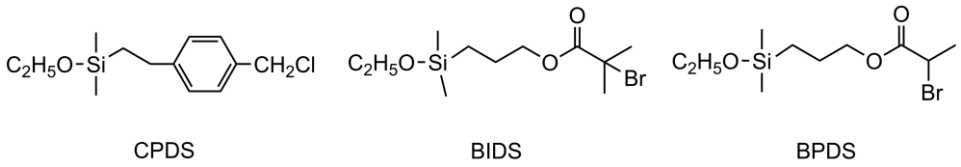

CPDS BIDS BPDS **(2.8)**

Although these are mostly used for premodification of silica surfaces, some other metal oxide surface might be also modified by siloxane type coupling agents.

Although less frequent, other controlled radical polymerization techniques, nitroxide nediated polymerization (NMP) and RAFT methods have been used for generating surface brushes on nanoparticle surfaces. It is important to note that, these two techniques are based on chain transfer mechanism. Due to this fact, simultaneous homopolymer formation is accompanied to the grafting and this sometimes reduces the grafting yields considerably.

An interesting procedure for RAFT mediated grafting of styrene from silica surface has been reported by Benicewicz et al [62]. They used a silane coupling agent bearing dithioester function. By using silica-bound RAFT agent they were able graft copolymerization of styrene and n-butyl acrylate at low monomer concentrations. The low concentrations were determined to be useful to avoid gelation and inter-

particle connections. There are only few papers describing successful grafting by RAFT method.

Similarly, nitroxide moieties attached to nanoparticle surfaces do not give satisfactory graft yields in ordinary polymerization conditions. Parvole *et al*.described an interesting nitroxide mediated grafting procedure based on bimolecular approach of Rühe, in which both nitroxy groups and azo initiators are sequentially introduced to silica surfaces [136]. Polymerization of n-butyl acrylate was demonstrated to give satisfactory graft yields in these conditions.

2.4.3.1 Grafting from nanoparticle surfaces by ring opening polymerization

Under appropriate conditions, ring opening polymerization (ROP) techniques can be utilized for surface grafting on nanoparticle surfaces. In an excellent work published by Carrot *et al*, grafting of ε-caprolactone has been achieved by ring opening polymerization from amine functional silica surface using an aluminum alkoxide catalyst [35]. ROP of epoxy groups have been achieved in the presence of aluminum isopropoxide. by initiation from suitable hydroxy functional surfaces to introduce poly(ethylene oxide) (PEO) onto silica nanoparticles.

3. EXPERIMENTAL WORK

3.1 Materials and Chemicals

3.1.1 Monomers

Methyl methacrylate (MMA, 99%, Aldrich):

It was distilled prior to use.

Ethylene glycol dimethacrylate (EGDM, 99%, Aldrich):

It was distilled under reduced pressure prior to use.

2-Methyl 2-oxazoline (MeOX, 99%, Aldrich):

It was purified by distillation over CaH_2.

Glycidyl methacrylate (GMA, 99 %, Aldrich)

It was used as purchased.

Methacrylic acid (MAA, 99 %, Aldrich):

It was used as received.

Divinyl benzene (DVB55, 55% mixture of isomers, technical grade, Aldrich):

It was used as received.

Tertiary-butylacrylate (tBA, 99%, Aldrich):

It was passed through a column containing basic alumina.

ε-Caprolactone (ε-CP, 99 %, Aldrich):

It was distilled over CaH_2 under vacuum.

Glycidol (96 %, Acros):

It was distilled under reduced pressure, before use.

Maleic anhydride (>99%, E. Merck):

It was used as received.

Styrene (St, 99%, Aldrich):

It was passed through a basic alumina column to remove the inhibitor before use.

3.1.2 Solvents

Dimethoxyethane (Acros):

It was distilled over metallic sodium before use.

Diethyl ether (98%, Carlo-Erba):

It was dried with calcium chloride and distilled over sodium wire.

Acetonitrile (98%, Aldrich):

It was distilled over CaH_2 before use.

Dichloromethane (J.T. Baker):

It was dried with calcium chloride and distilled over P_2O_5.

Tetrahydrofuran (THF, 99.8%, J.T.Baker):

It was used as received.

n-Hexane (95%, Aldrich):

It was used without further purification.

N,N-Dimethyl formamide (DMF, ≥ 99%, Aldrich):

It was used as received.

Methanol (Technical):

It was used for the precipitation of polymers without further purification.

Toluene (99%, Aldrich):

It was dried with calcium chloride and distilled over P_2O_5.

Acetone (Technical):

It was used for the precipitation of polymers without further purification.

3.1.3 Other chemicals

Dibenzoyl peroxide (DBPO, 98%, Aldrich):

It was recrystallized from ethanol.

CuBr:

It was freshly prepared by the procedure as described in the literature [137].

H-TETA (1, 1, 4, 7, 10, 10-hexakis [hexyl 1, 4, 7, 10-tetraazadecane]):

It was prepared by alkylation of triethylenetetramine with 1-bromohexane as described in the literature [138].

N,N,N′,N′-Tetraethyldiethylenetriamine (TEDETA, 97%, Aldrich):

It was distilled before use.

N, N, N',N'', N''-Pentamethyldiethylenetriamine (PMDETA, 99%, Aldrich):

It was distilled before use.

2,2'-Azobis-(isobutyronitrile) (AIBN, 98%, Aldrich):

It was recrystallized from ethanol.

Triethylamine (TEA, 99.5 %, Fluka):

It was used as received.

Ethylene glycol (95 %, Aldrich):

It was used as received.

2-Bromoethanol (99%, E. Merck):

It was used as received.

Poly (N-vinyl pyrrolidinone) (MW: 15.000, Aldrich):

It was used as received.

N,N'-Dicyclohexylcarbodiimide (DCC, 99%, Aldrich):

It was used as received.

Poly(ethylene glycol) monomethylether (Me-PEG, M_n : 2000 and M_n:5000, Fluka):

It was used as received.

Propargyl alcohol (99%, Aldrich):

It was used as received.

4-Pentynoic acid (99%, Aldrich):

It was used as received.

2-Bromoisobutyryl bromide (97%, Aldrich):

It was used as received.

TiO_2 nanopowders with 25–70 nm (Aldrich):

It was used as received.

Fumed silica with 200 ± 25 m^2g^{-1} of BET surface area (Aldrich):

It was used as purchased.

Poly (methyl methacrylate-stat-butyl acrylate) (BASF):

The copolymer (in aqueous emulsion 60 % solid content) was isolated by precipitation in acidified aqueous solution.

Tin (II) 2-ethylhexanoate (Sigma, 95 %):

It was used as received.

Poly(ethylene glycol) monomethylether (Me-PEG, M_n : 2000 and M_n:5000, Fluka):

It was used as received.

Sodium azide ($NaN_3 \geq$ 99%, Merck):

It was used as received.

Dodecyl amin (99%, Merck):

It was used as received.

Crystallized and lyophilized laccase (Fluka):

It was obtained from Fluka (Steinheim, Germany). (Lac; Benzenediol:oxygen oxidoreductase; from *Agaricus bisporus*, E.C 1.10.3.2, powder, deep brown, 8.85 U/mg)

3.2 Instrumentation

3.2.1 Nuclear magnetic resonance spectroscopy (NMR)

^{1}H NMR measurements were recorded in $CDCl_3$ with $Si(CH_3)_4$ as internal standard, using a Bruker AC250 (250.133 MHz) instrument.

3.2.2 Infrared spectrophotometer (FT-IR)

FT-IR spectra were recorded on a Perkin Elmer FTIR Spectrum One B spectrometer.

3.2.3 UV-Visible spectrophotometer

UV-Visible spectra were recorded on a Shimadzu UV-1601 UV-visible spectrophotometer.

3.2.4 Thermogravimetric analyses (TGA)

Thermogravimetric analyses (TGA) were performed by Perkin Elmer instruments Diamond TG/DTA Analyzer, with a heating rate of 10 $^{\circ}$C /min under air atmosphere.

3.2.5 Scanning electron microscopy (SEM)

Scanning Electron Microscopy (SEM) pictures of the composite films were taken by JEOL JSM 6335 F using Field Emission.

3.2.6 X ray diffraction (XRD)

Nanoparticles were examined by X ray diffraction (XRD) using a D/max-γA diffractometer (Cu K_α radiation) at a scanning rate of 10^{o} min^{-1} in the diffraction angle range 2θ = 10–90 ^{o}.

3.2.7 Transmission electron microscopy (TEM)

Transmission Electron Microscopy (TEM) images were obtained by HR TEM, JEOL JEM 2100. Scanning Electron Microscopy (SEM) pictures of the composite films were taken by JEOL JSM 6335 Fusing Field Emission.

3.2.8 Dynamic light scattering (DLS)

The hydrodynamic diameters of nanoparticles in each step were measured by Dynamic Light Scattering (DLS) (NanoS, Malvern Instruments, London, UK) in acetone medium (1% (w/w). DLS was applied with an angle of 170° by using He–Ne laser (4 mW) operated at 633 nm.

3.2.9 Optical photography

Particle shapes and sizes of the product were determined by optical photography using an image analyzing system consisting of a microscope (XSZ single zoom microscope), a CDD digital camera (TK 1381 EG), and a PC with the data analyzing system Image-Pro Plus.

3.2.10 Gel permeation chromatography (GPC)

Gel permeation chromatography (GPC) analyses were performed with a set up consisting of a Waters 410 Differential Refractometer, a Waters 515 HPLC Pump and an apparatus equipped with three Waters ultrastyragel columns (HR series 4, 3, 2 narrow bore), with THF as the eluent at a flow rate of 0.3 mL/min. Molecular weights were calculated on the basis of a calibration curve recorded with mono disperse polystyrene standards.

3.2.11 Fluorescence spectrophotometer

Fluorescence measurements were carried out using a Hitachi F-4500 fluorescence spectrophotometer at room temperature.

3.2.12 Transmitted-reflected light microscope

Fluorescence image of the microscope were obtained using a Olympus Bx60 Transmitted-Reflected Light Microscope equipped with Nikon digital camera. It has UplanFL 10X/0.30, UplanFL 20X/0.50, UplanFL 40X/0.75, UplanFL 100X/1.3 oil objectives and all objectives have DIC optics.

3.2.13 X-ray photoelectron spectra (XPS)

X-ray Photoelectron Spectra (XPS) of the samples were taken by SPECS PHOIBOS-150 Electron Analyser equipped with a SPECS XR-50 X-ray source using monochromatized Al Kα radiation (1486.6eV) for the excitation. Survey spectra were recorded in 0 to 1200 eV range with pass energy of 80 eV. All the peaks were referenced to a C1s signal at 285 eV. The pressure of the analyser chamber was 10^{-8} to10^{-9} Torr.

3.2.14 Environmental scanning electron microscopy (ESEM)

Shapes and sizes of the micelles were assigned by Environmental scanning electron microscopy (ESEM) technique, using Philips – FEI XL30, ESEM-FEG instrument operating at 5.00 kV in STEM mode.

3.3 Preperation Methods

3.3.1 Synthesis of 2-bromoethyl methacrylate (BEMA) monomer

Synthesis of BEMA was carried out by a new procedure as described in our previous report [139]. In this procedure boron ester of 2-bromoethanol was reacted with methacrylic acid in the presence of pyridine. The procedure is as follows: To a 250 mL volume of flask, there was added 75 g (0.6 mol) 2-bromoethanol, 12.37 g (0.2 mol) H_3BO_3 and 80 mL toluene. The flask was equipped with a Dean-Stark trap and a reflux condenser. The mixture was heated at 150 ^oC and water removal was completed within 3-4 h under continuous stirring. Then excess of toluene was distilled off and recovered via reservoir of the trap. To the cooled mixture 50.9 mL (0.6 mol) methacrylic acid, 0.1 g hydroquinone and 3 mL pyridine were introduced and the reaction content was heated to 160 ^oC for 24 h. After cooling, the reaction content was poured into 300 mL water. Organic phase was separated by a separatory funnel and dried with Na_2SO_4. The monomer was isolated by distillation under vacuum (112-114 ^oC /11 mm). The yield was 71.2 %.

^1H NMR, ($CDCl_3$), δ: 6.0 ppm (s, 1H, = CH_2 cis.), 5.45 ppm (s, 1H, = CH_2 Trans), 4.3 ppm (broad s, 2H, -COO-CH_2-), 3.4 ppm (broad s, 2H, -CH_2-Br), 1.8 ppm (s, 3H, CH_3-C=C).

In the FT-IR spectrum of the product typical C=O stretching vibration of the ester group appears at 1725 cm^{-1}. The other characteristic peaks associated with C=C, C-O and C-Br stretching vibrations appear at 1638, 1160 and 814 cm^{-1} respectively.

3.3.1.1 Synthesis of bromoethyl methacrylate based microspheres by suspension polymerization

PBEMA microspheres were obtained by the following procedure: 1 g of commercial poly(*N*-vinyl pyrrolidone) and 3 g Na_2SO_4 were dissolved with 300 mL of distilled water in a 1000 mL volume of three-necked flask equipped with a nitrogen inlet, dropping funnel and a reflux condenser. Then 12.1 g (62.5 mmol) BEMA, 4.95 g (25 mmol) EGDMA, 16.25 g MMA (162.5 mmol), 45 mL toluene (porogen) and 0.160 g (0.098 mmol) AIBN were added successively to the flask under nitrogen flow. The flask was mounted in a thermostated-oil bath and temperature was adjusted to 60 ^oC. The nitrogen stream was stopped and the system was closed. The reaction was conducted under constant stirring rate (1000 rpm) for 12 h. The reaction content was then, cooled and poured into 1 L of water and beaded product was collected by filtration. It was washed with excess of water (5×100 mL) and dried at 40 ^oC for 24h. The pearl-like bead product weighed 28 g. The product was fractionated by sieving and determined to be mostly (85 %) in 125-420 mμ size range.

3.3.1.2 Determination of bromide content of the microspheres

A half gram of bead sample was introduced to 15 mL of methanolic NaOH solution (20 %) and the mixture was boiled for 24 h under reflux condenser. The cooled mixture was filtered and washed with water (3×10 mL). The filtrate and washings were combined and made up 50 mL in a volumetric flask. Twenty five mL of this solution was neutralized with nitric acid solution (65 %) (approx. 4 mL) and mixed with 4 mL of $AgNO_3$ solution (1 M). The white precipitate was filtered, washed with water (5 mL) and dried at 40 ^oC for 16 h under atmospheric pressure. Dry weight of AgBr (0.073 ± 0.002 g) indicated a 1.55 mmol bromide per gram of the cross-linked polymer.

3.3.1.3 Surface initiated atom transfer radical polymerization of GMA from the bromoethyl groups

To remove soluble impurities in the cross-linked microspheres, 12 g of the sample was placed in a Soxhlet extractor. The extraction was performed using toluene (150 mL), in about 3 h. and dried. Meanwhile to a 100 mL volume of three necked flask equipped with a nitrogen inlet and a reflux condenser, 0.44 g CuBr (3.1 mmol), 2.01 g ligand, H-TETA (3.1 mmol), 14 mL GMA and 14 mL toluene were charged and stirred for 30-40 min to dissolve the copper salt under nitrogen flow. Two gram of the bead sample was added to the flask, then the system was closed and reaction mixture was gently stirred (to avoid mechanical disintegration) with magnetic bar (400 rpm) at 60 ^{o}C for 24 h. The mixture was cooled, filtered, washed with toluene (2 ×25 mL), acetone (2 ×25 mL), and ethanol (50 mL) and dried under vacuum at room temperature for 24 h. Dry product weighed 10.4 g. The bead particles were still in spherical form. To inspect free homopolymer formation, the filtrate (before washing) was added into 40 mL methanol. The precipitate was filtered and washed with water (30 mL). Dried product weighed 0.28 g indicating approximately 1.87 % of free homopolymer formation in the grafting process.

Kinetics of the surface grafting was performed at the same polymerization conditions. For this purpose in each set of the experiments, 0.2 g of PBEMA sample was employed as macroinitiator. The polymerizations were carried out in degassed tubes using 43 ±2 mg CuBr (0.31 mmol), 0.2 g (0.31 mmol) H-TETA and 2 g (13.7 mmol) GMA. At the end of predetermined times, the reactions were quenched and the products were isolated as described above. The grafting degree, G (g per gram), monomer conversion in grafting, p were defined (reaction (3.1)) as follows:

$$G = \frac{m_G - m_o}{m_o} \qquad p = \frac{m_G - m_o}{m_{GMA}} \qquad \textbf{(3.1)}$$

Where, mG is mass of the graft copolymer, m0 is mass of PBEMA sample and mGMA is mass of GMA used in the surface grafting process.

3.3.1.4 Synthesis of model initiator, bromoethyl acetate

To a 100 ml flask, there was added 3.6 mL (0.05 mol) bromoethanol and 4.3 mL (0,06 mol) acetyl chloride. The mixture was stirred for 3h at room temperature and

poured into 100 mL water. The organic layer was separated and washed with 100 mL K_2CO_3 solution (1%) and dried with anhydrous $MgSO_4$ (0.5 g). Distillation of the crude product (81 ^oC / 5 mm) gave 7.1 g (84.0 %) colorless liquid. ^1H NMR, ($CDCl_3$), δ: 4.30 ppm (t, 2H, CH_2-O), 3.50 ppm (t, 2H, CH_2-Br), 2.05 ppm (s, 3H, CO-CH_3,).

3.3.1.5 The use of bromoethyl acetate as initiator for atrp of mma

A typical ATRP mixture containing CuBr (0.067 g, 0.47 mmol), H-TETA (0.31 g, 0.47 mmol), MMA (5 mL, 46.8 mmol) and 5 mL toluene was prepared in a 100 mL round bottom flask under nitrogen atmosphere. The initiator, bromo ethyl acetate (0.079 g , 0.47 mmol) was added to the flask placed in an oil bath at 70 ^oC and the reaction was conducted for 5 h. After removal of the copper catalyst via silica column, the polymer was precipitated in n-hexane 30 mL, filtered and dried at 50 ^oC for 12h under vacuum. The yield was 0,7 g (14.8 %). GPC trace of the polymer revealed Mn: 18500 (Mw: 36000).

The same polymerization procedure was repeated using bromo methyl propionate and benzyl bromide as ATRP initiators instead of bromo ethyl acetate. The polymerization yields were determined to be 56.0 % and 96.0 % for the case of benzyl bromide and bromo methyl propionate respectively. GPC traces of the corresponding polymers indicated Mn: 30400 (Mw: 39500) and 45800 (Mw: 70000) for the initiation with benzyl bromide and bromo methyl propionate respectively.

The initiation efficiencies (I_{eff}) were estimated (reaction (3.2)) simply by the relationship;

$$I_{eff} = \frac{M_{th}}{M_n} = \frac{([M]/[I]).\ p\ .\ M_o}{M_n} \qquad \textbf{(3.2)}$$

Where M_{th} is theoretical molecular weight, Mn is number average molecular weight determined by GPC. [M] and [I] are concentration of the monomer and initiator respectively. P denotes the conversion and M_o is molecular weight of the monomer (MMA). From these data the initiation efficiencies of bromo ethyl acetate**,** benzyl bromide and bromo methyl propionate were calculated as 0.08, 0.12 and 0.33 respectively.

3.3.1.6 Surface initiated ring-opening polymerization of 2-methyl 2-oxazoline from the bromoethyl groups

One gram of the bead sample, 10 ml acetonitrile and 8.5 mL (0.1 mol) MeOx were introduced to a 100 mL volume flask and nitrogen was flushed for 5 minutes. Then the system was closed and the reaction was conducted at 110 ^{o}C by gentle stirring (400 rpm) for 24 h. The mixture was cooled and poured into water. The bead product was filtered, washed with water (3 ×50 mL), ethanol (20 mL) and dried at 50 ^{o}C under vacuum for 24 h. Dry product weighed 1.62 g.

The kinetic experiments were carried out in sealed tubes for each reaction time, using 0.2 g PBEMA sample, 3 mL acetonitrile and 2 mL of MeOx. The grafting was monitored by mass increases of PBEMA samples. The grafting degrees were assigned as described above.

3.3.1.7 Hydrolysis of polyoxazoline brushes

Dry sample with PMeOx surface graft (1 g) was mixed with 10 mL HCl solution (4.0 M) and boiled for 48 h. The mixture was filtered and washed with water several times. Then the solid residue was digested in 20 mL NaOH solution (5 M) and left to stand for 24 h. The product was filtered and washed with water (5x100 mL) and dried under vacuum at 50 ^{o}C for 18 h. The dry product weighed 0.84 g.

3.3.1.8 Determination of amine content of the hydrolysis product

Dry sample of the hydrolysis product (0.2 g) was mixed with 5 mL HCl solution (4.66M) and left to stand overnight. The mixture was filtered and 2 mL of the filtrate was titrated with 0.1 M NaOH solution. The titer consumption (88.6 mL) revealed an amine content of 5.75 mmol·g^{-1}.

3.3.2 Synthesis of P(S-DVB) micro-beads by suspension polymerization

P(S-DVB) resin was prepared in spherical bead form by crosslinking copolymerization of styrene-divinyl benzene mixture (with 9/1 M ratio) in aqueous suspension using Gum Arabic as stabilizer, according to the method given in the literature [140]. The bead product was dried, sieved and 210–422 μm size of fraction was used in further reactions.

3.3.2.1 Acetoxy mercuration of P(S–DVB) beads

In a 250 mL three necked round bottom flask equipped with reflux condenser, first 21 g of P(S–DVB) (210-422 μm) microspheres were wetted with 50 mL of dry acetic acid and then 10 g HgO, 40 mL acetic acid and 20 mL acetic anhydride were added to the reaction mixture. The reaction content was refluxed for 3 h at 120 ^{o}C and the resulting mixture was poured into a large excess of water (1.0 L). The microspheres were collected by filtration and washed with excess of water and alcohol (50 mL x 2). Air dried (the product was not dried in vacuum to avoid sublimation of the mercury) microspheres product was weighted 27 g (28.6 wt % of mass increase). These results revealed that maximum 12 % of styrene units (in mol mol^{-1}) have been acetoxymercurated.

3.3.2.2 Chlorine exchange reaction

In a 500 mL flask, mercurated microspheres (27 g) were mixed with 200 mL saturated NaCl solution and shaken for 24 h at room temperature. Then, the reaction mixture was filtered and collected microspheres were washed with excess of water and alcohol (30 mL x 2) and dried under open atmosphere at room temperature for 24 h. The dry yield of the chloromercurated product was 26.2 g.

3.3.2.3 Reaction with 2-bromoacetyl bromide

The chloromercurated microspheres (25 g) were mixed with 50 mL of dioxane in a 250 mL flask and the mixture was shaken for 30 min in a continuous shaker. Then, 25 mL (123.8 mmol) 2-bromoacetyl bromide was introduced to the reaction mixture and shaking was continued for 24 h at room temperature. The reaction mixture was poured into iced-water and the microspheres were filtered off. The solid residue was washed with (40 mL x 2) methanol to remove alcohol-soluble mercury bromide and filtered. The dried product (Step 1) microspheres weighed 21.4 g.

3.3.2.4 Determination of the bromine content

The bromide content of the Step-1 microspheres was determined by simple titration. For this purpose, 0.2 g of the bromoacetylated polymer was mixed with 10 mL methanolic NaOH solution (5 M) in a 50 mL flask and refluxed for 4 h. The mixture was filtered and washed with distilled water and the filtrate was transferred into a volumetric flask and diluted to 250 mL with distilled water. The NaBr content of the

solution was assayed colorimetrically by mercuric thiocyanate method [141]. This analysis gave 0.84 mmol bromine per gram of the polymer.

3.3.2.5 Graft copolymerization of styrene from the supported P(S-DVB) microspheres

In a 100-mL three-necked round-bottom flask fitted with nitrogen inlet, 5g (4.2 mmol) bromoacetyl functional microspheres product was swelled in 10 mL dry toluene then 30 mL styrene (0.262 mol), 2.73 g (4.2 mmol) H-TETA and 0.6 g CuBr (4.2 mmol) were added to the reaction mixture under nitrogen atmosphere. The reaction was conducted at constant temperature (90 ^{o}C) under continuous stirring for 6 h. The reaction mixture was then cooled, diluted with THF and filtered. Vacuum dried (at 60 ^{o}C for 24h) product (Step 2) weighed 12.5 g.

3.3.2.6 ATRP of GMA from the active chain ends of polystyrene brushes

To a 100 mL three necked round bottom flask equipped with a nitrogen inlet and a reflux condenser, there was added 30 mL toluene and 6 mL GMA (45 mmol). Then 10 g of the Step 2 microspheres (with 3.36 mmol active chain ends) was introduced to the flask and left in contact for 1.0 h to swell. To this mixture, 2.18 g (3.36 mmol) H-TETA and 0.482 g CuBr (3.36 mmol) were added under nitrogen atmosphere. The reaction was continued for 4.0 h at 60 ^{o}C under nitrogen atmosphere. The microspheres were isolated from the mixture by filtering and washed with THF (4x 50 mL) to eliminate residuals. The product was dried under vacuum at room temperature for 24h. The yield of the resulting material (Step 3) was 12.02 g.

3.3.2.7 Amino functionalization of grafted P(S-SVB) microspheres

The epoxy groups carrying P(S-DVB)-*g*-P(S-GMA) microspheres were aminated with 0.5 M 1,6 diaminohexane solution (i.e., spacer-arm) at pH 10.0 and at 65 ^{o}C in a reactor containing 10 g microspheres and was stirred magnetically for 5 h. After the reaction, the spacer-arm attached P(S-DVB)-g-P(S-GMA) microspheres were washed with distilled water. The microspheres were equilibrated in phosphate buffer (20 mL, 50 mM, pH 7.0) for 6 h, and transferred to the same fresh medium containing GA (20 mL, 0.5 volume % GA). The activation reaction was carried out at 25°C for 12 h, while continuously stirring the medium. After the reaction period, the microspheres were cleaned by washing sequentially with distilled water, acetic

acid solution (0.1 M, 100 mL) and phosphate buffer (0.1 M, pH 7.0). The resulting microspheres were used for the immobilization of lipase.

3.3.2.8 Immobilization of lipase on microspheres

P(S-DVB)-*g*-P(S-GMA) and P(S-DVB)-*g*-P(S-GMA)-HMDA-GA microspheres (5.0 g,) were equilibrated in phosphate buffer (50 mM, pH 7.0) for 2 h, and transferred to the same fresh medium containing lipase (100 mL, 2 mg mL^{-1}). Immobilizations of *Rhizomucor miehei* lipase on both microspheres were carried out at 4 °C for 3 to 18 h, while continuously stirring the reaction medium. After this period, the enzyme-immobilized microspheres were immediately transferred ethylene diamine solution (5.0 mg mL^{-1} ethylene diamine) in same buffer solution to block the free reactive groups on both the microspheres. Physically bound enzyme from the microspheres was removed by washing with a solution containing ionic detergent (sodium cholate, 50 mM) and salt (NaCl, 1.0 M) at pH 8.0 for 2 h. The amount of immobilized lipase on the P(S-DVB)-*g*-P(S-GMA) and P(S-DVB)-*g*-P(S-GMA)-HMDA-GA microspheres were determined by measuring the initial and final concentrations of protein within the immobilization medium and in wash solutions using *Coomassie Brilliant Blue* as described by the Bradford [142]. A calibration curve constructed with lipase solution of known concentration (0.05–0.50 mg mL^{-1}) was used in the calculation of protein in the enzyme and in wash solutions.

3.3.2.9 Activity assays of lipase

The activity of free and immobilized lipase was determined by olive oil hydrolysis [143]. A 100 mL olive oil emulsion was prepared by mixing olive oil (50 mL) and gum Arabic solution (50 mL, 7 wt %, w/v). The assay mixture consisted of emulsion (5 mL), phosphate buffer (2.0 mL, 100 mM, pH 7.5) and free enzyme (0.5 mL, 1.0 mg mL^{-1}) or immobilized enzyme (0.1 g microspheres). Oil hydrolysis was carried out at 35 °C for 30 min in a shaking water-bath at 150 rpm. The reaction was stopped by the addition of 10 mL of acetone–ethanol solution (1:1, v/v). The liberated fatty acid in the medium was determined by titration with 50 mM NaOH solution. These activity assays were carried out over the pH range 4.0–9.0 and temperature range 20–60 °C to determine the pH and temperature profiles for the free and the immobilized enzymes.

3.3.2.10 Determination of the kinetic parameters of the enzyme preparations

The kinetic constants were estimated by the reaction of the free and immobilized lipase on the P(S-DVB)-*g*-P(S-GMA)-HMDA-GA microspheres with tributyrin as substrate (5- 50 mM) and titrating the reaction product, butyric acid with 50 mM NaOH as described above. The experiments were conducted under the optimized assay conditions. The apparent K_m and V_{max} values for the free and immobilized lipase were calculated from Lineweaver–Burk plots (reaction (3.3)) by using the initial rates of the enzymatic reaction:

$$v^{-1} = \{K_m / V_{max} [S]^{-1}\} + v^{-1}_{max} \quad \textbf{(3.3)}$$

Where, [S] was concentration of the substrate, *v* and V_{max} represented the initial and maximum rate of reaction, respectively. K_m was the Michaels constant. One lipase unit corresponded to release of 1 μmol fatty acid per minute under assay conditions. The specific activity is the number of lipase units per mg protein.

3.3.2.11 Thermal and storage stability of the immobilized lipases

The thermal stabilities of the free and immobilized lipase on the P(S-DVB)-*g*-P(S-GMA)-HMDA-GA microspheres were determined by incubation in substrate-free phosphate buffer solution (50 mM, pH 7.5) at two different temperatures (55 and 65 °C) under continuous shaking at 150 rpm. At 15 min time intervals, the remaining activities of the free and immobilized lipase were measured as described above.

3.3.2.12 Enzymatic synthesis of banana flavor esters

Industrially important esters (i.e., ethyl acetate and iso-amyl acetate; banana flavor esters) were synthesized in screw-capped flasks (20 mL) using immobilized lipase on the P(S-DVB)-*g*-P(S-GMA)-HMDA-GA microspheres (0.1 g) for both solvent-free medium and non-aqueous medium. For solvent free system, the enzymatic esterification reactions were carried out with various acetic acid / ethyl alcohol and / or acetic acid : iso-amyl alcohol molar ratios (i.e., 0.25:1.0, 0.5:1.0, 0.75:1.0, and 1.0:1.0) containing of 20 μL distilled water) on an orbital shaker at 150 rpm and at 40◦C and 55◦C, respectively, for 24 h. For non-aqueous medium, ethyl acetate and iso-amyl acetate synthesis reactions were carried out in *n*-hexane (15 mL) containing 50 mmol acetic acid and 100 mM ethyl alcohol and/or 50 mmol acetic acid and 100 mM iso-amyl alcohol with shaking at 150 rpm at 40 ◦C and 55 ◦C, respectively.

Along the 24 h reaction, the amount of remaining acid was determined by titrimetric method using 50 mM NaOH and phenolphthalein as an indicator. The conversion (%) of esters was calculated based on the conversion of the acetic acid to esters after a given time. The initial reaction rate was determined in the linear region. All of the experiments were carried out in triplicate. The control experiments (no enzyme) were performed and it was observed that ester yield is less than 2%.

3.3.2.13 Operational stability of immobilized lipase in ester synthesis

A batch-wise fashion was adopted to investigate the operational stability of the immobilized lipase in ester synthesis using acetic acid: ethyl alcohol and/or acetic acid: iso-amyl alcohol molar ratios 0.5:1.0. The activity was determined as described above, and each reaction was terminated after 12 h reaction period. After any run, the same enzyme immobilized on the P(S-DVB)-*g*-P(S-GMA)-HMDA-GA microspheres were washed two times with 5.0 mL ethyl acetate or iso-amyl acetate and reintroduced into a fresh medium, this being repeated up to 10 cycles for ester synthesis.

3.3.3 Synthesis of PDVB microspheres via precipitation polymerization

PDVB microspheres were prepared by precipitation polymerization technique as described in the literature [24]. For this purpose, AIBN (0.2 g, 1.22 mmol, 4 wt % relative to DVB55) was added to the solution of DVB55 (11 mL, 76.8 mmol, 4 vol % relative to total volume) and 274 mL acetonitrile in a dry 500 mL volume of three-necked flask equipped with a mechanical stirrer and a nitrogen inlet. The flask was placed in thermostated oil bath and the temperature was adjusted to 70 ^{o}C. The nitrogen flow was stopped and the reaction was conducted for 48 h at this temperature under continuous stirring (32 rpm). The reaction content was cooled to room temperature and polymer precipitated was filtered, washed with tetrahydrofuran (20 mL), acetone (20 mL) and methanol (20 mL). The product was dried at 45 ^{o}C under vacuum for overnight. The yield was 3 g (30 %).

3.3.3.1 Hydrobromination of PDVB microspheres

Hydrobromination was performed according to a procedure as described in the literature [144]. PDVB microsphere (2g) was suspended using 80 mL n-heptane in 250 mL of round bottom flask and dibenzoyl peroxide (0.18g, 0.74 mmol) was added

to the mixture under magnetic stirrer. Hydrogen bromide (HBr) was generated by drop-wise addition of concentrated sulfuric acid (15 mL, 0.28 mol) to solid KBr (59.5 g, 0.50 mol) in a separated vessel was introduced to the mixture by means of a delivery tube. After 8 h, the generation of HBr was stopped and the stirring was maintained for another 2 hours. The suspension mixture was filtered and product was purified by washing with dichloromethane, methanol and diethylether before drying in a vacuum oven at 40^{o}C for overnight. The dried product was weighted 2.4 g.

The amount of bromine on the particles was determined by titration; the brominated particles (0.1 g) were mixed with magnesium oxide (1 g, 25 mmol) and sodium carbonate (0.5 g, 4.71 mmol) and fused at 550 ^{o}C for 10 h as described in the literature [145]. Sodium bromide in the cooled mixture was transferred into 100 mL volumetric flask by appropriate dilutions and washings and slightly acidified (pH: 5) by adding nitric acid (%65). This solution was titrated with $AgNO_3$ in presence of sodium chromate as color indicator. This estimation revealed bromine content of 1.46 mmol/g.

3.3.3.2 Azidation of PDVB microspheres

Bromoethyl group on PDVB microspheres was converted into ethyl azide function by condensation with NaN_3. For this purpose, PDVB microsphere (1 g) was suspended in 20 mL dimethylformamide and NaN_3 (0.5 g, 7.7 mmol) was added to the mixture. Then, 0.1 mL distilled water was added to enhance solubility of sodium azide. The flask was closed and covered with aluminum foil to protect from light exposure and shaken for 24 h at room temperature. The bead product was isolated by filtration and successive washings with water (20×2 mL), methanol (20 mL) and diethylether (20 mL) and dried overnight under vacuum at room temperature.

3.3.3.3 Synthesis of alkyne functional ATRP initiator

Initiator was synthesized by dropwise addition of 2-bromoisobutyryl bromide (1.5 mL, 12 mmol) to propargyl alcohol (0.68 mL, 11.5 mmol) and triethylamine (TEA, 1.65 mL, 11.9 mmol) solution in diethylether (50 mL) at 0 °C under a nitrogen atmosphere. After addition, the reaction mixture was stirred overnight at room temperature. The reaction mixture extracted with water and organic phase was dried with Na_2SO_4. The solution was concentrated and the crude product was purified by column chromatography over silica gel eluting with hexane/ethyl acetate (10/1) to

give the product as a colorless liquid (yield: 1.9 g, 85%). ^{1}H NMR ($CDCl_3$): 1.90 (s, 6H,), 2.47 (t, 1H,), 4.71 (s, 2H,)

3.3.3.4 Preparation of alkyne functional poly(ethylene glycol)

PEG (M_n: 2000 g/mol, 3.0 g, 1.5 mmol) was dissolved in 25 mL of CH_2Cl_2. 4-Pentynoic acid (0.22 g, 2.25 mmol) and DMAP (0.18 g, 1.5 mmol) were successively added to the reaction mixture. After stirring 5 min at room temperature, a solution of DCC (0.46 g, 2.25 mmol) in 15 mL of CH_2Cl_2 was added to the reaction mixture and stirred overnight at room temperature. After filtration of the salt, the solution was concentrated and product was purified by column chromatography over silica gel eluting with CH_2Cl_2/ethyl acetate mixture (1:10) and then with CH_2Cl_2/ MeOH (10:1). Finally, concentrated solution of alkyne-PEG was precipitated in diethyl ether and filtered (yield: 2.81g, M_{nGPC}: 2400 M_w/M_n: 1.08).

3.3.3.5 Preparation of alkyne functional poly(methyl methacrylate)

CuCl (66.8 mg, 0.67 mmol), PMDETA (97.2 μL, 0.67 mmol), alkyne functional initiator (96 mg, 0.46 mmol), methyl methacrylate (5 mL, 46.6 mmol) and 5 mL toluene as a solvent were placed in a Schlenk tube. Three freeze-pump-thaw cycles were performed and the tube was stirred in oil bath at 80 °C for 20 min. At the end of the reaction, the mixture was diluted with THF and the copper complex was removed out by passing through a neutral alumina column. The diluted mixture was precipitated in hexane and the solid was collected after filtration and dried at room temperature in a vacuum overnight.

3.3.3.6 Synthesis of alkyne functional poly(*tert*-butyl acrylate)

A Schlenk tube was charged with CuBr (51.1 mg, 0.35 mmol), PMDETA (74.3 μL 0.35 mmol), alkyne functional initiator (73.1 mg, 0.35 mmol), *tert*-butyl acrylate (5 mL, 34.1 mmol). Three freeze-pump-thaw cycles were performed and the tube was stirred in oil bath at 80°C for 40 min. After the given time, the mixture was diluted with THF. Then the copper complex was removed out by passing through a neutral alumina column, and THF was removed by rotary evaporation. The mixture was precipitated in cold methanol/water (80/20 v/v). After decantation, the polymer was dissolved in CH_2Cl_2, extracted with water and the water phase was again extracted with CH_2Cl_2 and combined organic phase was dried over Na_2SO_4. Finally, the

organic phase was evaporated to give alkyne functional poly(*tert*-butyl acrylate). The polymer was dried for 24 h in a vacuum oven.

3.3.3.7 PEG grafted PDVB microspheres via Click reaction

PDVB microspheres (100 mg containing 1.45 x 10^{-4} mol azide groups) were suspended in 4 mL of DMF in a Schlenk tube. Alkyne-PEG-2000 (0.7 g, 2.92 x 10^{-4} mol), CuBr (20.94 mg, 1.45 x 10^{-4} mol), and PMDETA (30.4 μL, 1.45 x 10^{-4} mol) were added and the reaction mixture was degassed by three freeze–pump–thaw cycles and left in vacuo. The mixture was stirred at 40 ^{o}C for 48 h. The solid was separated from the mixture by centrifugation. The collected solid was redispersed in DMF and separated by centrifugation. This purification cycle was repeated three times for dilute acidic methanol solution and THF. After purification, the resulting products were dried overnight under vacuum, and a sample of PEG grafted PDVB microspheres (102 mg) was obtained.

3.3.3.8 PEG and PMMA grafted PDVB microspheres via Click reaction

PDVB microspheres (50 mg containing 0.73 x 10^{-4} mol azide groups) were suspended in 5 mL of DMF in a Schlenk tube. Alkyne-PEG-5000 (0.79 g, 1.46 x 10^{-4} mol), alkyne-PMMA (0.78 g, 1.46 x 10^{-4} mol), CuBr (10.45 mg, 0.73 x 10^{-4} mol), and PMDETA (15.2 μL, 0.73 x 10^{-4} mol) were added and the reaction mixture was degassed by three freeze–pump–thaw cycles and left in vacuo. The mixture was stirred at 40 ^{o}C for 48 h. The solid was separated from the mixture by centrifugation. The collected solid was redispersed in DMF and separated by centrifugation. This purification cycle was repeated three times for dilute acidic methanol solution and THF. After purification, the resulting products were dried overnight under vacuum, and a sample of PEG and PMMA grafted PDVB microspheres (60 mg) was obtained.

3.3.3.9 PEG and P*t*BA grafted PDVB microspheres via Click reaction

PDVB microspheres (50 mg containing 0.73 x 10^{-4} mol azide groups) were suspended in 5 mL of DMF in a Schlenk tube. Alkyne-PEG-5000 (0.79 g, 1.46 x 10^{-4} mol), alkyne-P*t*BA (0.73 g, 1.46 x 10^{-4} mol), CuBr (10.5 mg, 0.73 x 10^{-4} mol), and PMDETA (15.2 μL, 0.75 x 10^{-4} mol) were added and the reaction mixture was degassed by three freeze–pump–thaw cycles and left in vacuo. The mixture was stirred at 40 ^{o}C for 48 h. The solid was separated from the mixture by centrifugation.

The collected solid was redispersed in DMF and separated by centrifugation. This purification cycle was repeated three times for dilute acidic methanol solution and THF. After purification, the resulting products were dried overnight under vacuum, and a sample of PEG and P*t*BA grafted PDVB microspheres (70 mg) was obtained.

3.3.3.10 Enzyme adsorption and desorption experiments

Adsorption of laccase enzyme on the different types of microspheres was studied at various pHs in sodium acetate (1 mL, 0.05 M, pH 3.5–5.0). The enzyme initial concentration was 10 mg/mL in each corresponding buffer. Adsorption experiments were conducted for 120 min at 25 °C on orbital shaker. The equilibrium adsorption time was determined to be 120 min with pre-experiments. The amount of adsorbed laccase on the three types of microspheres was determined by following the initial and final concentrations of protein within the adsorption medium using Coomassie Brilliant Blue with crystalline bovine serum albumin (BSA) as standard [142]. The experiments were performed in replicates of three and the samples were analyzed in replicates of three as well. For each set of data present, standard statistical methods were used to determine the mean values and standard deviations.

Laccase was removed from the microspheres (after adsorption) by washing in % 10 PEG and 1.0 M $(NH_4)_2SO_4$ (desorbing buffer) for 90 minutes at 25 °C [146].

The desorption ratio of laccase was calculated by using the following expression;

Desorption ratio= (enzyme released/adsorbed enzyme on microspheres)x100

Activity Assays: Laccase activity was assessed by measurement of enzyme oxidation of 2,2-azinobis-(3-ethylbenzothiazoline-6-sulphonic acid) at 427 nm ($\varepsilon = 3.6 \times 10^4\ cm^{-1}\ M^{-1}$) [147]. The reaction mixture contained either free or immobilized enzyme in, 300 μL of 1 mM ABTS and 0.1 M Na-acetate buffer (pH 4.5). 1.0 Unit (U) of enzyme activity is defined as the amount of enzyme that oxidizes 1 μmol ABTS in 1 min. Specific activity is expressed as U/ mg-protein per mg support matrix.

Zeta Potential Analysis: Zeta-Meter 3.0+ (with Zeiss DR microscope, GT-2 type quartz cell, molybdenum cylinder anode, and platinum rod cathode electrode) was used for the zeta potential analysis by using sodium acetate buffer (pH 4.5, 0.1 M) as an environment. The microspheres (0.5 mg/mL) were suspended in the buffer by stirring overnight. In electrophoresis, the particles are moved by applying an electric field across the system. Microspheres were timed for both directions of the applied

electric field. The value of zeta potential as signed to dispersions was the average of the data obtained from 6 experiments. The applied voltage during the measurements was varied in the range 20–30 mV [148]. The zeta potential of microsphere suspensions was estimated from measured electrophoretic mobilities by employing the Smoluchowski equation. Electrokinetic charge densities were also calculated according to Saka et al [149].

3.3.4 Surface adsorption of poly(2-hydroxypropylene maleate) on SiO_2 and TiO_2 nanoparticle and its thermal curing

PHPM polyester was prepared by stepwise condensation of maleic anhydride with glycidol as reported by our group before [150]. A 10 % solution of the polymer (M_n = 13800 g/ mol) in dimethoxyethane was used in the adsorption experiments. Encapsulation of the nanopowders was achieved by surface adsorption of PHPM from acetone solution and followed curing as described for the microparticles. The nanopowder samples (6 g) were mixed with acetone solution (20 mL) of PHPM (22.3 % w/w) and stirred for 15 min. Thereafter, acetone was removed by rotary evaporator and the residue was heated at 180 $^{\circ}$C for 30 min for crosslinking of the polyester adsorbed.

3.3.4.1 Adsorption and thermal crosslinking of the polyester on the microparticle surfaces

To investigate the adsorption behavior of PHPM, a series of the polyester solutions (in 7.2–116 gL^{-1} concentrations) were prepared in acetone. 10 mL of these solutions were mixed and stirred with 1.0 g of dry pigment powders in micron sizes (100–210 μm) for 1 h at room temperature. The mixtures were filtered by suction and dried at 70 $^{\circ}$C under vacuum overnight. The samples were then cooled to room temperature and weighed. Non-adhered portions of the polyesters remaining in the filtrates were estimated by weighing the residues, after evaporation of the solvent. The samples were then cured at 180 $^{\circ}$C for 30 min in an oven for thermal crosslinking of the polyester adsorbed onto the particle surfaces. The samples were cooled and placed in a Soxhlet extractor to remove any soluble polyester residue. The samples were dried under vacuum at 50 $^{\circ}$C for 6 h.

3.3.4.2 Estimation of polyester adsorption on the microparticles by Langmuir isotherm approach

The equilibrium adsorptions, q_E (per gram of pigment) were calculated by the following relationship: $q_E = \frac{(c_0 - c)}{w_0}$, where c_0 is the initial polyester content of the acetone solution, c is polyester content of the acetone solution at the equilibrium and w_0 denotes the weight of the pigment sample.

The data collected were used to build up plots of $1/q_E$ vs $1/C_E$ plots (Langmuir plots), where q_E and C_E denote the equilibrium adsorption and equilibrium concentration, respectively. The maximum adsorptions were estimated from the intercepts of the plots.

3.3.4.3 Surface initiated polymerization of ε-caprolactone from the nanoparticle surfaces

The cured sample (5 g), 16 mL of redistilled ε-Caprolactone (0.144 mol) and 10 mL dimethoxyethane were charged in a 100 mL flask after 5 times of empty-fill cycles with dry nitrogen. To the mixture, 0.2 mL of tin (II) 2-ethylhexanoate was added with a hypodermic syringe while stirring and the temperature of the bath was adjusted to 80 ^oC. The reaction was continued for 8 h at this temperature. The mixture was cooled and precipitated in 100 mL ethanol, filtered, and washed with ethanol (2 × 30 mL). Then, superficially dried samples were suspended in acetone (40 mL) to remove free PCL. The acetone was removed by centrifugation (3000 rpm, 5 min). The samples were redispersed in acetone and centrifuged again. The resulting gel-like samples were then dried under vacuum at 50 $^\circ C$ for 6 h and stored in tightly closed bottles. Dry weights were found 6.5 g and 6.1 g for the samples with SiO_2 and TiO_2, respectively.

3.3.4.4 Preparation of polymer nanocomposite films

Commercial (methyl methacrylate-*stat*-butyl acrylate) copolymer (5 g, approx. 50 % MMA) was dissolved in 50 mL of acetone. The organically modified nanoparticles (0.5 g) were mixed with 10 mL of the above polymer solution. The mixtures were sonicated at 20 KHz (with 40 % power out) for 5 min. The pigment dispersions obtained were stable and no precipitation or phase separation was observed within three days of standing at room temperature. The dispersions were then applied onto

polished glass surfaces by means of film maker (Sheen Automatic Film Applicator) to give composite films with 60 μm of wet thickness. The surface films were left to stand under atmospheric pressure for 24 h at room temperature. The films were detached from the glass surfaces by hot water and dried at 40 ^{o}C overnight. The free-standing composite films were used for the surface characterizations with SEM.

3.3.5 Synthesis of $Zn(NH_3)_4(OH)_2$ solution

Fifty mL of 10 M KOH solution was added drop wise to 150 mL of ammonia solution in a 250 mL Erlenmeyer flask mounted in ice-bath while stirring. To this solution, there was added 50 mL of 4.5 M $ZnCl_2$ solution. The resulting clear solution was transferred into a volumetric flask and diluted to 250 mL, so as final concentration of Zn(II) to be 0.9 M.

3.3.5.1 Preparation of zinc oxide nanoparticles

Zinc oxide nanoparticles in different sizes were prepared by mixing 20 mL of 0.9 M $Zn(NH_3)_4(OH)_2$ solution with appropriate quantities of ethanol solution of 1 M dodecylamine(10- 80 mL). 40 mL ammonia solution (25%) was added to dodecylamine solution prior to addition to the zinc tetramine hydroxide solution. The reaction mixture was stirred at 1000 rpm in glass beakers open to air atmosphere. An air stream was bubbled through the mixture. The clear became opaque in a few hours by evaporating ammonia. The reaction was conducted for 18 h. The white precipitate was filtered, washed with water (2×30 mL), ethanol (2×20 mL) and dried at 40 ^{o}C under vacuum for overnight.

3.3.5.2 Preparation of poly(methyl methacrylate-*b*-glycidyl methacrylate)

Standard copper mediated ATRP polymerization technique was employed for preparing the block copolymer, P(MMA-*b*-GMA) . The first block, PMMA was generated as follows: To a 100 mL round bottom flask 10 mL MMA (94 mmol), 0.134 g CuBr (0.94 mmol), 0.195 mL PMDETA (0.94 mmol), 0.137mL ethyl 2-bromo *iso*-butyrate (0.94 mmol) and 20 mL toluene as a solvent were added under nitrogen flow. The flask was mounted in a thermo stated-oil bath and temperature was adjusted to 80 ^{o}C. The nitrogen stream was stopped and the system was closed. The reaction was conducted under constant stirring rate (1000 rpm) for 25 min. At the end of the reaction, the mixture was diluted with THF, filtered and the filtrate

was chromatographed through neutral alumina to remove the copper complex. The polymer was isolated by precipitation into n-hexane (50 mL per 10 mL solution), filtered and dried at room temperature under vacuum overnight. GPC traces of the polymer showed a molecular weight, M_n: 8450 g/mol and polydispersity index, PDI: 1.06.

Block copolymer with PGMA was prepared by a similar procedure in which using above PMMA was employed as macroinitiator.

Thus, 4 g PMMA (0.47 mmol) , 4 g glycidyl methacrylate (0.28 mmol), 0.68 g CuBr (0.47 mmol), 0.097 mL PMDETA (0.47 mmol) and 20 mL toluene were charged to a 100 mL volume of round bottom flask under nitrogen flow. The flask was mounted in a thermo stated-oil bath and temperature was adjusted to 60 ^{o}C. The reaction was conducted for 1h. Resulting block copolymer was isolated similarly. GPC trace of the block copolymer precipitated in n-hexane revealed a molecular weight of M_n :11200 g/mol) and PDI 1.134.

3.3.5.3 Encapsulation of zinc oxide nanoparticle with the block copolymer

Zinc oxide nanoparticles were encapsulated using by reaction the block copolymer (P(MMA-*b*-GMA)) in toluene solution. For this purpose, 1.67 g block copolymer was dissolved in 20 toluene and 0.25 g ZnO nanoparticle was dispersed in this mixture. The flask was equipped with reflux condenser and the reaction was conducted at 100 ^{o}C for 24 h. ZnO nanoparticles coated with the block copolymer were isolated from the mixture by centrifugation. To remove unbound polymer and other impurities the product was redispersed in toluene and in THF and isolated by centrifugation similarly. The product was dried under vacuum at 60 ^{o}C for overnight.

3.3.5.4 Preparation of polymer nanocomposite films

Commercial (methyl methacrylate-*stat*-butyl acrylate) copolymer (0.5 g, approx. 50 % MMA) was dissolved in 5 mL of acetone. To this solution polymer encapsulated ZnO nanoparticles (0.09 g) were added and the mixture was stirred for 15 min. The mixtures was then sonicated at 20 KHz (with 40 % power out) for 2 min. The resulting dispersions were stable and no precipitation or phase separation was observed upon standing three days at room temperature. The dispersions so obtained were then applied onto polished glass surfaces by means of film maker (Sheen Automatic Film Applicator). The composite films (with 60 μm of wet thickness)

were left to dry under atmospheric pressure for 24 h at room temperature. The freestanding composite films were detached from the glass surfaces by hot water. After drying at 40 $^{\circ}$C for overnight, they were used for the surface characterizations with SEM.

4. RESULTS AND DISCUSSION

4.1 Bromo Ethyl Methacrylate Based Hairy Functional Polymers

In this study, Synthesis and cross-linking copolymerization of 2-bromoethyl methacrylate (BEMA) in aqueous suspension is described for preparing bromoalkyl functional microbeads (125-420 µm). Highly transparent microspheres with accessible bromoethyl group density of 1.55 mmol·g^{-1} were prepared. The bromoethyl functions of the bead polymer were then, employed as initiation sites for surface initiated polymerization of either ring-opening polymerization of 2-methyl oxazoline or atom transfer radical polymerization of glycidyl methacrylate respectively (reaction 4.1).

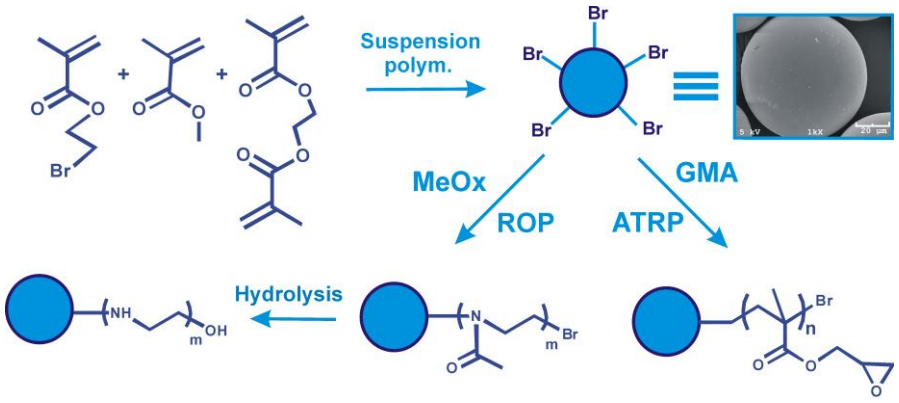

(4.1)

4.1.1 A new method for preparing bromoethyl methacrylate monomer

The monomer, 2-bromoethyl methacrylate (BEMA) was prepared in high purity by a new synthetic procedure as described recently by our group [139]. The procedure involves acidolysis of 2-bromoethyl borate with methacrylic acid. 1H-NMR spectrum of the monomer in Figure 4.1 shows isolated methyl group signal at 1.8 ppm. Protons of the double bond exhibit symmetrical doublet in 5.45-6.0 ppm range as expected. Proton signals of -COO-CH2- and -CH2-Br groups are observed as triplets at 4.3 and 3.4 ppm respectively. Three protons of CH3-C=C group gives a sharp singlet at 1.8 ppm. Having bromoethyl function, the monomer offers many transformation possibilities and can be considered as key monomer for preparing various functional polymers. Comparing with the commercially available monomer,

vinyl benzyl chloride constituting with a mixture of *meta* and *para* isomers, this monomer has advantage of the purity and higher reactivity of the bromoalkyl function.

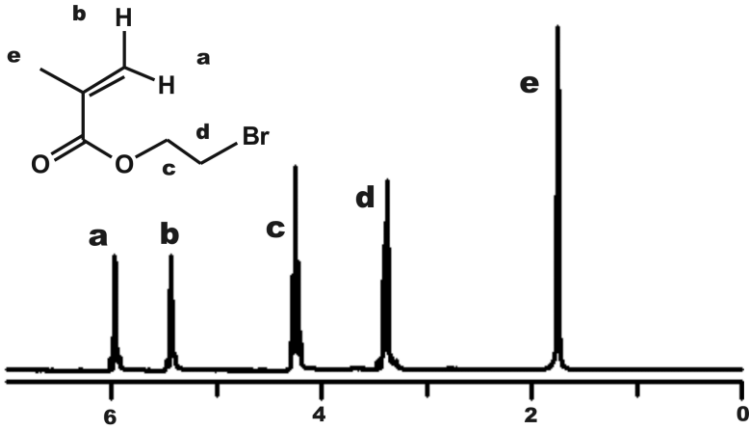

Figure 4.1: ^{1}H-NMR spectrum of the monomer, bromoethyl methacrylate (BEMA) in $CDCl_3$.

4.1.2 A suspension polymerization recipe for synthesis of bromo ethyl functional micro-beads

Cross-linked PBEMA microspheres were prepared by suspension polymerization methodology using MMA as diluting co-monomer to adjust bromoethyl group density of the resulting polymer. EGDMA was chosen as cross-linker and AIBN was employed as primary radical source. The polymerization and chemical structure of the resulting polymer is depicted in reaction (4.2).

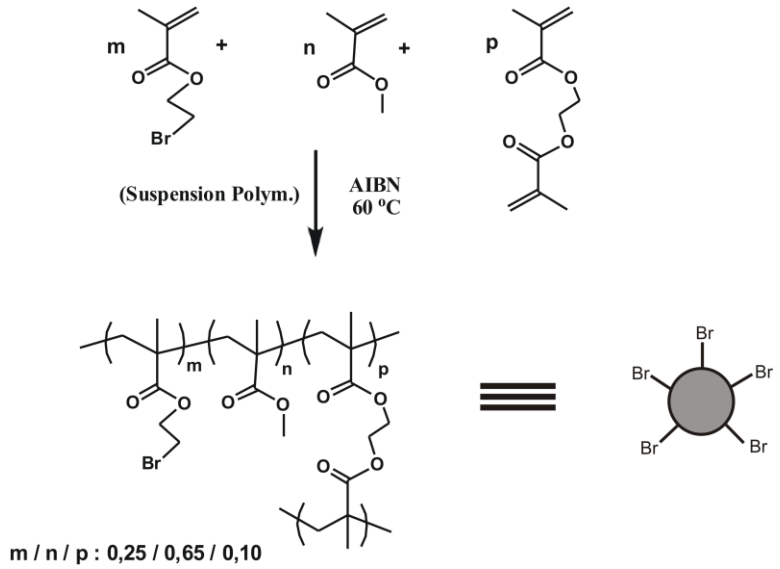

(4.2)

In principle, proper selection of the stabilizer is critical issue in suspension polymerization to obtain perfect spherical beads. The particle shape may also affect on thickness and homogeneity of the graft layer, when the product is employed as solid macroinitiator in the surface initiated ATRP.

In the present work, various polymers; poly(vinyl alcohol), Gum Arabic, poly(styrene-*alt*-maleic acid) and poly(N-vinyl pyrrolidone) (PNVP) were studied for stabilization of the suspension droplets of the monomer mixture in water. Experiments were conducted at various oil/water volume ratios with different stirring rates (500-1000 rpm). Except for the case of PNVP, the products obtained were amorphous gels or irregular beads in different sizes. Although, poly(styrene-*alt*-maleic acid) was successfully employed in our previous works, for preparing fine microbeads of GMA-MMA copolymer [151], this stabilizer did not work in the present case, most probably due to its increasing hydrophobicity of the stabilizing polymer by partial condensation of the carboxylate function with bromoethyl groups of BEMA. Changing the stabilizer ratio and stirring rates were not helpful and the resulting solid particles obtained were irregular. The experiments with Gum Arabic gave similar amorphous products.

Table 4.1: The recipe for suspension copolymerization of BEMA yielding transparent microspheres.

BEMA (monomer)	12.1 g (62.5 mmol)
EGDMA (cross-linker)	4.95 g (25 mmol)
MMA (co-monomer)	16. 25 g (162.5 mol)
Toluene (porogen)	45 mL
Poly(N-vinyl pyrrolidone) (stabilizer)	1 g
Water (continuous phase)	300 mL
AIBN (radical initiator)	0.160 g (0.098 mmol)
Stirring Rate	1000 rpm
Polymerization temperature	60 ^{o}C
Reaction Time	12 h
Appearance of the product	Colorless microspheres
Particle Size	125-420 μm
Accessible bromine content	1.55 mmolg^{-1}

The stabilization with PNVP gave colorless microspheres in relatively narrow size distributions (125-420μm). The recipe for the suspension polymerization procedure with PNVP is given in Table 4.1. Optical photography of the dry product in Figure 4.2 shows nearly spherical beads with smooth surfaces.

The fraction in 210-420 μm size range was employed for the surface initiated polymerizations in the following studies. Bromide content of this product was determined to be 1.55 mmol·g^{-1}. Considering with the initial molar composition of the monomer mixture in the suspension polymerization process, the theoretical bromide content must be 1.88 mmol·g^{-1}. Therefore, the practical bromide content accounts for about 82.5 % of the theoretical amount. Obviously, the remainder of the bromide is embedded in the cross-linked matrix and remains inaccessible in further reactions.

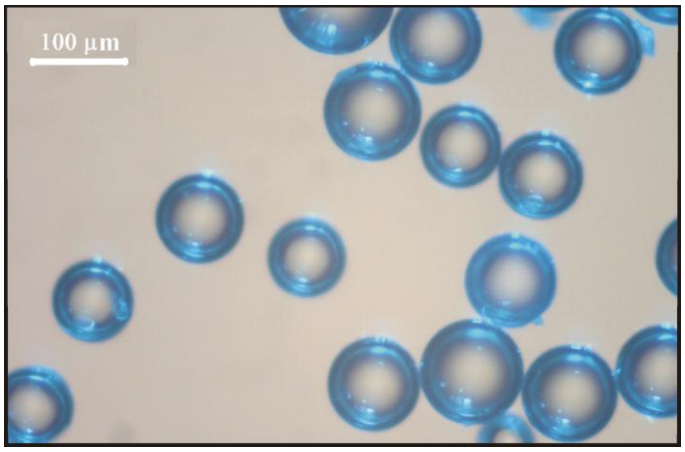

Figure 4.2: Optical photoimage of cross-linked PBEMA microparticles prepared by suspension polymerization using PNVP (1 %) as stabilizer.

4.1.3 Surface initiated ATRP from the bromoethyl groups

Since alkyl halides are well-known initiators for ATRP of acrylic and styrenic monomers, the bromoethyl groups on the beaded polymer surface were considered useful for creating polymeric surface brushes. Among controlled / living polymerization techniques, ATRP is especially useful for grafting from solid surfaces [8]. Negligible quantity of free-homopolymer formation is main advantage of surface initiated ATRP, in addition to nearly controlled chain growth in the grafting process [53].

This strategy has been employed successfully to generate surface grafts on solid PS or on inorganic pigment particles in micron or nanometer sizes [33, 54]. In the reported procedures, the surface grafts have been generated by ATRP from haloalkyl functions onto the surfaces. Common approach for incorporation of ATRP initiator groups onto solid particles involves esterification of surface hydroxy groups with 2-bromo isobutyryl bromide [3, 152]. Selective hydrolysis of the ester linkages after ATRP is useful for harvesting and analyses of the graft chains. However, hydrolytic

instability of this linkage is not desirable, especially when the graft chains are considered as functional group carriers. In this respect, utilization of a suitable co-monomer bearing haloalkyl function in preparing spherical bead polymer might be useful to generate surface brushes linked to the surface by non-hydrolysable covalent bonds. Perhaps vinyl benzyl chloride is the only haloalkyl functional monomer commercially available. Its cross-linked polymer has been reported as solid initiator for ATRP of dimethyl amino ethyl methacrylate [153].

However, cross-linked copolymer of this monomer (Merrifield resin) has been demonstrated to be too slow in surface initiated ATRP, due to less initiation efficiency of the chloromethyl group [154]. It was concluded that, bromoethyl groups on PBEMA microspheres could be used as efficient initiating sites for grafting by SI-ATRP, without necessity of surface modification.

Starting from the beaded polymer with known density of surface initiator groups is an apparent advantage of this approach. And also non-hydrolysability of the linkages between the graft chains and microspheres is an additional advantage of this material.

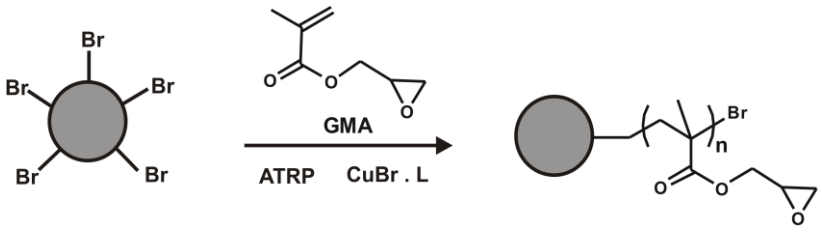

(4.3)

In conjunction with this, ATRP of GMA was studied in order to test radical initiation efficiency of the supported bromoethyl groups. The reaction was carried out with CuBr catalyst at 60 ^{o}C as depicted in reaction (4.3). This procedure resulted in 420 % graft yields within 24 h, indicating efficiency of those groups in initiation of ATRP. GMA was chosen for grafting monomer, due to numerous chemical transformation possibilities of the epoxy group on the graft chains [8].

In order to test radical generating ability of the bromoethyl function, bromo ethyl acetate was synthesized as a model compound by reacting bromoethanol with acetyl chloride. This compound was employed as initiator for ATRP of MMA at 70 ^{o}C in toluene (using constant [monomer] / [initiator] / [CuBr . L]: 100/1/1 ratios). For comparison of its initiation efficiency with those of the well known ATRP initiators, the polymerization was repeated with bromo methyl propionate and benzyl bromide in the same conditions. After 5 hours of the polymerization, the resulting polymers

were isolated. The initiation efficiencies were assigned simply by ratio of the theoretical to the practical molecular weights inferred from the GPC traces. These experiments revealed initiation efficiencies 0.08, 0.12 and 0.33 for bromo ethyl acetate, benzyl bromide and bromo methyl propionate respectively. These results showed that the initiation efficiency of bromoethyl acetate is less than that of bromo methyl propionate, but comparable with that of benzyl bromide.

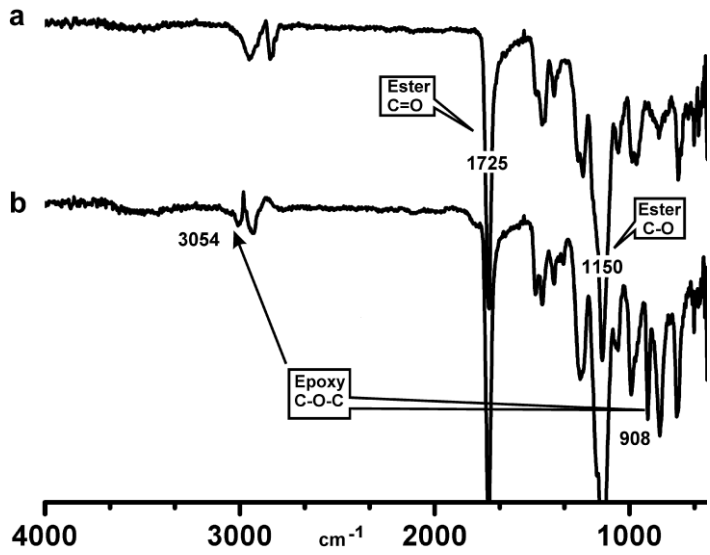

Figure 4.3: FT-IR spectrum of PBEMA microspheres before (a) and after surface grafting with GMA (b).

FT-IR spectrum of GMA grafted resin (Figure 4.3-b) exhibits methacrylate ester vibrations at 1725, 1255 and 1150 cm^{-1} associated with stretching vibrations of carbonyl, CO-O and COO-C bonds respectively. These bands appear also in the IR spectrum of the starting microspheres (Figure 4.3-a), but their intensities are significantly higher in the spectrum of grafted resin. The specific oxirane bands of the PGMA brushes, which are different from those of the base material, appear at 3054 (shoulder) and 908 cm^{-1} and these represent C-H and C-O stretching vibrations of the epoxy ring respectively.

Semi-logarithmic plot of the conversion-time data of the grafting with GMA (Figure 4.4) implies nearly first order kinetics (regression factor, R = 0.98) with a rate constant of $k = (6.6 \pm 0.04) \times 10^{-6}\ s^{-1}$. The graphic reveals a constant radical concentration in the graft copolymerization of GMA in these conditions. The slope of the curve however, increases beyond 24 h indicating somewhat greater rate constant at high conversions. This must be due to heterogeneity of the grafting at the earlier

stage of the reaction. Increasing lengths of the graft chains at higher conversions provide quasi-homogenous conditions and slightly higher polymerization rates.

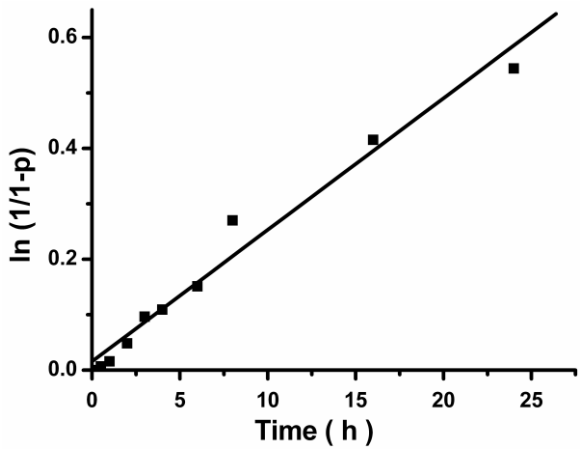

Figure 4.4: First order kinetic plot for the surface initiated graft copolymerization of GMA on PBEMA microspheres by ATRP.

Since the grafts are not detachable from the surface, we are unable to make a precise estimation for the rates of the chain growths and polydispersities. Considering the heterogeneity of the reaction, the surface grafting of GMA is not expected to proceed in thoroughly controlled fashion. Nevertheless, it is fact that initiation of ATRP of GMA from the bromoethyl groups on the solid microspheres is possible and provides reasonable graft yields.

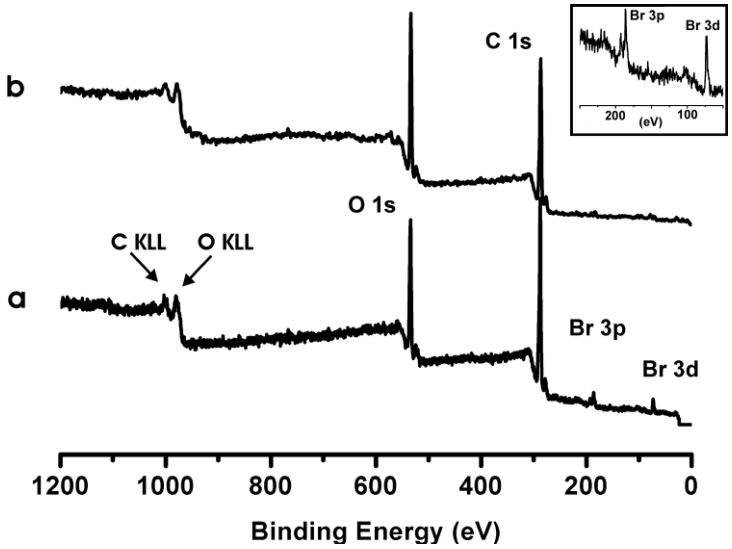

Figure 4.5: Full scale XPS of PBEMA microspheres before (a), and after surface initiated grafting with GMA(b). The window shows 3p and 3d core levels of the bromide on the PBEMA microspheres.

XPS technique was also employed in order to follow the changes in surface characteristics of the microspheres by the grafting process. Figure 4.5-a clearly shows core levels of the elements in PBEMA microspheres. Thus, the main elements, carbon and oxygen, exhibit binding energies for C 1s and O1s core levels at 285 and 534 eV respectively. These elements show also Auger KLL peaks at 1000 and 979 eV respectively. The typical bromine peaks in PBEMA are observed at 73 and 186 eV for Br 3d and Br 3p core levels (see window in Figure 4.5). However, after grafting with PGMA, these peaks become almost invisible (Figure 4.5-b). Considering with livingness of ATRP process, the chain ends of PGMA brushes must carry bromine atoms. Absence of the two peaks in the XPS must be due to dilution of the bromines by increasing volume of the microspheres in the grafting.

4.1.4 Surface initiated ROP from the bromoethyl groups

In the last part of the study, the bromoethyl groups of the PBEMA microspheres were also employed as initiator for ring opening polymerization (ROP) of 2-methyl oxazoline (MeOx) as given in reaction (4.4). Alkyl halides are known to polymerize also oxazoline monomers [155]. Since polymer of MeOx is precursor for linear polyethyleneimine, its grafting from the surface of PBEMA microspheres allows preparing amine functional surface grafts. The grafting in this study was simply achieved by heating cross-linked PBEMA sample with MeOx in the presence acetonitrile as solvent at 110 ^{o}C.

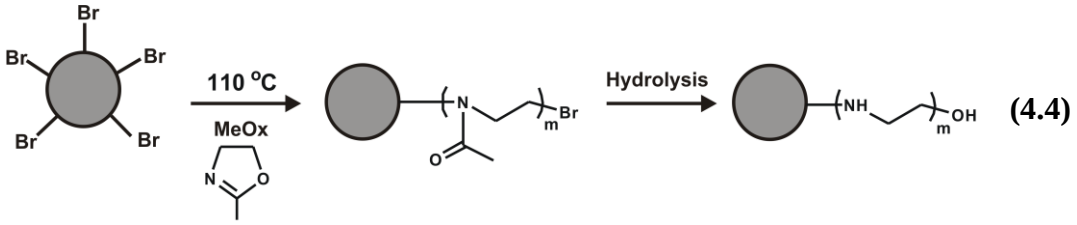

(4.4)

The mass increase in the reaction product indicated 62 % of grafting yield. FT-IR spectrum of the product in Figure 4.6-b clearly shows carbonyl stretching vibration band of the N-acetyl group at 1630 cm^{-1}, indicating presence of poly(N-acetyl ethyleneimine) grafts in the resulting product. Comparing with FT-IR spectrum of starting bead product in Figure 4.6-a, the characteristic bands originating from C=O and C-O vibrations of the methacrylate ester groups remain unchanged at the same positions.

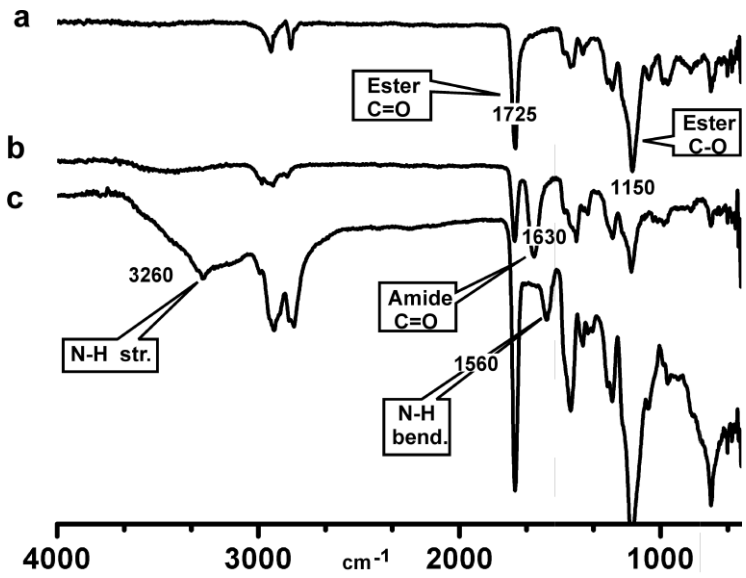

Figure 4.6: FT-IR spectrum of PBEMA microspheres before (a), after surface grafting with MeOx (b), and its hydrolysis product with poly(ethyleneimine) brushes(c).

Kinetics of the ring opening polymerization of MeOx is first order with a rate constant of k = (7.2 ± 0.01) $\times 10^{-7}$ s^{-1}as inferred from slope of the straight line (regression factor, R = 0.993) in Figure 4.7. As a result, the successful grafting in both cases implies sufficient reactivity of the bromoethyl groups of PBEMA microspheres for surface initiated ATRP of GMA and ROP of MeOx.

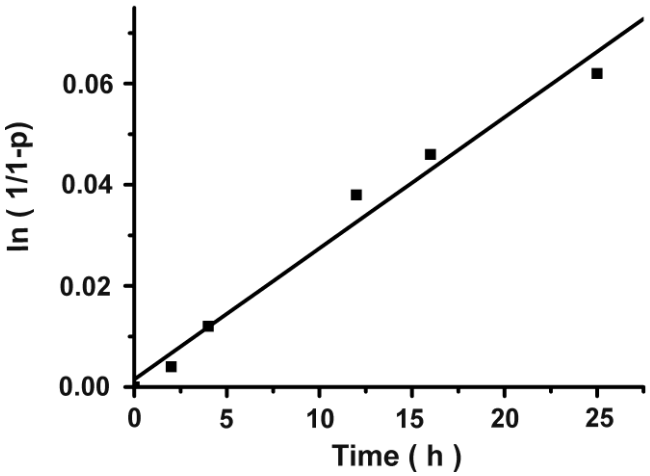

Figure 4.7: First order kinetic plot for the surface initiated ring opening polymerization of MeOx at 110 ^{o}C.

The microspherical product with PMeOx surface grafts were then subjected to acid hydrolysis. However, the original procedure of Jeong et al. [156] given for hydrolysis of linear PMeOx did not result in complete hydrolysis. The complete hydrolysis of

the PMeOx grafts however, was achieved by boiling with HCl solution (4.0 M) for 48 h and following neutralization with NaOH solution.

FT-IR spectrum of the hydrolysis product in Figure 4.6-c does not show the carbonyl vibration at 1630 cm^{-1} that indicates removal of the acetyl groups by hydrolysis. New peaks originating from stretching and plane bending vibrations of the amino groups appear respectively at 3250 and 1560 cm^{-1}. The unchanged C=O and C-O vibrations of the methacrylate ester groups in this spectrum implies selective hydrolysis of the acetamido groups in the PMeOx grafts to give PBEMA-g-polyethyleneimine structure.

Acid titration of this product revealed an amino group density of 5.75 $mmol \cdot g^{-1}$. By assuming full hydrolysis of the N-acetyl ethyleneimino groups of the graft chains, this corresponds to a 65 % of the grafting, in the ROP of MeOx which is slightly greater than the one estimated by the mass increase (62 %).

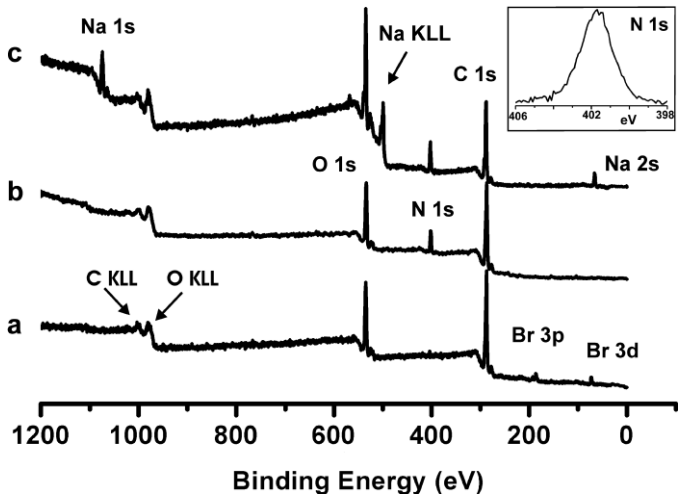

Figure 4.8: Full scale XPS of PBEMA microspheres before (a), and after grafting with PMeOx and hydrolysis product of the later (c). N 1s core level centered at 402 eV is given (inset).

Moreover, transformation of PMeOx surface grafts was also evidenced by XPS using Al Kα as excitation source. The sample possessing PMeOx surface brushes exhibits typical N 1s core level at 402 eV in its XPS (Figure 4.8-b). This peak appears at the same position after hydrolysis as expected (Figure 4.8-c). Presence of the nitrogen core level peak is also evidence for occurrence of the grafting with MeOx and successful hydrolysis yielding poly(ethyleneimine) brushes.

Unexpected sodium peaks appeared at 1074, 500 and 66 eV in Figure 4.8-c (corresponding to Na 1s, Na KLL and Na 2s levels respectively), are due to the contamination of NaOH solution used for neutralization of the acid-hydrolysis product. Retaining of the sodium even after successive washings with water might be due to reduced hydropohilicity of the poly(ethyleneimine) chains after neutralization with NaOH solution. Thereby, some trace of NaOH remains in the collapsed graft chains.

To inspect variation of the surface characteristics and shapes of the PBEMA microspheres in the surface grafting processes, SEM pictures of the products were taken and compared with that of the starting material (Figure 4.9).

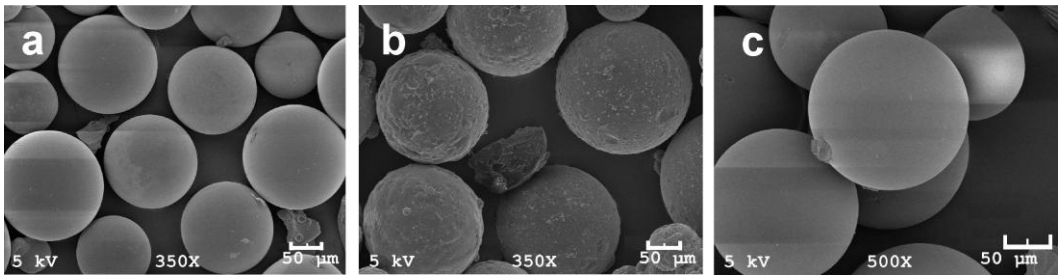

Figure 4.9: SEM images of the bare PBEMA microspheres (a), and their surface grafted counterparts with PGMA (b), and PMeOx (c).

Figure 4.9-a shows spherical PBEMA microparticles with smooth surface. The size enlargement of the particles is observed after grafting with PGMA while retaining the bead shapes, as seen in Figure 4.9-b. The reason for the roughness of the particle surfaces is unclear, but this might be due to high grafting with GMA. In the case for the sample with PMeOx surface grafts, the SEM picture (Figure 4.9-c) shows a slight increase in diameters of the particles and the surfaces as smooth as the virgin particles.

4.2 Synthesis of P(S-DVB) microbeads with epoxy functional brushes as enzyme carrier

Functional hairy poly(styrene-*b*-glycidylmethacrylate) (P(S-GMA)) brushes were generated by grafting from bromoacetylated poly(styrene-divinylbenzene) (P(S-DVB)) microspheres via surface initiated-atom transfer radical polymerization, (SI-ATRP). Two different approaches for the covalent immobilization of lipase onto microspheres were studied for the first time, direct immobilization of lipase to the

polymer brushes via their epoxy groups and immobilization of lipase via glutaraldehyde coupling after attachment of spacer arm (Hexamethylendiamine (HMDA)) to the polymer brushes.

The covalent immobilization of the lipase on microspheres after spacer-arm attachment and glutaraldeyhde coupling was found to be the most effective that of direct binding method. In this case, a maximum value of the immobilized enzyme activity 498.5 $U.g^{-1}$ was found with an enzyme loading of 27.6 mg per gram support. Thermal and storage stabilities were found to increase upon immobilization on the P(S-DVB)-*g*-P(S-GMA)-HMDA-GA microspheres. Finally, esterification reactions have been performed to produce ethyl acetate and iso-amyl acetate in solvent-free system and in n-hexane using lipase immobilized P(S-DVB)-*g*-P(S-GMA)-HMDA-GA microspheres. The immobilized lipase was effectively reused in successive batch runs in solvent-free system for iso-amyl acetate synthesis and the activity lost was only 21% after 10 cycles.

4.2.1 Properties of the functionalized microspheres

The crucial task in surface initiated ATRP is generation of the initiation sites on the solid surface. This can be carried out either by surface modification with suitable reagents possessing haloalkyl functionality or by preparation of the solid support using appropriate functional co-monomer. The linkage between solid core and initiator group is also important. Non-hydrolysibility of this linkage is preferable when the resulting functional material is to be processed under harsh conditions. Attachment of the initiator groups by ester linkage is common approach and has been widely employed by many authors [54, 157]. However, hydrolysis of this bond chemically or enzymatic means deters the use of this approach when the hairy carrier polymer is considered to recycle and reuse.

Taking these into consideration, in this work, the initiator group was introduced to the solid core by an alternative way in which chloromercurated surface of the P(S-DVB) microspheres was reacted with bromoacetyl bromide. The resulting bromoacetyl group was utilized as initiating points. Since the initiator group is being connected with the support and graft chains by C-C linkages, any leakage of graft chains from the support is avoided. This makes the material recyclable and reusable.

The length of the graft chain is also important to increase mobility of the graft chains and rate of the reactions as well. The reaction rates of the functional groups increase by increasing distance from the bead core as evidenced by many authors and this has been termed as spacer chain effect. Taking peculiarities of the spacer chain, first PS was grafted to the P(S-DVB) resin and P(GMA) was then introduced by followed ATRP from terminal bromoalkyl groups of the PS grafts (reaction 4.5).

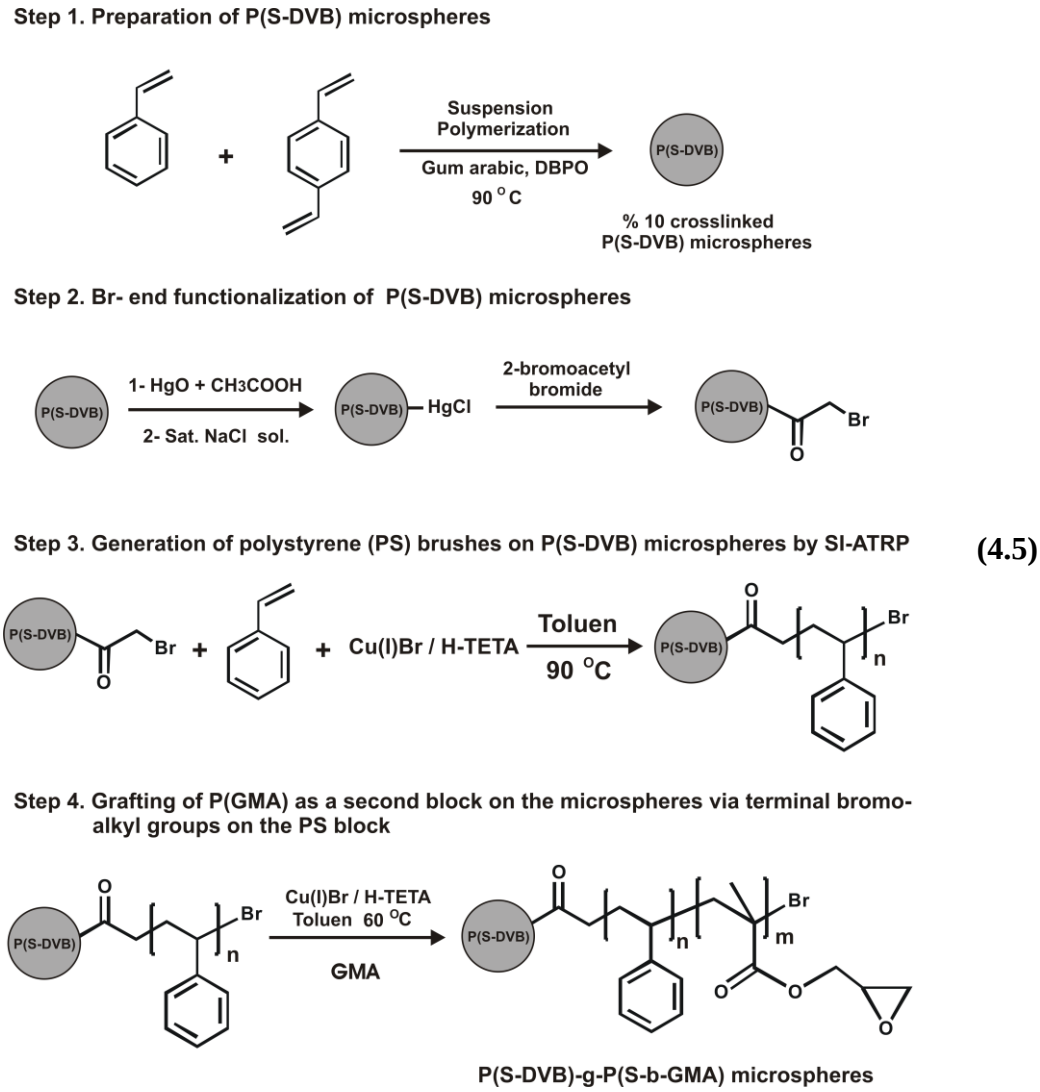

(4.5)

The chemical transformations in each step were followed by monitoring characteristic bands in FT-IR spectra of the products (Figure 4.10). In the spectrum of P(S-DVB-Br) (the product of Step 1; Figure 4.10-a) bearing bromoacetyl groups, typical stretching vibration band of the carbonyl (C=O) group is observed at 1719 cm^{-1} as a weak band. Apparently, low intensity of this band is due to low density of this group in the structure. Also, a very weak band associated with C-Br vibration is observable at 795 cm^{-1}. After grafting with PS (i.e., P(S-DVB)-*g*-PS; the product of

Step 2; Figure 4.10-b) the later becomes almost invisible which can be ascribed to its consumption by utilization in the grafting with styrene. However, the carbonyl band vibration at 1719 cm^{-1} becomes also invisible, due to the decreasing percentage of this group.

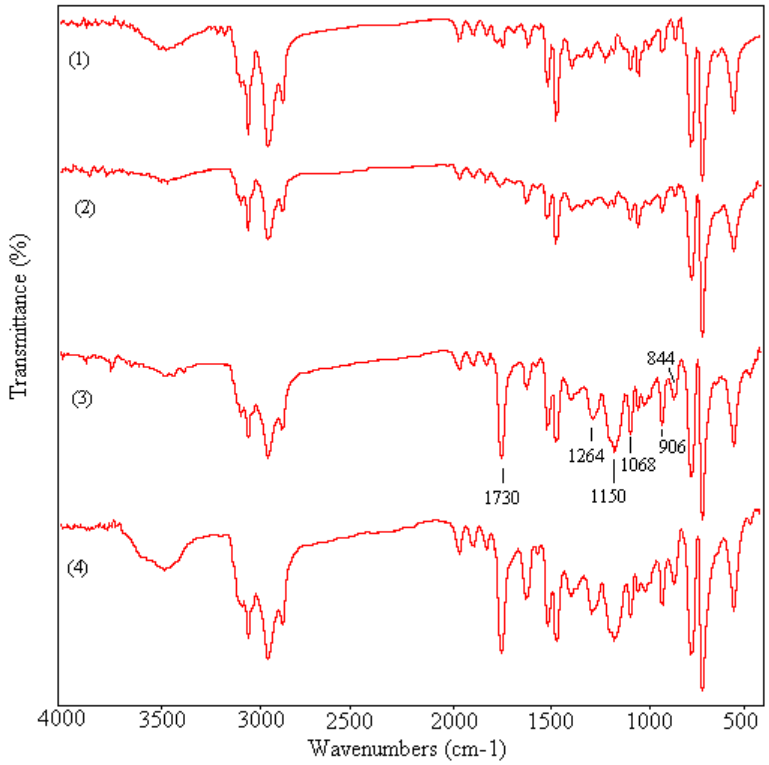

Figure 4.10: (a) P(S-DVB)-Br (the product Step 1; P(S-DVB)-Br); (b) polystyrene grafted (S-DVB) (the product Step 2; P(S-DVB-*g*-(PS)-Br); (b) the second block P(GMA) grafted on to the first styrene block (the product of Step 3; P(S-DVB)-*g*-P(S-GMA) and (d) Spacer-arm attached P(S-DVB)-*g*-P(S-GMA)-HMDA.

After additional grafting with GMA, typical methacrylate ester vibrations are observed at 1725, 1255 and 1150 cm^{-1} (which are associated with stretching vibrations of carbonyl, CO-O and COO-C bonds respectively) (the product of Step 3; Figure 4.10-c). The typical bands arising from the epoxy functionality are not discernible around 1000 cm^{-1}, because this region is overcrowded contains many bands. Nevertheless, the shoulder around 1170 cm^{-1} can be ascribed to C-O-C stretching vibration of the epoxy group. However, decreasing intensity of this band after modification with the amino compound implies that this band comprises also the vibration of glycidylic ether group. Another change is observed at 3100-3500 cm^{-1} range can be considered as O-H vibration band arising from ring opening of the epoxy function (Figure 4.10-d). The FTIR spectra of P(S-DVB)-*g*-P(S-GMA)-

HMDA have also the characteristic N-H amine stretching bands at between 3500 and 3300 cm^{-1} (the bands more broadened and expended after attachment of 1,6 diaminohexane) and 1600 cm^{-1}.

Scanning electron microscopy (SEM) micrographs presented in Figure 4.11 shows a smooth surface structure of the P(S-DVB)-*g*-P(S-GMA)-HMDA microspheres. The non-porous surface properties of the microspheres would reduce diffusion limitation of the substrate and product during enzymatic hydrolysis and esterification reactions.

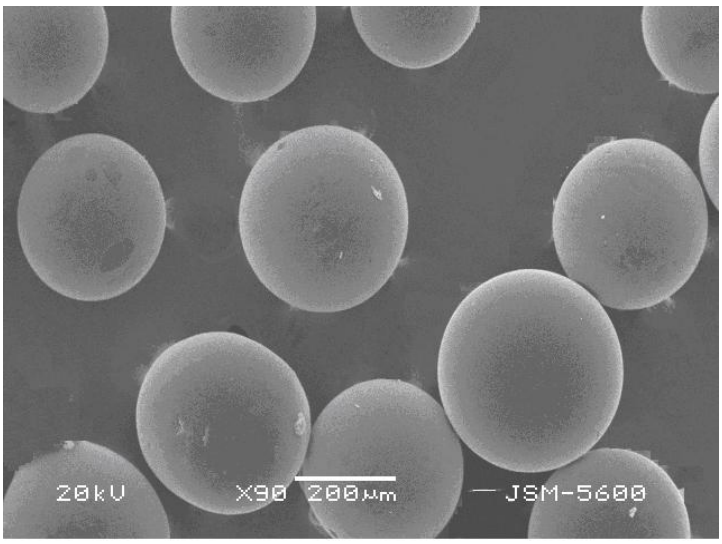

Figure 4.11: Scanning electron micrograph images of P(S-DVB)-*g*-P(S-GMA) microspheres.

The specific surface area of the P(S-DVB)-*g*-P(S-GMA) microspheres was measured by BET method and was found to be 12.3 $m^2 g^{-1}$ microspheres. The amount of epoxy groups on the P(S-DVB)-*g*-P(S-GMA) microspheres was determined to be 0.18 mmol per gram g microspheres. The amino group content of the P(S-DVB)-*g*-P(S-GMA)-HMDA microspheres was fond to be 0.32 mmol g^{-1} microspheres, respectively.

4.2.2 Immobilization of lipase on the P(S-DVB)-*g*-P(S-GMA) based microspheres

Polymer brushes offer certain advantages over other materials as they are covalently anchored to the substrate providing excellent mechanical stability and present high surface area template with functionality controllable by monomer type and brush length. The epoxy groups of P(GMA) coated onto styrene grafted P(S-DVB)-*g*-P(S) microspheres, (i.e., P(S-DVB)-*g*-P(S-GMA)), were converted into amino groups by

the reaction with 1,6 diaminohexane, P(S-DVB)-*g*-P(S-GMA)-HMDA. The aim was to determine an efficient relationship between enzyme and support by moving the enzyme away from the surface of the microspheres, via incorporation of spacer-arms. Lipase was then covalently immobilized on both P(S-DVB)-*g*-P(S-GMA) and spacer-arm-attached and glutaraldehyde activated P(S-DVB)-*g*-P(S-GMA)-HMDA microspheres.

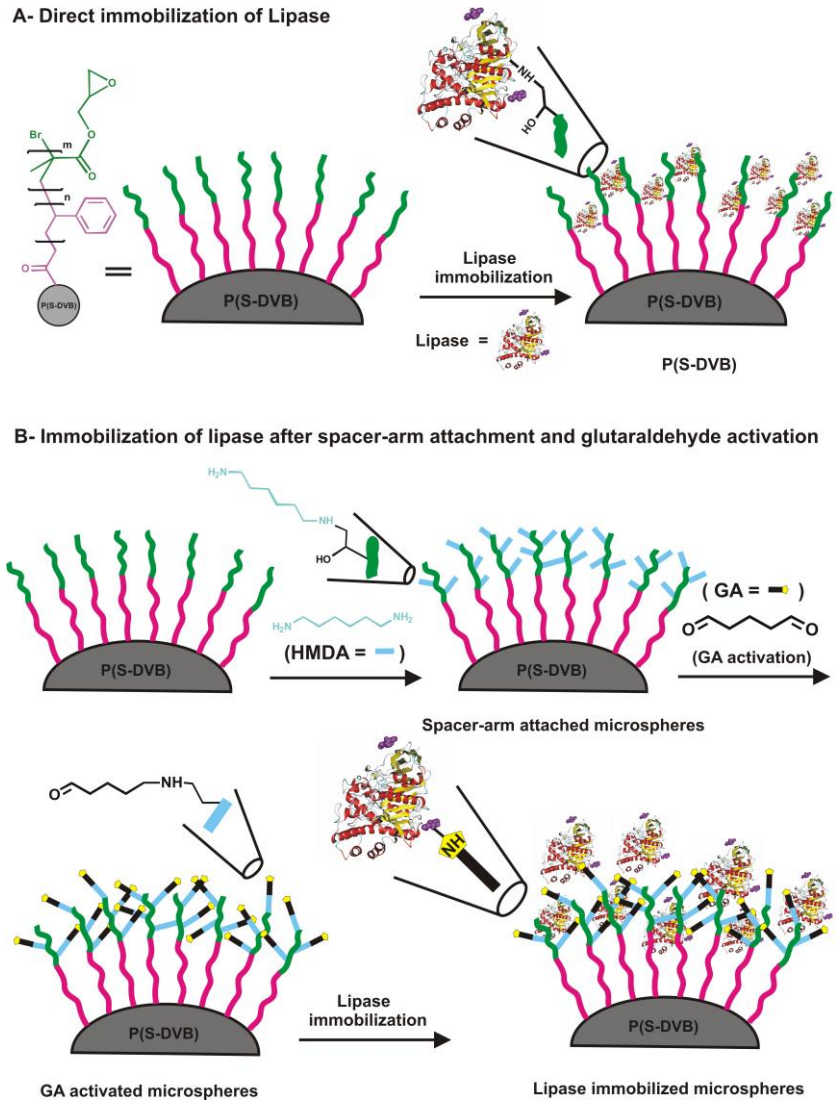

(4.6)

In the direct method in the reaction (4.6), lipase was immobilized on the P(S-DVB)-*g*-P(S-GMA) microspheres via a coupling reaction between the free amino groups of enzyme and epoxy groups of the support. In the case of P(S-DVB)-*g*-P(S-GMA)-HMDA-GA microspheres (S), the coupling reaction between amine groups of the enzyme and aldehyde groups of the supports, could be considered via shift base formation. Glutaraldehyde can readily react with amino groups; therefore, the

aldehyde group content should be close to the amino group content on the microspheres. The -SH groups of lipase can also react with glutaraldehyde after the amine groups have been used. It is important to note that -NH_2 groups are more liable than -SH groups to react with glutaric dialdehyde. Most proteins contain many lysine residues, usually located on the protein surface (i.e., exposed to the aqueous medium) because of the polarity of the amine group.

In addition, lysine residues are generally not involved in the catalytic site, which allows moderate covalent linkage to preserve protein conformation and thus biological activity [158]. In addition, the attachment of spacer-arm (i.e., 1,6-diaminohexane) to the P(S-DVB)-*g*-P(S-GMA) microsphere surface could prevent undesirable side interactions between large enzyme molecules and support. In this way, more areas for the immobilized lipase could become accessible to lipid substrate. The attachment of the spacer-arm was resulted an increase in the apparent activity of the immobilized lipase with respect to the enzyme immobilized via the direct epoxy groups coupling. The maximum lipase immobilization capacities of the P(S-DVB)-*g*-P(S-GMA) and P(S-DVB)-*g*-P(S-GMA)-HMDA-GA microspheres were 19.3 and 27.6 mg g^{-1}, respectively. The retained activity yield of the lipase immobilized on the spacer-arm-attached microspheres was about 84.8%, and it was 62.1% for the enzyme immobilized through epoxy groups. The measured specific activity of the free lipase was 21.3 U mg $protein^{-1}$. The specific activity of lipase immobilized on P(S-DVB)-*g*-P(S-GMA)-HMDA-GA microspheres was 498 U g^{-1} microspheres. Without spacer arm, the lipase, in attempting to maximize its contact with the surface, could lose its active conformation, and consequently, low specific activity (255 U g^{-1} microspheres) results.

The spacer-arm attached P(S-DVB)-*g*-P(S-GMA)-HMDA microspheres itself possessed good enzyme immobilization capacity 27.6 mg protein g^{-1} microspheres. However, the relative of the immobilized lipase on spacer-arm attached and glutaraldehyde activated support was about 22.7% higher than that of the lipase immobilized directly on the P(S-DVB)-*g*-P(S-GMA) via epoxy group coupling. The improvement could be attributed to the physical and chemical changes that occurred as a result of the spacer-arm attachment and glutaraldehyde activation. Recalling that the spacer-arm and coupling agent (i.e., HMDA and glutaraldehyde, respectively) have six- and five-carbon length and it should act as an extra total

eleven-carbon spacer length in this immobilization method. Thus, the external hydrophobic amino acid residues on the enzyme molecule could not interact too much with hydrophobic polystyrene surface as compared to direct coupling of lipase on the microspheres surface. By incorporating the eleven-carbon spacer-arm on the P(S-DVB)-*g*-P(S-GMA) microspheres, a decrease in the surface hydrophobicity also resulted to further contribute to the improvement in lipase immobilization.

All these factors resulted in better immobilization of lipase on the spacer-arm attached microspheres. In this respect, the polystyrene chain would contribute to a higher hydrophobicity of P(S-DVB)-*g*-P(S-GMA) but the effect would be off set by the amino groups of spacer-arm, which is hydrophilic in nature. As reported previously, too strong hydrophobic functional group should also be avoided as it is reported to be responsible for significant loss of lipase enzymatic activity [159]. Therefore, the rest of the immobilization study was carried out using the P(S-DVB)-*g*-P(S-GMA)-HMDA-GA microspheres.

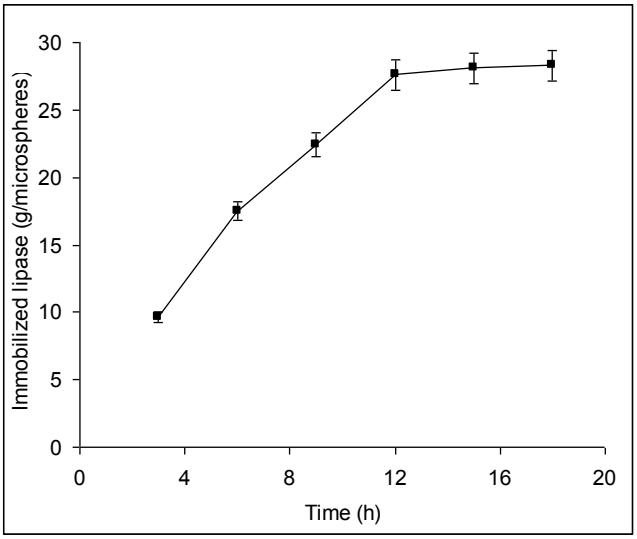

Figure 4.12: Effect coupling duration time on the immobilization efficiency of the lipase on the P(S-DVB)-*g*-P(S-GMA)-HMDA-GA microspheres.

The effects of enzyme coupling time on the immobilization capacity were studied with P(S-DVB)-*g*-P(S-GMA)-HMDA-GA microspheres and are presented in Figure 4.12. An increase in the coupling duration time led to an increase in the immobilization efficiency (from 9.6 to 27.6 mg g^{-1} microspheres) but this relationship leveled off at around 12.0 h. Further increase in the coupling duration time (up to 18 h) did not lead to a significant change in the immobilization capacity.

4.2.3 Effect of pH and temperature on the free and immobilized lipase activity

The effect of pH on the activity of the free and immobilized lipase on the P(S-DVB)-*g*-P(S-GMA)-HMDA-GA was studied at 40 ◦C in the pH range between 4.0 and 9.0. The optimum pH of free lipase was 7.5, which corresponds closely to the optimum found for immobilized lipase, which is 8.0 (Figure 4.13). The pH profile of the immobilized lipase also closely follows that of free lipase. This shift depended on the method of immobilization as well as the structure of the matrix. It should be noted that the shift to neutral and basic region of the optimal pH upon immobilized could be expected as a result of the diffusional constraint of the support retaining a higher concentration of enzyme product, fatty acids, on the surface of the microspheres that immobilized lipase present.

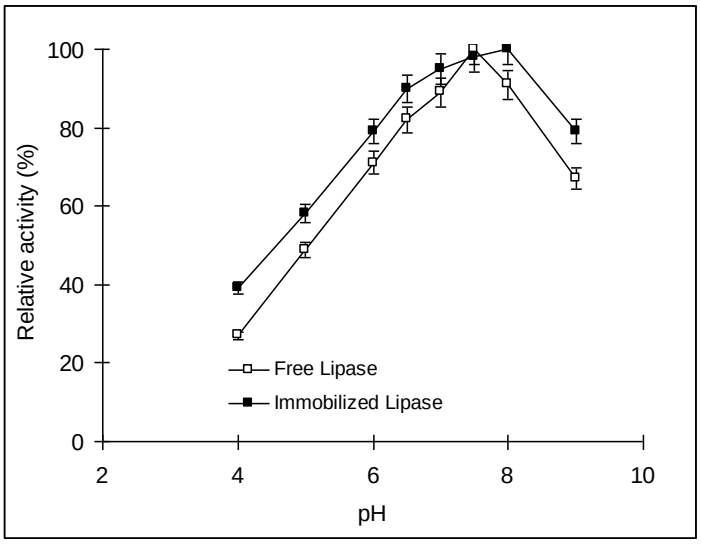

Figure 4.13: Effect of pH on the activity of free and immobilized lipase on the P(S-DVB)-*g*-P(S-GMA)-HMDA-GA microspheres; the relative activities at the optimum pH were taken as 100% for free and immobilized lipase, respectively.

It should noted that additional interaction of the support with enzyme due to the presence of amino functional groups on the spacer arm might have also reduced the sensitivity of enzyme to less alkaline pH. This charged group would have better interactions with the hydrophilic sites on the lipase molecule while the hydrophobic sites were still available for catalyzing the esterification reaction. As previously reported, the hydrophobic sites of the lipase molecule are mainly responsible for the catalytic activity [160-162]. The changes in the activity profile of the immobilized enzyme compared to free enzyme could probably be attributed to the stabilization of

lipase molecules resulting from multipoint covalent attachment on the surface of the hydrophobic/hydrophilic microspheres, which limited the transition of enzyme conformation against the change of pH. Other researchers have reported similar observations upon immobilization of lipase and other enzymes [163, 164].

The effect of temperature on the free and immobilized enzyme activity was investigated in phosphate buffer (0.1 M, pH 7.5) in the temperature range 20–60°C. The apparent temperature optimum for free enzyme was about 40°C, while that for the immobilized enzyme and the form stabilized by immobilization was about 45°C (Figure 4.14). In the literature, most immobilized lipases exhibited higher optimum temperature values than their free counterpart [165, 166].

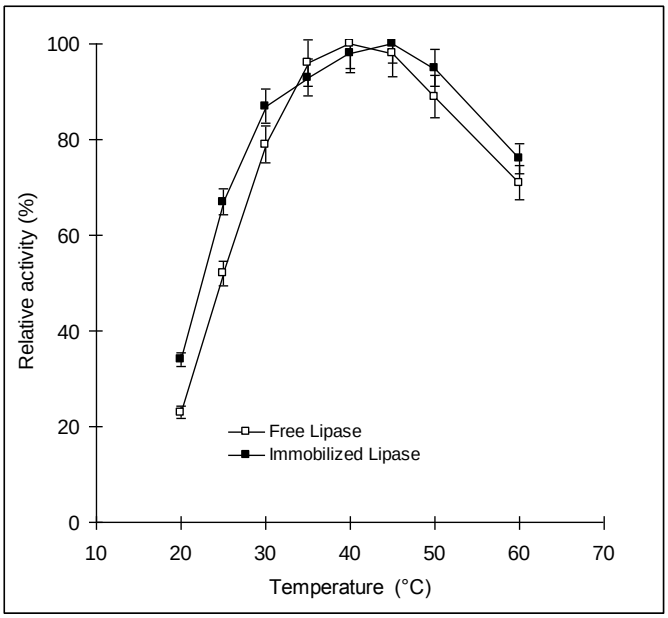

Figure 4.14: Effect of temperature on the activity of the free and immobilized lipase on the P(S-DVB)-*g*-P(S-GMA)-HMDA-GA microspheres; the relative activities at the optimum temperature were taken as 100% for free and immobilized lipase, respectively.

The multi-point covalent attachment of the lipase molecule on the microspheres surface via glutaraldehyde coupling could reduce the conformational flexibility of the enzyme and might result in higher activation energy for the molecule to reorganization to a proper conformation for the binding to its large substrate (i.e., oil olive). Thus, the immobilized lipase showed its catalytic activity at a higher reaction temperature compared to that of the free counterpart.

4.2.4 Kinetic parameters of the free and immobilized lipases

The K_m value was known as the criterion for the affinity of enzymes to substrates, and the lower value of K_m represented the higher affinity between enzymes and substrates. In this work, kinetic constants of free and immobilized lipase, i.e. K_m and V_{max} values were determined by using tributyrin as substrate. The activities of the free and immobilized lipase for various concentrations of the substrate (5–50 mM) were plotted in Lineweaver–Burk plots, and K_m and V_{max} values were calculated from the intercepts on *x*- and *y*-axis, respectively.

The kinetic data for hydrolysis of tributyrin was fitted to the Michaelis-Menten equation. For the free and immobilized lipase the apparent K_m values were found to be 22.7 and 34.3 mM, respectively. The K_m value of immobilized lipase was the same order of magnitude, and was only 1.15 times higher than that of the free enzyme. The V_{max} values for the free and immobilized lipase were calculated as 23.4 and 20.3 U mg^{-1} enzyme, respectively. The V_{max} value of the immobilized enzyme decreased about 1.5-fold compared to the free enzyme.

These results indicated that the presented immobilization method changed the reaction velocity and substrate affinity of the *R. miehei* lipase. Several reasons can account for the variations of the V_{max} values of the enzyme upon immobilization [167, 168]. These variations are attributed to several factors such as the covalent attachment of the enzyme molecule on the microspheres surface might have induced an inactive conformation to the enzyme molecules.

It should be noted that the immobilization process does not also control the proper orientation of the immobilized enzyme on the support. This improper fixation and/or the change in the property of the active sites might hinder the active site for binding of substrates (i.e., tributyrin) to the immobilized lipase molecules.

The efficiency factor η can be calculated (reaction (4.7)) from the maximum reaction rates of the immobilized enzyme over that of the free counterpart:

$$\eta = v_{immobilized} / v_{free} \qquad \textbf{(4.7)}$$

where $v_{immobilized}$ and v_{free} was the reaction rate of the immobilized and free enzyme, respectively. From this calculation, nano-structured microspheres-enzyme system provided an efficiency factor of 0.87 for the immobilized lipase. The ratio A_{max}/K_m

defines a measure of the catalytic efficiency of an enzyme–substrate pair. In this study, the catalytic efficiencies (A_{max}/K_m) of the free and immobilized lipase were found to be 10.3 and 5.9, respectively. The catalytic efficiency of lipase was decreased about 1.7-fold upon immobilization.

Lipases have a higher level of hydrophobicity than conventional proteins, and the total percentage of hydrophobic amino acid residues (i.e., Ile, Leu, Val, Met, Tyr, Phe) in lipases isolated from various microbial sources is varied between 28% and 33% [163]. The lipases have inherent affinity toward hydrophobic media, and the hydrophobic / hydrophilic nature of the di-block polymer grafted and aminated supports could provide a proper micro-environment for lipase, and thus, reasonable retained immobilized lipase activities were obtained with the presented support-enzyme system. The retained lipase activity was obtained up to 84.8% in this study, and is comparable with the related literature [169, 170].

4.2.5 Thermal stability of the free and immobilized lipase

The effect of temperature on the stability of the free and immobilized lipase is shown in Figure 4.15. The pattern of heat stability indicated that a smaller rate of thermal inactivation was observed for the immobilized lipase on the P(S-DVB)-*g*-P(S-GMA)-HMDA-GA microspheres than that of the free enzyme. At 55 °C, the free enzyme lost about 78% its initial activity after 120 min of heat treatment, while the immobilized enzyme showed significant resistance to thermal inactivation (lost about 17% of its initial activity in the same period). At 65 °C, the free lipase lost all its initial activity after 75 min heat treatment. Under the same conditions, the immobilized lipase retained about 41% of its initial activity.

As in this figure, the free enzyme at 55 and 65 ºC led to a steep loss of catalytic activity compared to immobilized counterpart, which is typical of most enzymes [171], whereas a marked enhancement of thermal stability was achieved with enzyme immobilization since no activity decay was observed after 60 and 15 min exposure at 55 and 65ºC, respectively. These results suggest that the thermostability of immobilized lipase becomes significantly higher at higher temperature. If the heat stability of enzymes increased upon immobilization, the potential application of these enzymes would be extended.

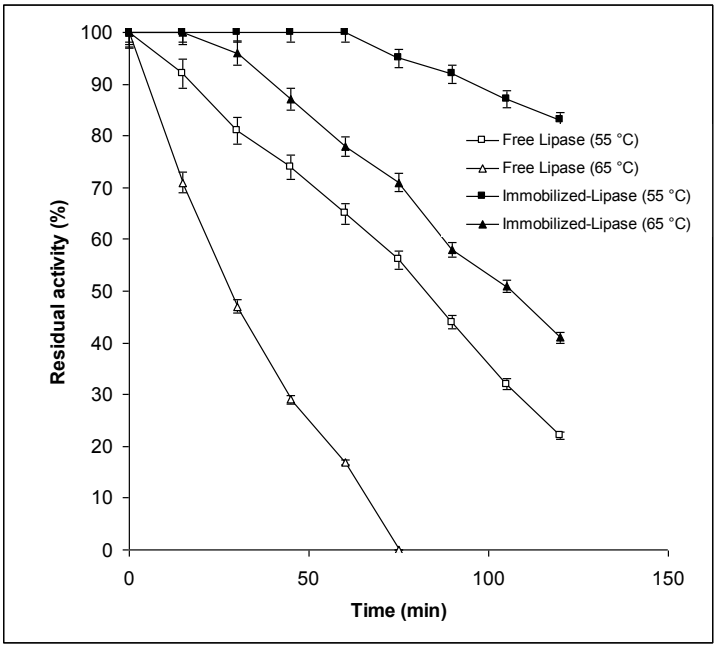

Figure 4.15: Thermal stability of the free and immobilized lipase at two different temperatures.

4.2.6 Enzymatic activity in banana esters synthesis

The biosynthesis of esters is currently of much commercial interest because of the increasing popularity and demand for natural products amongst consumer [172]. The activity of the immobilized lipase was investigated on the basis of the esterification of ethanol and iso-amyl alcohol with acetic acid to produce banana flavours (i.e., ethyl acetate and iso-amyl acetate).

The enzyme activity was defined based on the percentage of acid conversion. The optimum temperature for the synthesis of ethyl acetate from ethanol and acetic acid by immobilized enzyme, the esterification reaction was carried out at different temperatures (35-65ºC) and 1/4 acid: alcohol molar ratio. The effect of temperature on esterification reaction was presented in Figure 4.16. For ethyl acetate production, maximum ester synthesis activity was observed at 40◦C with 1/2 acetic acid: ethyl alcohol molar ratio. On the other hand, the temperature from 35 to 55◦C, there were remarkable increase in the amount of synthesized iso-amyl acetate and after 55◦C the ester synthesis yield decreased. Only 7% and 13% conversions were observed at 65ºC for ethyl acetate and iso-amyl acetate, respectively. This may be due to the thermal denaturation of enzyme.

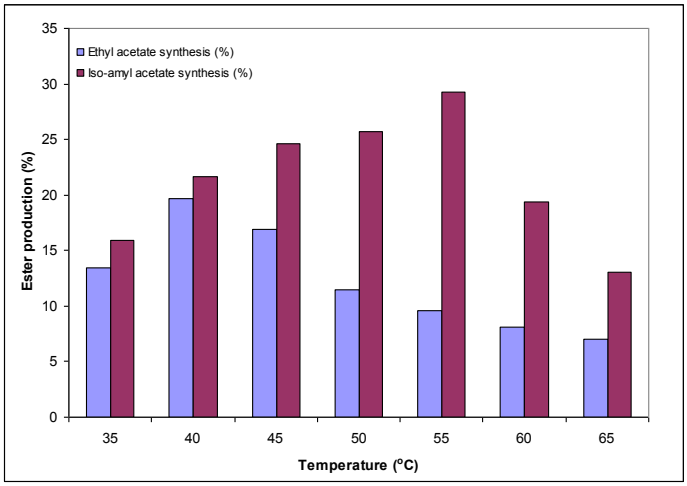

Figure 4.16: Effect of temperature on the enzymatic production of ethyl acetate and iso-amyl acetate using immobilized lipase on the P(S-DVB)-*g*-P(S-GMA)-HMDA-GA microspheres.

The effect of acid to alcohol molar ratio (i.e., acetic acid: ethyl alcohol, and acetic acid : iso-amyl alcohol molar ratio (i.e., 0.1:1.0, 0.25:1.0, 0.5:1.0, 0.75:1.0, and 1.0:1.0) at optimal temperatures for each individual ester was investigated using immobilized *Rhizomucor miehei* lipase in a solvent-free system. As seen in Figure 4.17, the highest amount of ethyl acetate was synthesized (19.7%) with 1/4 acetic acid: ethyl alcohol molar ratio. On the other hand, the amount of synthesized iso-amyl acetate increased from 13.4 to 39.7% with increasing acetic acid to isoamyl alcohol molar ratio from 0.1:1.0 to 0.75:1.0 molar ratio.

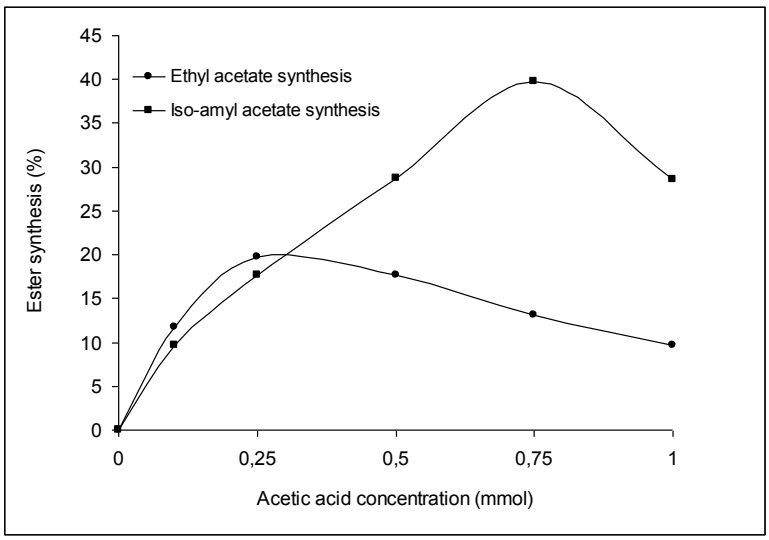

Figure 4.17: Effect of acid: alcohol ratio on the ester synthesis activity of the immobilized lipase.

As shown in Figure 4.17, the molar ratio of acid: alcohol was further increased, the conversion (%) decreased, and it could be due to the inhibition of the lipase activity by high acetic acid concentration. As previously reported, in the lipase-catalyzed esterification reaction, the first step consists of the preferential binding of the acid molecule to the enzyme molecule [169]. At high alcohol molar ratio, the high level alcohol concentration may promote the binding of alcohol molecules to the immobilized lipase, during the first reaction step, competing with the acetic acid. As a result, a decrease in the amount of bound acid occurs. Thus, this situation would lead to a decrease in the reaction rates, since the reaction will be limited by the amount of acid in the vicinity of the enzyme [173].

The synthesis of ethyl acetate by immobilized *Rhizomucor miehei* lipase was also studied in non-aqueous medium. The ethyl acetate and iso-amyl acetate synthesis experiments were carried out under 1:2 acid/alcohol molar ratio for both esterification reaction. The amount of synthesized ethyl acetate and iso-amyl alcohol was 34.6 and 59.3% in the presence of n-hexane. The amounts of the synthesized ethyl acetate and iso-amyl alcohol were increased in the presence of n-hexane compared to solvent-free systems. As reported previously, the presence of an organic solvent can shift the equilibrium towards ester synthesis by a total transfer of ester into the organic phase [171, 174]. Similar results related to the increment in the amount of ester synthesized in organic medium were reported in literature earlier. For example, Karra-Chaabouni et al. [175] produced ethyl valerate and hexyl acetate in hexane, heptane and solvent-free medium. They found remarkably higher ester yield in both hexane and heptane medium than those obtained in the absence of organic solvents.

4.2.7 Operational stability in esters synthesis

In general, enzymes are difficult to be recovered and reused. Therefore, the reusability of an immobilized enzyme is of key importance for industrial applications, and an increased stability could make the immobilized enzyme more advantageous than its free counterparts. In this study, the immobilized lipase on P(S-DVB)-*g*-(S-GMA)-HMDA was repeatedly used as the biocatalyst for the esterification reactions and subsequently recovered and reused.

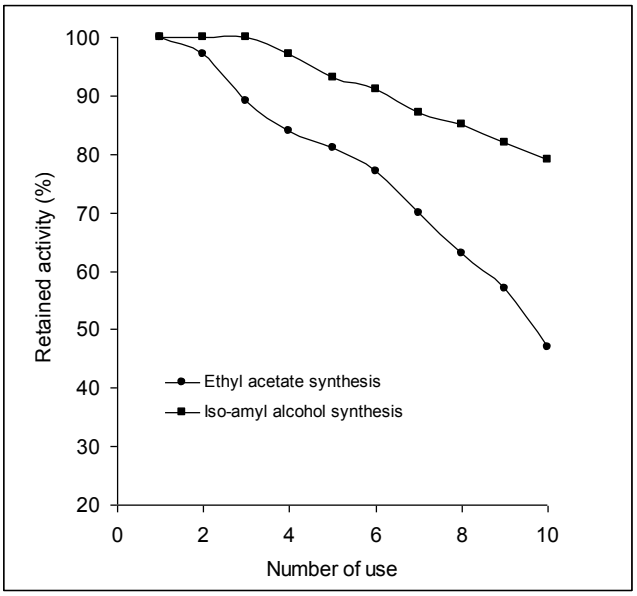

Figure 4.18: Operational stability of immobilized lipase during ethyl acetate and iso-amyl acetate synthesis. The same enzyme microspheres were used for each batch during repeated use.

As seen in Figure 4.18, the activity of immobilized enzyme slightly decreased as the number of reuses increase.The same activity values for iso-amyl acetate synthesis were obtained within the first 3 cycles. In this case, the activity retention of the enzyme immobilized for iso-amyl acetate synthesis was found to be slightly better than that of the ethyl acetate synthesis. As seen in this figure, immobilized enzyme was retained 47% and 79% its initial activity during synthesis of ethyl acetate and iso-amyl alcohol after 10 cycles of use, respectively, possibly resulting from the inactivation of lipase upon use. This result showed that lipase immobilized on the nano-structured microspheres could be used successfully for industrial applications requiring long-term reaction stability. Thus, this immobilization method led to increased enzyme reusability.

4.3 Modification of poly(divinylbenzene) microspheres by hydrobromination-Click chemistry protocol and their protein adsorption properties

Hydrophobic and/or hydrophilic polymer grafted poly(divinylbenzene) (PDVB) microspheres were synthesized by the combination of hydrobromination and the click chemistry processes. First, PDVB microspheres, prepared by precipitation polymerization, were azide functionalized by successive hydrobromination and azidation processes. Alkyne functional polymers, namely poly(methyl methacrylate)

(Alkyne-PMMA) and poly(*tert*-butyl acrylate) (Alkyne-P*t*BA), and poly(ethylene glycol) (Alkyne-PEG) were prepared by atom transfer radical polymerization (ATRP) and esterification reaction, respectively. Finally, azide functionalized microspheres were coupled with alkynylated polymers with high efficiency by copper catalyzed azide-alkyne click reactions. . Finally, use of microspheres as the support matrix for the reversible protein immobilization via adsorption is investigated. The system parameters such as adsorption conditions (i.e., enzyme concentration, medium pH) and desorption were studied and evaluated with regards to the biocatalytic activity and adsorption capacity (reaction 4.8).

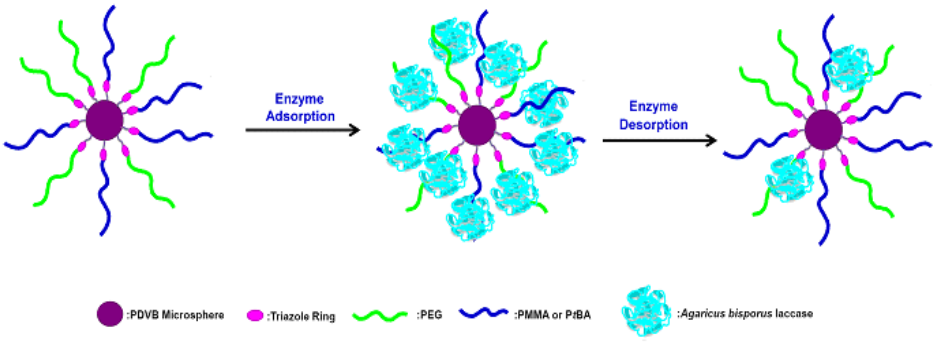

(4.8)

4.3.1 Synthesis of PDVB microbeads by precipitation polymerization method and its azide functionalization

Nearly monodisperse (~2.5 μm), spherical PDVB beads were prepared by precipitation polymerization technique and the residual double bonds on the surface were activated to primary bromine by anti-Markovnikov addition of hydrogen bromide according to the procedure described in the literature [144]. After the reaction, the brominated particles with 1.46 mmol/g of bromine content (estimated by titration method [176] were obtained. Ethyl bromide groups formed this way were then converted into azide functions by condensation with NaN_3 in DMF solution (reaction (4.9)).

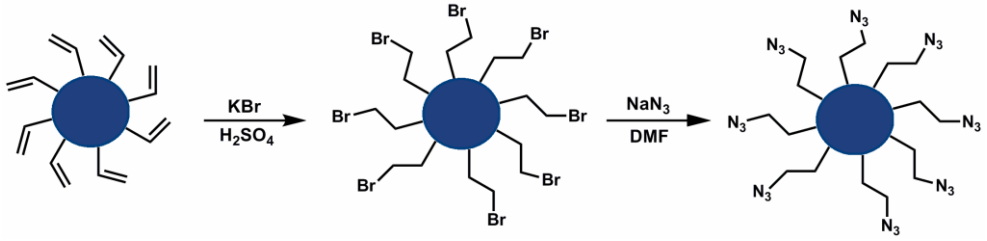

(4.9)

The magnified photo-images of the starting bead polymer and its derivatives obtained by the modification in each steps show nearly perfect microspheres (Figure 4.19).

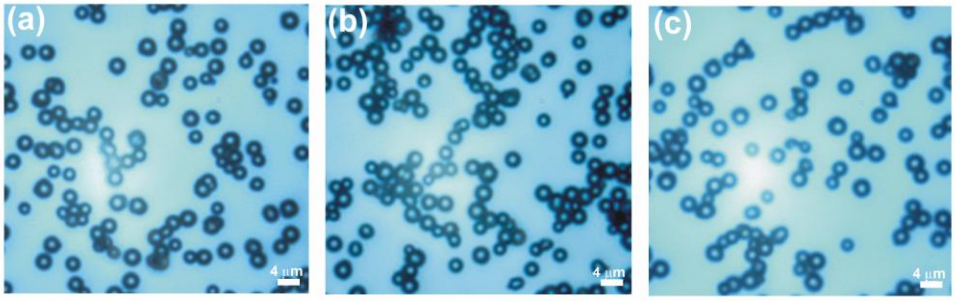

Figure 4.19: Optical microscope image of PDVB (a), brominated PDVB (b), azide functionalized PDVB microspheres (c).

The chemical transformations in each step were monitored by FT-IR spectroscopy. Typical stretching vibration band of the vinyl groups is observed at 1628 cm^{-1} and other peaks at 1405, 1014 and 989 cm^{-1} are associated with plane and out of plane deformation bands of =C-H group (Figure 4.20).After addition of HBr, these peaks are almost invisible in the FT-IR spectrum, indicating high yield of transformation in this step. A new peak appeared at 1172 cm^{-1} can be ascribed to C-Br stretching vibration. In the FT-IR spectrum of azidated sample this peak disappears completely and characteristic vibration band of N_3 group is observed as a sharp peak at 2100 cm^{-1}. These results establish occurrence of the proposed transformation in each step and presence of azide functions on the bead particles.

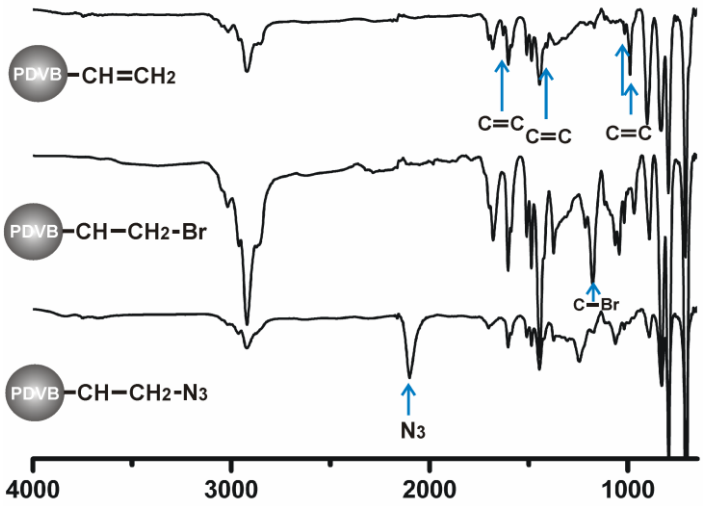

Figure 4.20: FT-IR spectra of bare PDVB, hydrobrominated PDVB and azido functional PDVB spherical beads.

4.3.2 Preperation of alkyne terminal polymers

Alkyne terminal PEG-2000 and PEG-5000 were successively prepared by a simple esterification reaction between hydroxy terminal PEG and 4-Pentynoic acid. The other two alkyne polymer, PMMA and P*t*BA, were obtained via ATRP technique by using alkyne functional initiator. The results and conditions for the preparation of alkyne functional polymers were summarized in Table 4.2.

Table 4.2: Preparation of alkyne functional polymers.

Polymer	Method	Time (min)	Conv.[d] (%)	M_{ntheo}[e] (g/mol)	M_{nGPC}[f] (g/mol)	M_w/M_n[f]
Alkyne-P*t*BA[a]	ATRP	60	32	4100	5130	1.30
Alkyne-PMMA[b]	ATRP	20	35	3800	5400	1.20
Alkyne-PEG1[c]	Esterif.	overnight	75	-	5430	1.02
Alkyne-PEG2[c]	Esterif.	overnight	93	-	2440	1.02

[a] $[M]_0/[I]_0/[CuBr]_0/[PMDETA]_0$ =100/1/1/1, T = 80 °C
[b] In Toluene, $[M]_0/[I]_0/[CuCl]_0/[PMDETA]_0$ = 100/1/1/1, T = 80 °C.
[c] Polymers were synthesized by the esterification reaction between 4-pentynoic acid and poly(ethylene glycol) monomethyl ether at room temperature.
[d] Determined by gravimetrically.
[e] Calculated by using $M_{n\ theo} = ([M]_0/[I]_0 \times (\%)\ Conv. \times 100 + M_{wI})$
[f] Determined by GPC based on polystyrene standards.

4.3.3 Grafting of the polymers onto surface via Click chemistry

The click reaction (reaction (4.10)) was performed using Cu(I) catalyst in DMF at 40 °C. After the coupling reaction, polymer grafted PDVB microspheres could be easily collected by centrifugation. The catalyst and the excess polymers were removed by washing DMF, dilute acidic methanol and THF.

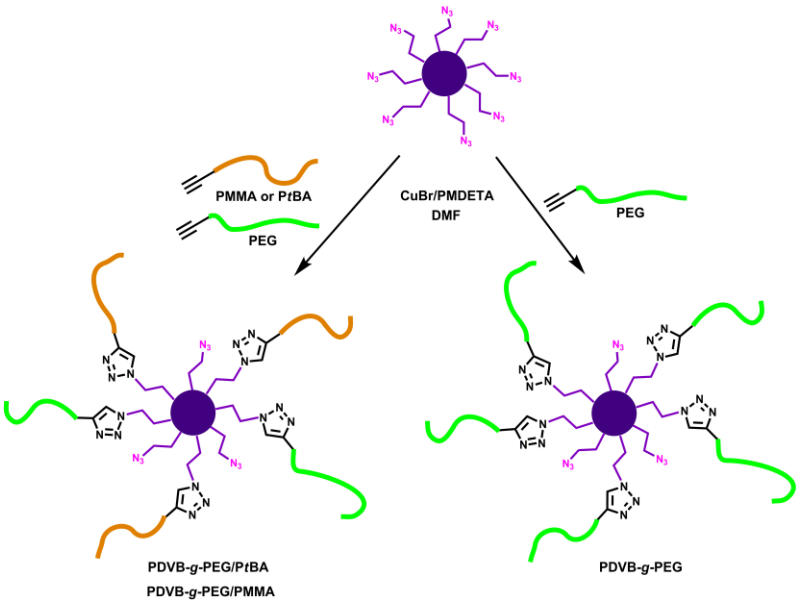

(4.10)

Polymer grafted microspheres were characterized by FT-IR (Figure 4.21), where a reduction of azide vibration peak at 2099 cm^{-1} was observed together with a concomitant increase in at 1085 cm^{-1} corresponding to the ether linkage of PEG grafts. The absorptions of carbonyl groups of hydrophobic segments were also noted at 1728 cm^{-1}. Comparison of the peak areas at 2099 cm^{-1} before and after the click reaction clearly indicates that most of the azide groups have successfully reacted.

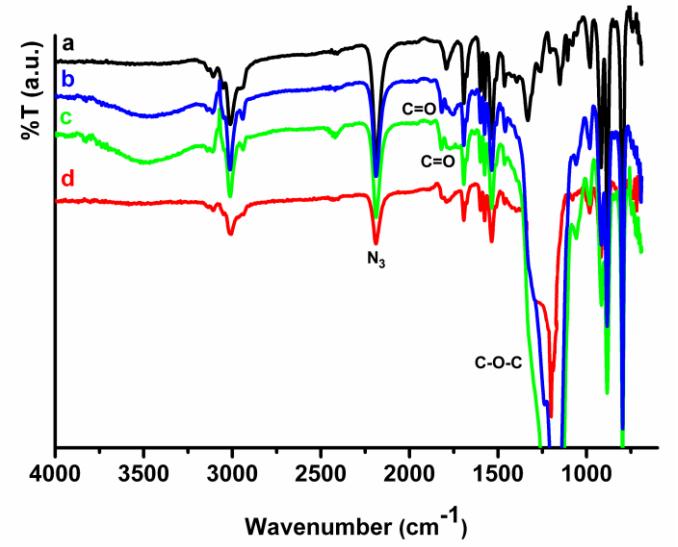

Figure 4.21: FT-IR spectra of azidated PDVB microsphere (PDVB-N_3) (a), poly(ethylene glycol) and poly(*tert*-butyl acrylate) grafted PDVB microsphere (PDVB-*g*-PEG/P*t*BA) (b), poly(ethylene glycol) and poly(methyl methacrylate) grafted PDVB microsphere (PDVB-*g*-PEG/PMMA) (c) and poly(ethylene glycol) grafted PDVB microsphere (PDVB-*g*-PEG) (d).

TGA analysis also confirmed the presence of grafted chains on microspheres surface (Figure 4.22). Azidated microspheres exhibited additional 13 % weight loss that corresponds to azide group decomposition. Grafting efficiency was calculated by using percentage of this weight loss as 17 %, 20 % and 27 % for PDVB-*g*-PEG, PDVB-*g*-PEG/ P*t*BA, and PDVB-*g*-PEG/PMMA respectively. Other evidence obtained from TGA measurements is char yield calculated as 19.4 %, 30.1 %, and 31.9 % which changed proportionally with grafting efficiency.

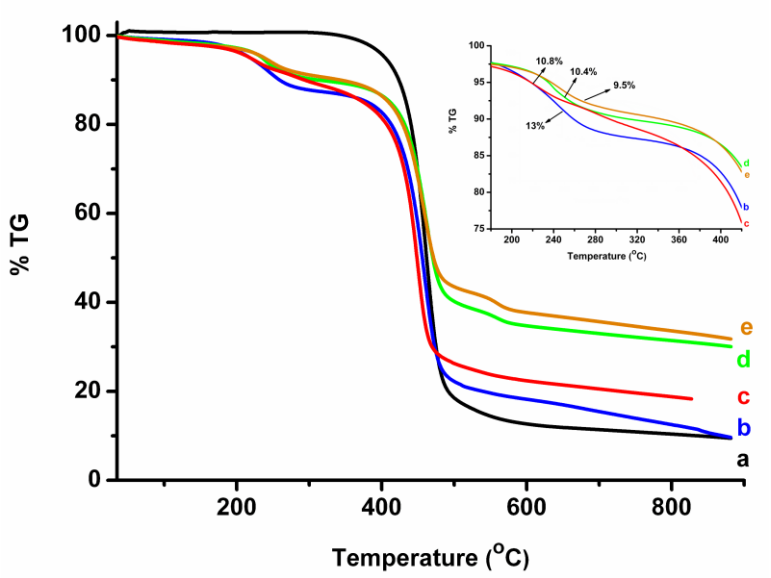

Figure 4.22: TGA traces of PDVB microspheres (a), azidated PDVB microsphere (PDVB-N_3) (b), poly(ethylene glycol) grafted PDVB microsphere (PDVB-*g*-PEG) (c), poly(ethylene glycol) and poly(tert-butyl acrylate) grafted PDVB microsphere (PDVB-*g*-PEG/P*t*BA) (d), and poly(ethylene glycol) and poly(methyl methacrylate) grafted PDVB microsphere (PDVB-*g*-PEG/PMMA) (e).

4.3.4 Protein adsorption

In this part, PDVB-*g*-PEG, PDVB-*g*-PEG/P*t*BA and PDVB-*g*-PEG/PMMA were investigated as the platform for the reversible biomolecule immobilization via adsorption. *A. bisporus* laccase was used as model protein to examine the adsorption and desorption properties of modified microspheres. Finally, these microspheres were evaluated in terms of protein adsorption capacities as well as activity retention in the immobilized form.

Since pH influences the stability and conformational structure of proteins, this parameter should be controlled during adsorption of enzyme to obtain reproducible results. Figure 4.23 shows the amount of enzyme adsorbed onto microspheres at different pH values. Close to the isoelectric point (pI) of *A. bisporus* laccase, at pH 4.0, the adsorption amount exhibits a maximum, which is a rather general phenomenon in protein adsorption. Since the biomolecule do not have a net charge in the pI the electrostatic repulsion between adsorbed protein molecules is at a minimum. Hence, the proteins could attain closer packing on the surface of the microspheres than those with a net charge.

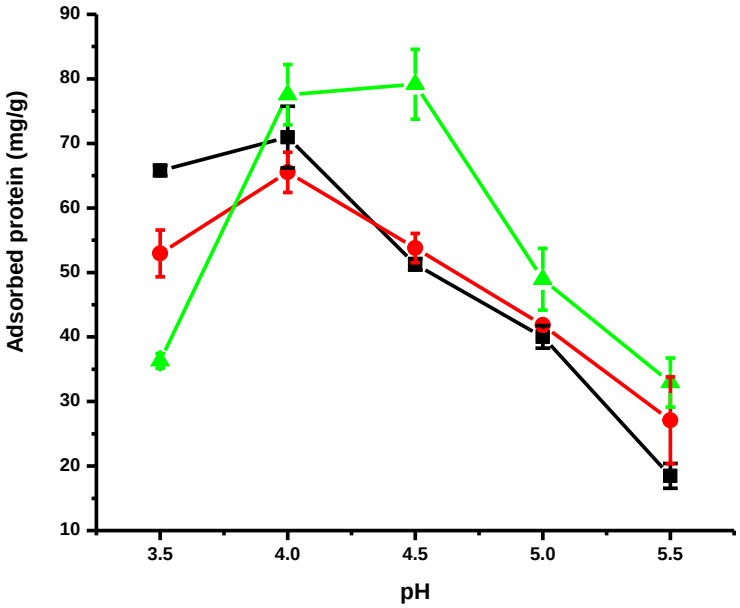

Figure 4.23: Effect of pH on the adsorptive amount of microspheres (Adsorption buffer; pH 4.0, 50 mM acetate buffer; adsorption time: 2 h; T: 25 ^{o}C; ■ (PDVB-g-PEG), • (PDVB-g-PEG/P*t*BA), ▲ (PDVB-g-PEG/ PMMA)).

Another reason for the maximum might be due to from a higher structural stability and therefore a smaller tendency to spread at the interface of microspheres at the pHs closer to their isoelectric regions as also reported for the other systems [177]. Figure 4.24 presents the relation between enzyme concentration and adsorptive amount. As can be seen, with the increase of enzyme, adsorption amount increases correspondingly up to 10 mg/mL and less significant increase was obtained at 20 mg/mL. Comparison of the adsorbed amounts per g support for pH 4.0 shows that the surface of PDVB-g-PEG /PMMA attracts more enzyme molecules (77.5 mg/g support) as compared to PDVB-g-PEG (71 mg/g support) and PDVB-g-PEG/ P*t*BA, (65 mg/g support). Higher adsorption capacity of PDVB-g-PEG /PMMA could be explained by the presence of both PEG and PMMA on the surface that caused both hydrophobic and hydrophilic interactions during the protein adsorption because of its dual functionality while PDVB-g-PEG surface attracts protein molecules only by hydrophilic interactions. In contrast, among all matrices, the lowest protein adsorption to PDVB-g-PEG/ P*t*BA might be due to the branched structure of P*t*BA that might prevent the good contact between the matrix and biomolecule and this could affect the enzyme loading capacity as well as the biocatalytic activity.

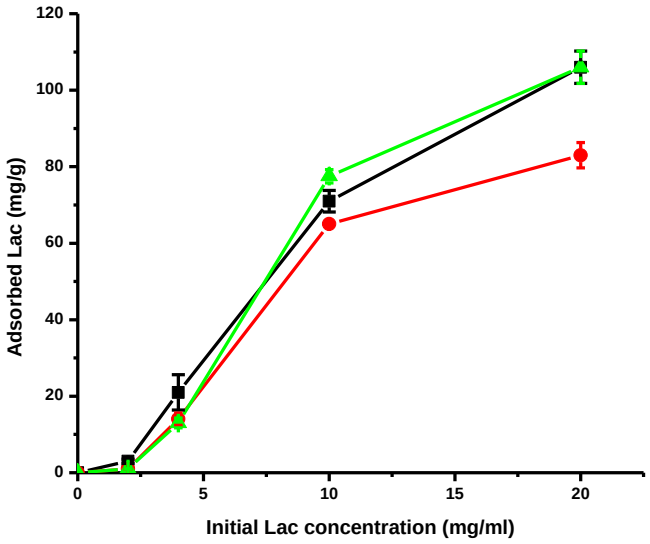

Figure 4.24: Effect of enzyme concentration on the adsorptive amount of microspheres (Adsorption buffer; pH 4.0, 50 mM acetate buffer; adsorption time: 2 h; T: 25 ^{o}C; ■ (PDVB-g-PEG), • (PDVB-g-PEG/P*t*BA), ▲ (PDVB-g-PEG/ PMMA)).

In fact, the ability to immobilize proteins with high binding capacities on surfaces while maintaining their activity is one of the most critical parameter for the biotechnological applications [178]. Specific activities of the immobilized laccases were shown in Table 4.3 after adsorption of 10 mg/mL and 20 mg/mL enzymes. According to the data, higher specific activities were observed for all supports after 10 mg/mL enzyme loading process. The performance of adsorptive immobilized enzyme is largely determined by the chemical and physical nature of carriers. The density of the binding functionality is one of the important facts in non-covalent binding. It affects the microenvironment of the carrier. The conformational flexibility of the enzyme is mainly related to the number of links to the enzymes in the microenvironment and loading capacity is depend on the number of binding sites [179]. In our case, the highest adsorption capacity was obtained by PDVB-*g*-PEG/ PMMA, in contrast, replacing the PMMA with P*t*BA in the structure led to reduced enzyme loading and activity because of the improper matrix structure that prevented to protect the flexible biomolecule conformation for the efficient immobilization. The highest specific activity was observed by using PDVB-*g*-PEG. It could be explained by the fact that hydrophobic tails on the microspheres PDVB-*g*-PEG/ PMMA and PDVB-*g*-PEG/ P*t*BA could interact with each other via the hydrophobic

forces at the polar reaction medium (acetate buffer). This could create a network like assemblies that forced to lock the enzyme probably in improper conformation that might cause a drop in the activity in contrast to PDVB-*g*-PEG in which a mild microenvironment is available for the enzyme because of rather weak hydrophilic forces. Additionally, PEGs and PEGylated surfaces are of extreme importance to the field of biomedical engineering due to their ability to control biomolecular interactions with device surface. They have been used to prevent biofouling in bio-microsystems, tissue engineering applications, drug delivery, and cell patterning [180]. It can be stated that all these properties might contribute to provide a biocompatible surface and use of (PDVB-*g*-PEG) could be advantageous with regard to the biocatalytic activity.

Table 4.3: Effect of enzyme loading on the biocatalytic activity of immobilized enzymes.

Microspheres	**Initial laccase amount (mg/mL)**	**Specific activity Unit.(mg protein)$^{-1}$.(g support)$^{-1}$**
PDVB-*g*-PEG	10	1.14
PDVB-*g*-PEG	20	0.76
PDVB-*g*-PEG/PMMA	10	0.46
PDVB-*g*-PEG/PMMA	20	0.39
PDVB-*g*-PEG/P*t*BA	10	0.26
PDVB-*g*-PEG/P*t*BA	20	0.21

PEG (10 %) and $(NH_4)_2SO_4$ (1 M) were used as desorption agents to remove proteins from microspheres. Approximately, 100 % desorption was observed for all matrices when PEG and $(NH_4)_2SO_4$ were applied together during 90 min. It is clear that to achieve almost fully desorption is important for the matrix regeneration due to the possible reusability especially in industrial applications. It is also observed that PEG alone desorbs 76 % whereas $(NH_4)_2SO_4$ desorbs 95 % of adsorbed laccase for PDVB-*g*-PEG/P*t*BA. However, the amount of laccase desorbed by PEG from the PDVB-*g*-PEG/ PMMA was 80 % and it was 67 % by $(NH_4)_2SO_4$. It can be stated that in the case of PDVB-*g*-PEG/ PMMA, hydrophobic interactions were more effective in the laccase adsorption as compared to (PDVB-*g*-PEG/P*t*BA [146]. Hence, PDVB-*g*-PEG/ PMMA seem to be more efficient platform to attract the biomolecules via hydrophobic forces that is important for the specific protein adsorption techniques especially useful for the biomolecules with the hydrophobic natures. On the other hand, due to the highest protein capacity, this microsphere might be a promising

protein purification or removal media by further optimizations for adjusting the ratio of surface functionalities according to the desired systems.

Zeta potential (ZP) is an indicator of the surface charge property of colloid or particle in solution and varied depends on the surface potential and the thickness of electric double layer. The degree of repulsion between charged particles in dispersion has been indicated by zeta potential. High zeta potential shows stability of small particles and resistance to aggregation. To further understanding the interaction of protein molecules (laccase) and microspheres, their electrical property should be known. Table 4.4 shows the ZP and electrokinetic charge densities for the microspheres before and after enzyme loading and desorption in the presence of PEG and $(NH_4)_2SO_4$. As can be seen from the Table, the ZP values were registered as negative and electrically stabilized.

Table 4.4: Zeta potential and electrokinetic charge densities for the microspheres before and after enzyme loading and desorption in the presence of PEG and $(NH_4)_2SO_4$.

Polymer		**Zeta potential[a] (mV)**	**Electrokinetic charge density[a] (C/m^2)**
PDVB-*g*-PEG	Carrier	-54.00±1.585	-47.00×10^{-3}
	Enzyme loading[b]	-77.89±1.36	-81.20×10^{-3}
	Desorption	-58.79±0.54	-52.86×10^{-3}
PDVB-*g*-PEG/ P*t*BA	Carrier	-88.64±2.66	-101.84×10^{-3}
	Enzyme loading[b]	-101.02±2.99	-131.23×10^{-3}
	Desorption	-92.24±3.25	-109.71×10^{-3}
PDVB-*g*-PEG/ PMMA	Carrier	-88.40±3.09	-101.34×10^{-3}
	Enzyme loading[b]	-101.40±3.19	-132.24×10^{-3}
	Desorption	-90.17±1.98	-105.12×10^{-3}

[a]All measurements were repeated 5 or 6 times.
[b]10 mg enzyme was loaded to each carrier

After enzyme loading as a result of adsorption, the ZPs were changed to more negative values, indicating that loaded enzyme is negatively charged at the operational conditions. It was also found that desorption of enzyme resulted in a decrease in the ZPs. When the PDVB-*g*-PEG, PDVB-*g*-PEG/P*t*BA, and PDVB-*g*-PEG/ PMMA carriers were compared with each other, PDVB-*g*-PEG, carrier was

showed less negative zeta potential value because of its less negative charge on its surface. This phenomenon was also verified by the calculation of electrokinetic charge densities. Similar ZP values, after biomolecule desorption could be a good indication of almost complete matrix regeneration which is important for the matrix recovery.

4.4 A General Method for Organic Modification of Inorganic Nanoparticles

A novel strategy was developed for tailoring nanoparticle surfaces with poly (ε-Caprolactone) (PCL). Thus, a self-curable polyester, poly(2-hydroxypropylene maleate) (PHPM) was adsorbed on the nanoparticle surfaces and heated to 180 °C to give a crosslinked polyester layer with residual hydroxyalkyl groups on their surfaces. Surface initiated polymerization (SIP) of ε-Caprolactone from hydroxyalkyl groups on the surfaces yielded core-shell nanoparticles with crosslinked core and PCL shells (22.2-71.4 %) as depicted in reaction (4.11). The core-shell nanoparticles were then employed in preparing the stable and the homogenous dispersions with poly(methyl methacrylate-*stat*-butyl acrylate) solutions. An application of the solutions onto glass substrates yielded uniform and nearly transparent free standing films (40–60 μm) with good homogeneity.

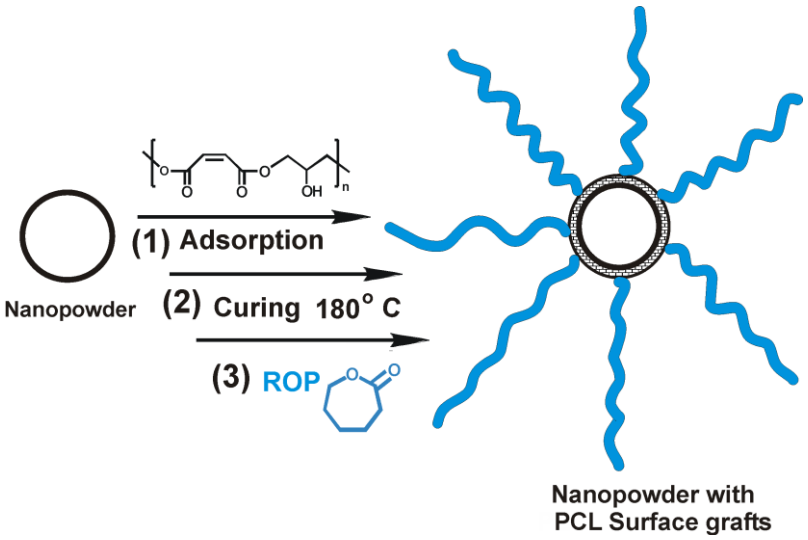

(4.11)

4.4.1 Surface adsorption of poly(2-hydroxypropylene maleate)

Stepwise heating of glycidol-maleic anhydride mixture gave unsaturated polyester (reaction (4.12)) in moderate molecular weights, as described before [150]. The resulting polyester with hydroxy groups in each repeating unit was demonstrated to

be highly adhesive to the various substrates such as glass, metal or wood and undergo rapid crosslinking upon curing at 180 °C.

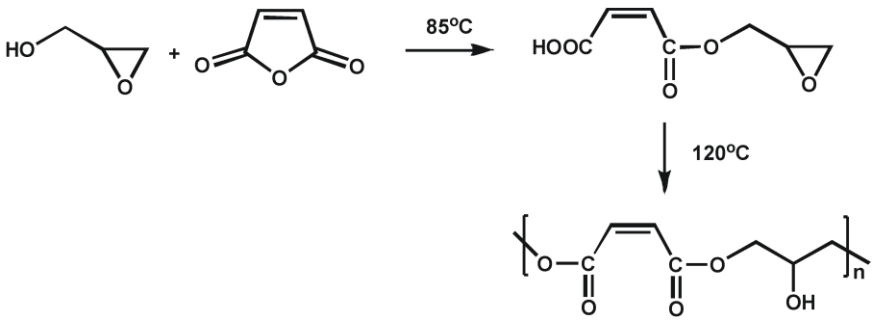

(4.12)

In the present work, this chemistry was employed in coating TiO_2 and SiO_2 nanoparticles with crosslinked polyester, poly(2-hydroxypropylene maleate) for further surface modification with poly(ε-Caprolactone). In the first step, the self-curable polyester was adsorbed on the nanoparticle surfaces from acetone solution as illustrated in reaction (4.13).

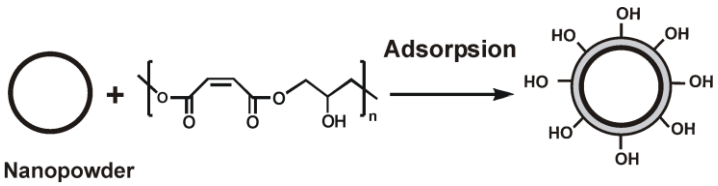

(4.13)

In order to inspect adhesion capability of the polyester onto the nanopowders, adsorption experiments were carried out with micropowders of TiO_2 and SiO_2. Experiments revealed that the equilibrium adsorption data obey Langmuir adsorption isotherm. The maximum adsorptions were estimated from the intercepts of the linear $1/q_E$ versus $1/C_E$ plots (Langmuir plots), where q_E and C_E denote the equilibrium adsorption and equilibrium concentration, respectively. The relevant data are collected in Table 4.5.

Table 4.5: Adsorption of the polyester on microparticle surfaces.

Micropowder	Adsorption of the polyester (g/g)[a]	Weight loss of encapsulated pigment (by TGA at 400 °C)
TiO_2	0.246	21.5 %
SiO_2	0.281	21 %

[a] based on Langmuir plots.

The maximum polyester adsorptions were determined to be 0.246 and 0.281 g per gram of TiO_2 and SiO_2, respectively. These values were also confirmed by TGA of

the samples after polyester adsorption from PHPM solutions (3 g/10 mL acetone). The thermograms taken under air atmosphere indicated the presence of 21–21.5 % (w/w) of polymer layer, which decomposes around 390 °C. These values correspond to 0.26 and 0.28 g of organic mass per gram of TiO_2 and SiO_2, respectively.

4.4.2 Encapsulation of the nanoparticles by thermal crosslinking of the surface adsorbed polyester

The self-curable polyester adsorbed nanoparticles were cured at 180 °C for 30 min as given in reaction (4.14).

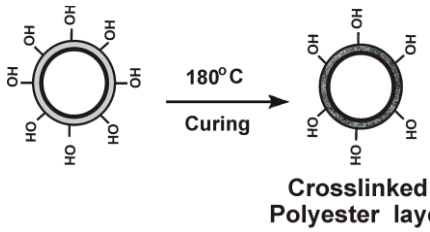

(4.14)

This process resulted in encapsulation of the nanoparticles by crosslinked polyester after curing process. Figure 4.25-b shows FT-IR spectrum of the silica sample with adsorbed polyester. In this spectrum typical ester carbonyl and carbon–carbon double bond vibrations appear at 1720 and 1640 cm^{-1}, respectively. Bare silica nanoparticles show no peaks in this region (Figure 4.25-a). After curing of the sample, intensity of the second peak decreases as shown in Figure 4.25-c. This implies the addition of the hydroxy groups to the maleate double bonds while crosslinking of the polyester as described before [150].

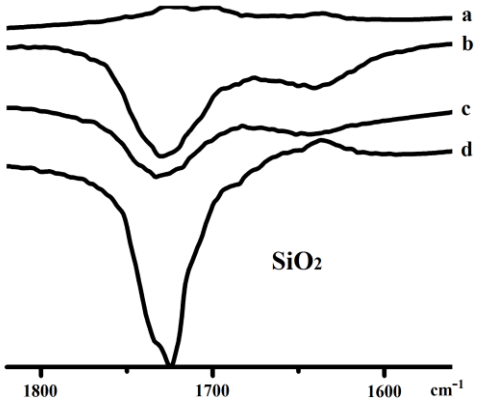

Figure 4.25: FT-IR spectra of the fumed silica (a), the SiO_2 nanopowder with adsorbed Poly(2-hydroxypropylene maleate) (PHPM) (b), the SiO_2 nanopowder with cured PHPM capsules (c) and encapsulated SiO_2 nanopowder with Poly(ε-Caprolactone) surface grafts (d) in 1600-1800 cm^{-1} range.

Extents of crosslinking in the curing process were estimated by comparison of the integral ratios of the two peaks in Figures 4.25 -b and -c. The percentage crosslinking of the adsorbed polyester was assigned by the formula:

$$\left(\frac{I^0_{C=C}}{I^0_{C=O}} - \frac{I_{C=C}}{I_{C=O}} \right) / \frac{I^0_{C=C}}{I^0_{C=O}} \times 100 \qquad \textbf{(4.15)}$$

where, $I_{C=C}$ denotes integral of the double bond vibration band at 1640 cm^{-1} for the cured samples, $I_{C=O}$ is integral of the carbonyl peak at 1720 cm^{-1} in the IR spectra of the cured samples and superscript "zero" represents integrals of the corresponding peaks for non-cured samples. This estimation revealed 18.7 % of double bond consumption in the cured polyester adsorbed on the SiO_2 nanopowder. Since equal percent of the hydroxy groups were involved in the crosslinking, the powder surface contained residual hydroxy groups (81.3 %) and an equal percent of double bonds as well.

Similar comparison of the integral ratios of those peaks in Figure 4.26 gave 28.6 % double bond consumption in the thermal curing of the polyester adhered to TiO_2 surface. Amounts of polyester adhered to the nanopowder surfaces were also assigned by TGA of the cured samples.

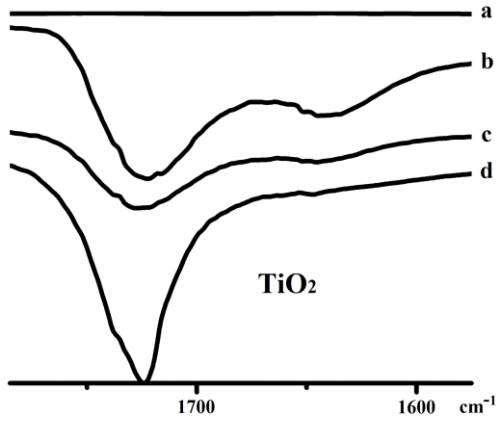

Figure 4.26: FT-IR spectra of TiO_2 nanoparticles, naked (a), with adsorbed polyester (b) with cured polyester capsules (c) and with Poly(ε-Caprolactone) surface grafts (d) in 1600–1800 cm^{-1} range.

To avoid char formation, the TGA measurements were carried out under air atmosphere. TGA thermograms of encapsulated SiO_2 and TiO_2 nanoparticles given in Figures 4.27 and Figure 4.28, respectively show that the polyester layer decomposes around 390 $^{\circ}C$ under air atmosphere. In Figure 4.27, an average 2 % of weight loss below 200 $^{\circ}C$ originated from humidity of the encapsulated silica

nanopowders. Taking this into consideration, the portion of the crosslinked polyester capsule must be at least 16 %, which corresponds to 0.19 g of organic part per gram of the silica particles.

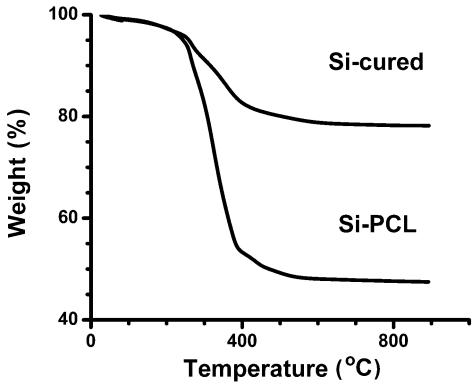

Figure 4.27: TGA of the SiO_2 nanopowders with crosslinked polyester capsules and with Poly(ε-Caprolactone) surface grafts.

Practically no weight loss is observed for the case of TiO_2 nanoparticles within 50–200 ^{o}C (Figure 4.28). Figure shows 12 % of weight loss for the TiO_2 sample carrying cured polyester at the same heating rate (10 $^{\circ}$C /min). This implies 0.136 g polyester on the surface of 1 g of the starting TiO_2 nanopowder.

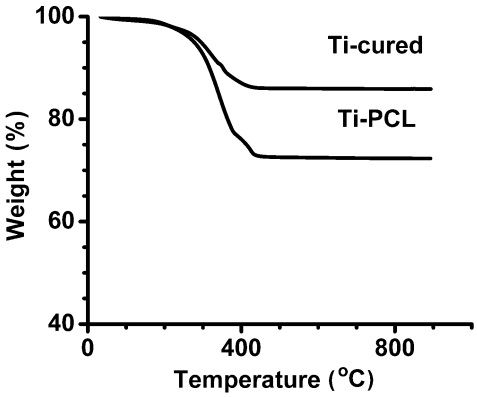

Figure 4.28: TGA curves of the TiO_2 nanoparticles with crosslinked polyester capsules (upper curve) and with Poly(ε-Caprolactone) surface grafts (lower curve).

XRD patterns of the resulting hybrid particles were the same as those of the virgin nanopowders. Figure 4.29 represents XRD of pure and cured silica powders. The broad signal at 23^{o} (2θ) indicates amorphous structure of SiO_2 nanopowder in both virgin and cured polyester.

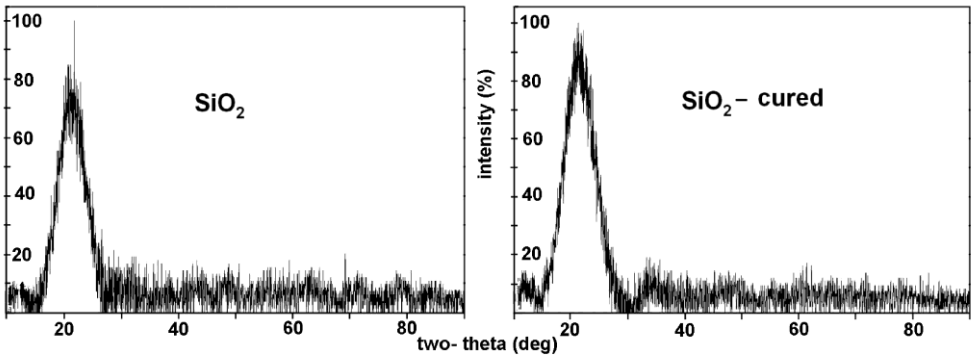

Figure 4.29: XRD spectra of virgin silica nanopowder (left) and silica nanoparticle with cured polyester capsule.

Commercial TiO_2 nanopowder shows typical XRD pattern of rutile and anatase (20 %) mixture as indicated by the supplier (Aldrich) (Figure 4.30). The TiO_2 sample coated with the crosslinked polyester shows the same XRD pattern. These results indicate that the crystalline structures of the nanopowders did not change in the thermal curing process at 180 ^oC

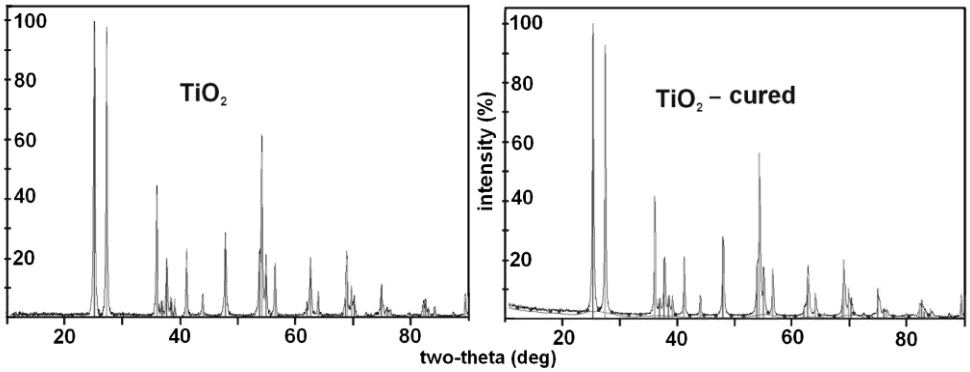

Figure 4.30: XRD spectra of the commercial TiO_2 nanopowders showing rutile and anatase crystalline structures, before (left part) and after curing of the adsorbed polyester (right part).

4.4.3 Cationic ring opening polymerization of ε-caprolactone from the residual hydroxy groups

ε-Caprolactone was polymerized from the surface of the nanoparticles via residual hydroxy groups of the crosslinked polyester, using tin (II) 2-ethylhexanoate as catalyst. Eight hours of the polymerization yielded appreciable quantities of PCL hairy grafts on the nanoparticle surfaces, as inferred from the mass increases (ca. 30 % and 22 % for the case of SiO_2 and TiO_2 samples respectively). The organically modified nanoparticles so obtained were well dispersible in toluene, acetone and THF.

TEM image of the silica with PCL surface grafts in the Figure 4.31 represents non-spherical silica nanoparticles with visible organic layers around the particles. The Figure shows that, 20-100 nm size of the silica particles are entrapped within polymer stacks of 50-250 nm. Considering with few tents of microns for the sizes of the starting fumed silica (as specified by the supplier, Aldrich), the observed sizes are significantly small.

Most probably, the formation of smaller SiO_2 particles is due to the mechanical disintegration of the starting particles, under sonication during the process. The thickness of the surrounding organic layer seems not uniform; however it is comparable with the dimensions of the inorganic species.

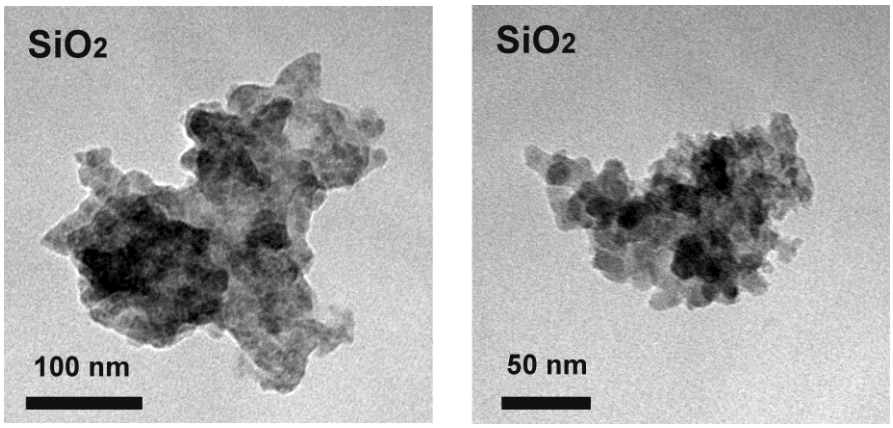

Figure 4.31: TEM micrographs of the Poly(ε-Caprolactone)-shelled SiO_2 nanopowders.

Similar organic layers are observable also in the TEM micrograph of TiO_2 sample possessing PCL grafts (Figure 4.32). The picture on the right hand represents a nearly spherical particle of 100 nm size having organic shell with a thickness of 7–9 nm. Smaller crystallites appeared around this particle implies possible disintegration of the main particle by sonication.

The TEM image on the left hand shows similar small crystallites (15-40 nm) bundled up in the polymer matrix. Thickness of the organic shell in this case is somewhat less i.e. 7–9 nm, which is consistent with low graft density of PCL (22.2 %) for TiO_2 sample. In comparison to the initial size of TiO_2 particles (50-70 nm), their sizes are significantly small (5-20 nm), due to grinding effect of the sonication as in the case for the silica sample.

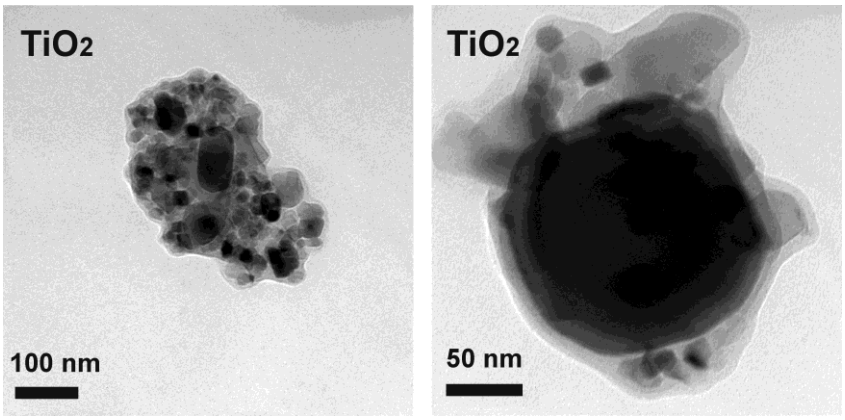

Figure 4.32: TEM micrographs of the Poly(ε-Caprolactone)-shelled TiO_2 nanopowders.

In addition, dynamic light scattering (DLS) measurements were performed on the particles in order to inspect their size changes by the surface modifications in each step. Figure 4.33-a shows that, the silica nanopowders with adsorbed PHPM have an average hydrodynamic diameter of 125 nm. After curing their average particle size (120 nm) remains almost the same (Figure 4.33-b). The similarity of the sizes of the particles in both cases might be considered as evidence for non-existence of further particle growth via interparticle crosslinking by the polyester bridges in the curing process. Significant size growth (250 nm) is observed after graft copolymerization of ε-Caprolactone from SiO_2 nanoparticle surface as expected (Figure 4.33-c).

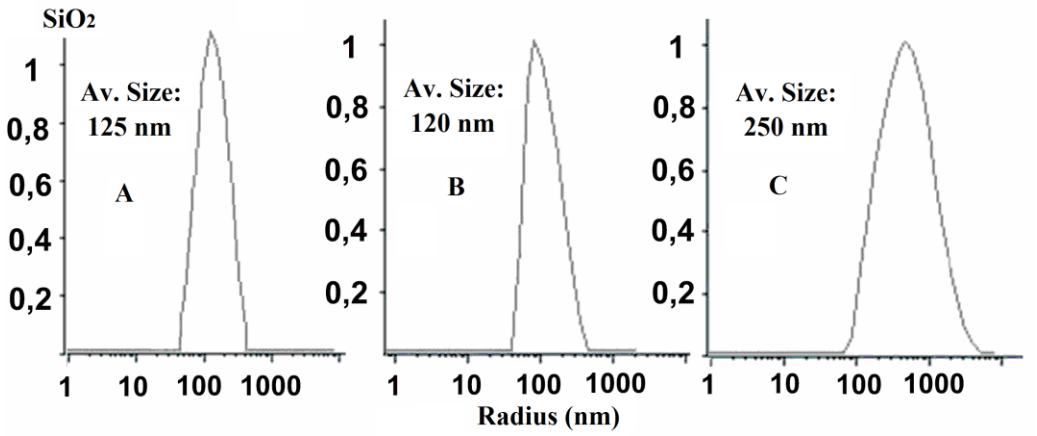

Figure 4.33: DLS profiles of the SiO_2 nanoparticles after PHPM adsorption (A), cured at 180 °C (B) and surface grafted with PCL (C).

Unimodal DLS curve for the PCL grafted sample implies absences of the free homopolymer in the product. Taking densities of 1.146 and 2.6 for PCL and SiO_2 respectively, increasing volume per nanoparticle implies 78 % percent of grafting which nearly matches with the value assigned from TGA (71.4 %). Presumably the

difference arises from the solvent, acetone used as dispersing medium for the DLS measurements. Acetone is a good solvent for PCL and the surface grafts tend to take expanded form rather than globular form in this solvent. Thus, apparent volume of the nanoparticle increases more than that of the expected. These results inferred from DLS are also in consistent with those of TEM pictures described above.

Similar progressive volume increases are observed in DLS of the surface modified titania samples, as seen in Figure 4.34. PHPM adsorbed titania samples showed also unimodal DLS curves indicating nearly narrow size distributions in each step. The average particle size with PHPM adsorbed sample is in 25- 30 nm range before and after crosslinking. Hence, volume of the particles does not change practically after the curing process. Absence of significantly larger particles can be ascribed to non-occurrence of particle growth by inter connection with the polyester adsorbed on the particle surfaces. By introducing PCL surface grafts, their average particle size increases from 30 to 40 nm. Similar estimation based on the final diameter of the particles with titania core revealed a 27.4 % (w/w) grafting yield, which is slightly greater than that assigned by TGA (22.2 %). This result is also in fairly consistent with the particle dimensions observed in the TEM images described above. Compared to the size of PCL grafted silica sample, small increase in the size of titania is due to the low grafting yield as indicated by TGA measurements.

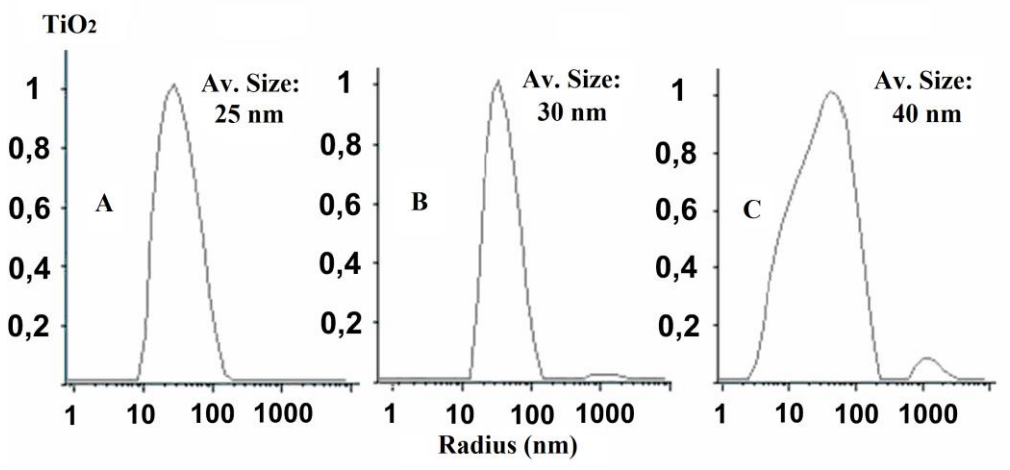

Figure 4.34: DLS profiles of the TiO_2 nanoparticles after PHPM adsorption (A), after curing at 180 $^{\circ}$C (B) and after surface grafting with PCL (C).

Avoidance of particle growth by coalescence with the helps of surface polyesters must be due to dispersing effect of the sonication and relatively less quantity of the polyester employed for the adsorption. Amount of the polyester (0.223 g per gram)

were chosen lower than maximumadsorption capacities (0.281 and 0.246 g/g for SiO_2 and TiO_2 respectively), which were estimated from Langmuir plots (see Table 4.5). The use of PHPM in less quantity was considered to be crucial to avoid remaining of the non-adsorbed free polyester. Proper selection of the polyester ratio in combination with the sonication must be responsible for preventing undesired particle growth in the encapsulation processes.

TGA of the nanoparticles with silica core and PCL shell indicates 51 % of weight-loss, which corresponds to 1.04 g of total organic portion per gram of naked silica nanopowder. Since 0.19 g of this quantity comes from PHPM, net weight of the PCL must be 0.85 g per gram of bare silica.

Considering molar mass of the repeating unit of PHPM (172 $gmol^{-1}$) and 18.7 % of hydroxy group consumption in the curing process, the density of the initiating hydroxy groups is calculated to be:

$$\frac{0.19}{172}\times(1-0.187)=9\times10^{-4}\ \text{molg}^{-1}$$

If all the hydroxy groups are assumed to be involved in initiation of the polymerization, the number of ε-caprolacone repeating units per initiation site would be:

$$\frac{0.85/114}{9\times10^{-4}}=8.25$$

Where, 114 is molar mass of ε-Caprolactone repeating unit.

Similar estimation for the core-shell nanoparticles of TiO_2 indicates 0.56 mmol of initiating hydoxyl groups per gram of bare TiO_2. TGA curve of these particles with PCL shells shows 28 % mass loss indicating 0.389 g organic portion or 0.253 g PCL per gram of TiO_2. This reveals that 4 repeating units per hydroxy group take place on the surface. The characteristics are collected in Table 4.6 for comparison.

In this study we have not attempted to increase the grafting degrees any further. Since ring opening polymerization of ε-Caprolactone from OH groups is living in nature; the degree of grafting can be increased by continuing the polymerization from the chain ends.

Table 4.6: Some characteristics of the nanoparticles prior and after grafting with PCL.

Characteristics	SiO_2	TiO_2
Hydroxyl group consumption in curing of the PHPM adsorbed on the particle surface[a]	18.7 %	28.6 %
PHPM content of the cured sample[b]	16 %	12 %
Total organic content of the particle with PCL surface grafts[b]	51 %	28 %
ε-caprolactone repeating unit per OH initiating site	8.25	4.0
Percentage grafting of PCL	71.4 %	22.2 %

[a] estimated from FT-IR spectra; [b] from TGA.

4.4.4 Nanocomposite films

The PCL hybrids of the nanoparticles obtained were used for preparing composite films with commercial poly (methyl methacrylate-*stat*-butyl acrylate) having good film forming and adhesion capabilities. This was performed simply by mixing acetone dispersions of the modified nanoparticles with acetone solutions of the base polymer, so as final concentration of the nanoparticles to be approximately 15 wt %. The mixtures were sonicated to give fairly stable and fine dispersions, so that no phase separations were observed upon standing for over 6 h at room temperature. The resulting dispersions were applied onto glass substrates by means of standard film maker (60 μm). The obtained dry films on the glass substrates were smooth and nearly transparent. SEM pictures of the free-standing composite films given in Figures 4.35-a and 4.35-b represent homogenous surfaces.

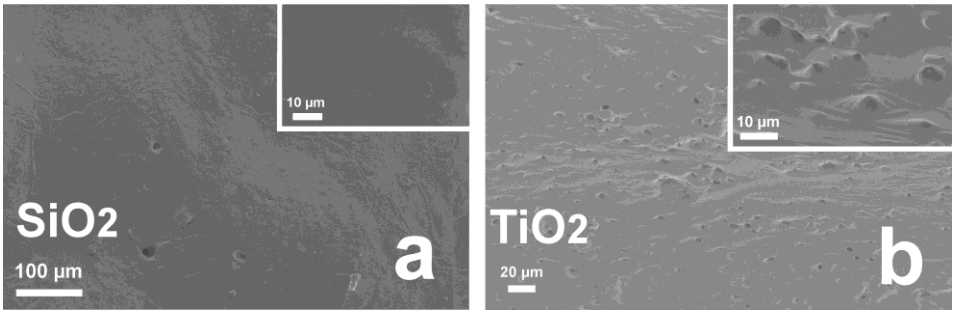

Figure 4.35: SEM pictures of free-standing poly (methyl metacrylate-*stat*-butyl acrylate) composite films with SiO_2 (a) and TiO_2 (b) nanopowders.

Some solid nanosize dots appeared on TiO_2 composite films (Fig.4.35-b) might be due to its less PCL content, in comparison to those of the silica containing films. Nevertheless, no phase separation is observed in this case as well.

4.5 Size Controlled Synthesis of Zinc Oxide Nanocrystallites and Generation of Core-Sell Structures by Post Treatment with Glycidylmethacrylate Block Copolymers

A novel, simple and convenient procedure was developed for size-controlled synthesis of ZnO nanoparticles, using zinc tetramine complex as precursor. In the procedure, ammonia of the zinc complex was gradually exchanged with dodecylamine (DDA) in alcohol-water mixture to give ZnO nanoparticles with surface tethered amine molecules. A series of nanoparticles was prepared using various [DDA] /[Zn (II)] ratios (1/3-1/15) by this method and they were characterized by UV, FT-IR, TGA, DLS, PL and ESEM techniques. Those investigations revealed that, the particle size is directly proportional to metal/ligand molar ratio and proper choice of this ratio allows preparing nanoparticles in any desired size. Unexpectedly, the room-temperature process presented gave 30-200 nm size of rod like nanoparticles having hexagonal crystalline (Wurtzite) structure as inferred from XRD. The reaction with poly (glycidyl methacrylate)-*block*-poly(methlymethacrylate) in toluene resulted in encapsulation of the nanoparticles by ring opening of epoxy groups of PGMA block with coordinated amino groups on the particle surfaces. The core cross-linked hybrid nanoparticles with PMMA hairy grafts so obtained did not show any fluorescence emission neither in UV region nor in the visible range. Homogenous and stable dispersions of the core-shell nanoparticles in acetone solutions of poly (methylmetacrylate-*co*-butyl acrylate) were demonstrated to give nearly transparent and freestanding films (40-60 μm) with good homogeneities by casting on glass substrates.

4.5.1 Size-controlled synthesis of ZnO nanoparticles

Zinc tetramine complex is completely water soluble and known to be present in the solution under equilibrium in reaction (4.16).

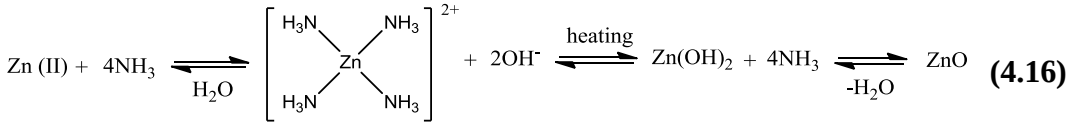

(4.16)

Obviously, the equilibrium is in favor of the complex in the presence of excess ammonia. Easy removal of ammonia from the solution shifts the equilibrium to the zinc hydroxide side, dehydration of which yields zinc oxide. Since ammonia itself is

volatile at the elevated temperatures, the complex decomposes to give zinc oxide as residual solid. Addition of some dodecyamine (DDA) to this system is normally expected to establish new equilibrium in which some percent of ammonia ligand will exchange with the non-volatile amine, DDA via simple disproportionation. Therefore, in the presence of DDA the competitive reactions; i) ligand exchange, ii) zinc oxide formation occur simultaneously. In ordinary conditions, the first reaction must be faster than the second one, if electron-donating behavior of the amino group is equal or comparable with that of ammonia.

Additionally to avoid the differences originating from solubility behavior of dodecylamine and ammonia, the reaction was performed in alcohol-water mixture yielding homogenous solution. It was concluded that molar ratio of DDA to Zn(II) influences paramount effect on the particle sizes of zinc oxide generated by slow evaporation of ammonia.

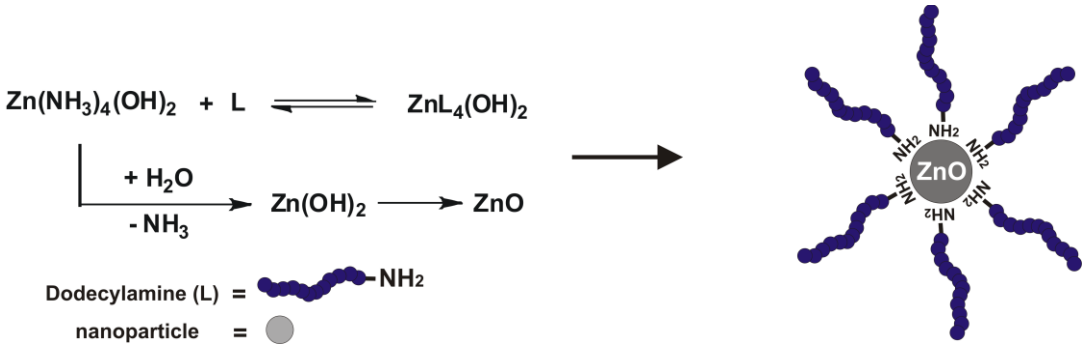

Figure 4.36: Schematic representation of size controlled ZnO nanoparticle formation in aqueous alcohol solution by simultaneous ligand exchange with DDA.

Therefore, this system is expected to give zinc oxide and zinc-DDA complexes simultaneously. Similar disproportionation between zinc oxide and zinc-DDA will result in formation of zinc oxide particles surrounded by partially ligated zinc (II) ions as depicted in Figure 4.36. To remove unbound DDA the crude product was redispersed in toluene and THF and isolated by centrifugation successively.

FT-IR spectrum of the dried product (Figure 4.37) represents N-H stretching vibration of the amino group at 3200 cm^{-1} as broadband and a plane bending vibration band of this group at 1660 cm-1. This result reveals that DDA remains attached to zinc oxide particle surfaces by coordinating, even after washing with

toluene and THF. The other typical aliphatic vibration bands of DDA are observed at 1375, 1450 and 1470 cm^{-1}, as expected.

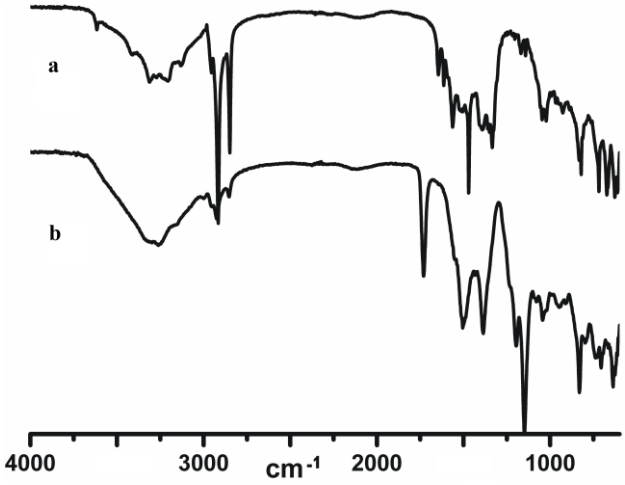

Figure 4.37: FT-IR spectrum of ZnO nanoparticles bearing coordinating DDA ligands before (a) and after encapsulation with PMMA-*b*-PGM (b).

TGA of the samples (Figure 4.38) represent mass loss between 15% - 49 %, which is proportional to the L/M ratio of the feeding composition. Thus, the sample prepared by L/M: 0.44 (mol/mol) represents 48.7 % mass lose around 300 ^{o}C, from which the practical ligand to metal ratio (reaction (4.17)), n_L / n_{ZnO} is,

$$n_L / n_{ZnO} = \frac{0.487 / 185.3}{(1\text{-}0.487) / 81} = 0.415 \qquad \textbf{(4.17)}$$

Where 185.3 band 81 are formula weights of DDA and ZnO, respectively. This value is close to that in the feed composition, 0.44.

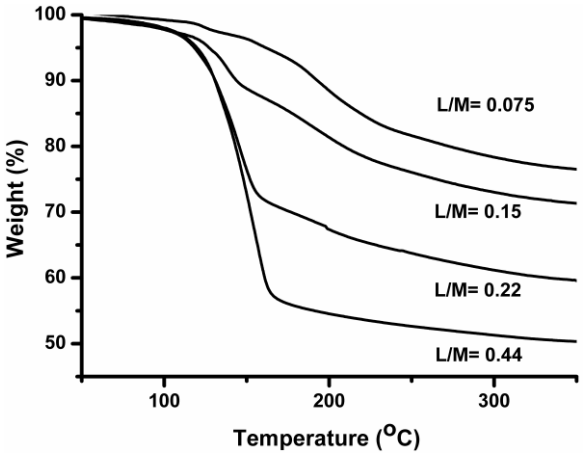

Figure 4.38: TGA of the ZnO nanoparticles stabilized with coordinating DDA ligands.

The ligand/metal ratios estimated from TGA of the other samples nearly match with the DDA/zinc molar ratios of the feed compositions (Table 4.7).

Table 4.7: Composition and size characteristics of the ZnO nanoparticles inferred from TGA and DLS measurements.

Entry	[L]/[M]	% mass loss (by TGA)	n_L/n_{ZnO}	Av. P. Size (by DLS)	$\left(\frac{V_{ZnO}}{V_{Org}+V_{ZnO}}\right)^{1/3}$	Part. Size (by ESEM)
1	0.440	48.7	0.415	62.0 nm	31.6 nm	30–100 nm
2	0.222	32.3	0.210	78.8 nm	48.5 nm	ND
3	0.150	24.2	0.140	168.2 nm	114.0 nm	110–280 nm
4	0.075	15.1	0.077	234.5 nm	179.5 nm	170–300 nm

Highly symmetric unimodal curves in the DLS profiles imply narrow size distribution of the nanoparticle samples. If we assume a close packing model for ZnO, the ratio of the molecules at the surface of the particle as given reaction (4.18) would be;

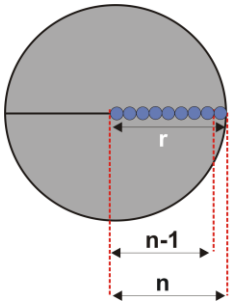

$$\frac{N_S}{N} = \frac{\frac{4}{3}\pi n^3 - \frac{4}{3}\pi (n-1)^3}{\frac{4}{3}\pi n^3} = 1 - \left(\frac{n-1}{n}\right)^3 = \left[1 - \left(1 - \frac{1}{n}\right)^3\right] \qquad \textbf{(4.18)}$$

Where, N_S and N are the number of total and surface molecules respectively and n designates the number of molecules located on the radius of the nanosphere.

In case n >>1, the ratio $N_S/N \approx 3/n$

If the particle shape cylindrical, this ratio (reaction (4.19)) would be;

$$\frac{N_S}{N} = \frac{2\pi nc + 2\pi n^2}{\pi n^2 c} \qquad \textbf{(4.19)}$$

Where c, denotes the number of molecules located alongside with height of the cylinder.

If c >> n, this ratio would approximate to $N_S/N \approx 2/n$

Then the number of ligand molecules per nanoparticle N_L can be written in terms of the surface ZnO molecules, N_S as follows; $N_L = aN_S$

Where, a denotes the number of ligand molecules per Zn atom at the surface of the particle. Therefore (reaction (4.20)),

$$N_L = aN_S = \frac{3a}{n} = \frac{3ab}{r} \qquad r = 3ab\,\frac{N}{N_L} = 3ab\,\frac{[M]}{[L]} \qquad \textbf{(4.20)}$$

Where, r is diameter of metal oxide sphere and b is average distance between Zn atoms. Diameter of ZnO portion should be:

$$= 6ab\,\frac{[M]}{[L]}$$

Average diameter of ZnO portion can be estimated by correlation of TGA and DLS results. Dimensional fraction of the ZnO portion can be calculated from cubic root mean of its volume fraction (reaction (4.21)).

$$\left(\frac{V_{ZnO}}{V_{Org} + V_{ZnO}}\right)^{1/3} \qquad \textbf{(4.21)}$$

By multiplying with the particle size measured by DLS one can find the average diameter of ZnO particles(reaction (4.22)).

$$2r = \left(\frac{V_{ZnO}}{V_{Org} + V_{ZnO}}\right)^{1/3} d \quad \text{or} \quad 2r = \left(\frac{V_{ZnO}}{V_{Org} + V_{ZnO}}\right)^{1/3} d = 6ab\,\frac{[M]}{[L]} \qquad \textbf{(4.22)}$$

In the case for cylindrical particles, the factor 6 must be exchanged with 4. Therefore, if this mechanism is correct a plot of the ZnO particle size versus M/L (mol/ mol) must a straight line with a slope of 6ab or 4ab. Figure 4.39 shows a linear plot of ZnO particle dimension against M/L ratio with a slope of 14.5 nm and a satisfactory regression factor, R= 0.9725. Linearity of this plot reveals that, ZnO particle size can be controlled precisely by proper selection of ligand/metal molar ratio.

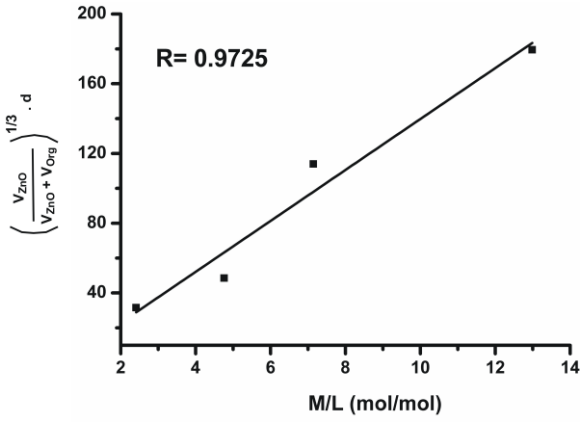

Figure 4.39: A plot of ZnO particle dimension versus metal/ligand molar ratio.

Interestingly, XRD pattern shown in Figure 4.40 represents hexagonal crystalline structure (a =. 5.20658 A^o, b= 3.24992 A^o). The 2θ values (31.767, 34.421, 36.252, 47.538, 56.592, 62.856, 66.372, 67.945,69.083, 72.566, 76.956, 81.384, 89.610^o) indicate typical Wurtzite structure of natural ZnO crystallites which is unusual, because current belief suggests [181] that, nanocrystallinity is only attained by annealing around 400 ^{o}C.

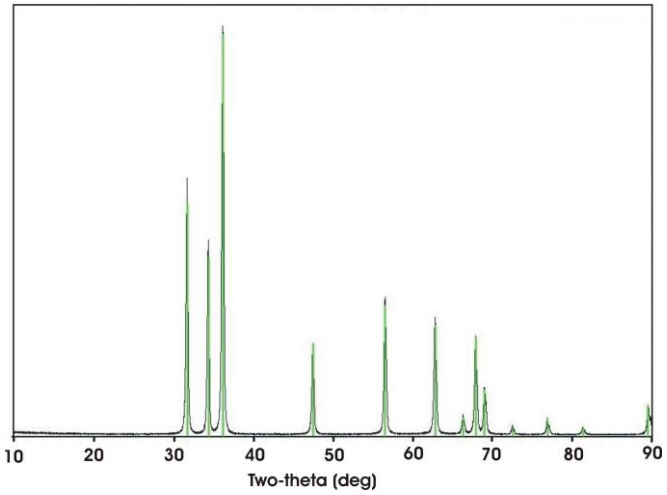

Figure 4.40: XRD difractogram of ZnO nanoparticles prepared (L/M :0.44) by the ligand exchange method at room temperature.

Although the hydrothermal method of nanoparticle synyhesis allows also preparing crystalline nanoparticles in supercritical solvents [124], formation of crystalline particles at room temperature is very exciting. Formation of crystalline ZnO in the present case might be due to homogeneity of the reaction medium and template effect of the coordinating amine molecule. UV-visible spectrum of the nanoparticle sample (L/M: 0.44) showed a broad absorption band in 200-380 nm range, which represents typical, UV screening effect of ZnO nanoparticles.

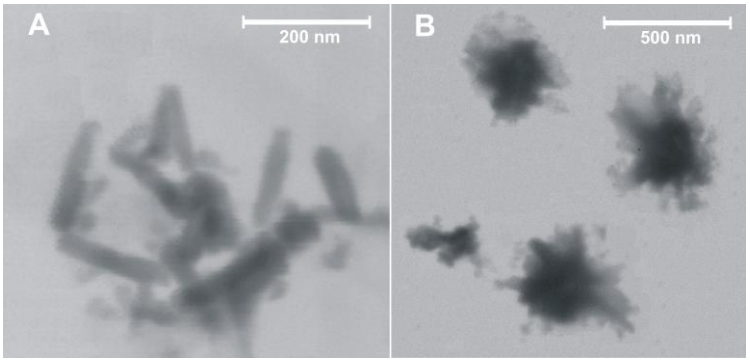

Figure 4.41: ESEM image of ZnO nanoparticle with L/M:0.44 before (A) and after reacting with PMMA-*b*-PGMA (B) taken from acetone dispersions.

The crystalline structures of the nanoparticles are also observed in ESEM images of the samples. Figure 4.41 shows rod-like nanocrystals of the sample with L/M: 0.44 (*Entry1*). The rod diameters are about 15-20 nm and the lengths are in 100-150 nm range.

4.5.2 Encapsulation of the nanoparticles

The coordinating amino groups on ZnO nanoparticles were expected to react with epoxy groups of the block copolymer, PMMA-*b*-PGMA. Multiepoxy functionality of PGMA block was considered to result in encapsulation of ZnO nanoparticle core by crosslinking reaction via amino groups. The reaction of ZnO nanoparticles (0.25 g) with the block copolymer, PMMA-*b*-PGMA (6.7 g per gram of the nanoparticle sample) was carried out in toluene dispersion at 100 ^{o}C for 24 h (Figure 4.42).

FT-IR spectrum of the product in Figure 4.37 (b) clearly represents a strong vibration band of the carbonyl group at 1720 cm^{-1} and a O=C-O vibration of the methacrylate ester bond around 1150 cm^{-1}. This result implies covalent linking of the block copolymer onto the nanoparticle surfaces. Generation of a crosslinked matrix by reaction with complexed amino groups around ZnO core is interesting, because nucleophilicity , hence electron donating ability of the amino groups must be reduced considerably after coordination with Zn (II) ions.

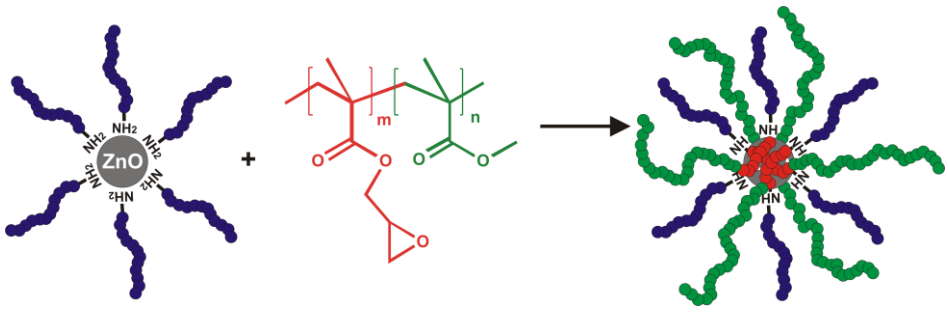

Figure 4.42: Encapsulation of ZnO nanoparticles by reaction of coordinated amino groups with epoxy groups of PMMA-PGMA block copolymer in toluene.

This result suggests that, coordinated amino groups are still reactive enough to react with epoxy groups of PGMA block at 100 ^{o}C. Moreover, DLS measurements of the encapsulated nanoparticles indicate considerable increases in their sizes. Figure 4.43 shows DLS of ZnO nanoparticle with L/M:0.44 as a representative example. The initial average size of the particle (62 nm) increases almost by a factor of four after treatment with the block copolymer and becomes 212 nm.

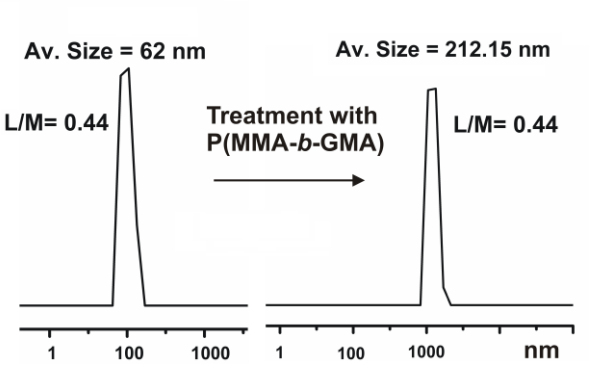

Figure 4.43: DLS of ZnO nanoparticle sample (with L/M:0.44) showing size increment after reacting with PMMA-*b*-PGMA.

This clearly indicates attachment of the block copolymer via its PGMA block. Obviously, the resulting nanoparticles must have core-shell structures with ZnO nanoparticles in the crosslinked core and linear PMMA chains at the outer side. Fluorescence spectra of the nanopartcles before and after reacting with PMMA)-PGMA block copolymer did not exhibit any emission band above 500 nm. The complete suppression of the fluorescence can be ascribed to deactivating effects NH and OH groups. The literature dealing with fluorescence emission of ZnO nanocomposites with polymers is controversial. Du et al. reported that fluorescence of ZnO nanoparticles in the visible range is completely fades in PMMA matrix and yields only UV emission around 340 nm [182]. By contrast, Lu et al. reported an intense fluorescence emission at 550 nm from ZnO/polymer nanocomposite films obtained by polymerization of polyhydroxyethyl methacrylate in the presence of 3-(trimethoxysilyl)propyl methacrylate capped ZnO nanoparticles [183]. In fact, fluorescence phenomena of ZnO-polymer composites have not been well understood yet. Interestingly, TGA curves of the core-shell nanoparticle samples recorded in nitrogen atmosphere did not show marked mass loss up to 600 ^{o}C. For this reason, we were not able to assign organic contents of the core-shell nanoparticles by TGA. The mass losses detected were even lower than those of the pristine samples bearing coordinated DDA molecules. This surprising result must be originated from the high temperature stability induced by ZnO nanoparticles as it has already been reported by Hong et al. [184].

4.5.3 Film formation of ZnO core-shell nanocrystals

Two samples with L/M: 0.44 and 0.22 were employed for testing their film forming abilities. This was performed by mixing 0.09 g encapapsulated ZnO nanoparticle dispersion in acetone (5 mL) with 5 mL acetone solution of 0.5 poly(MMA)-*stat*-poly(butyl acrylate). The mixture was stirred for 10 min at room temperature and applied onto glass slides by standard film maker (60 μm wet thickness).

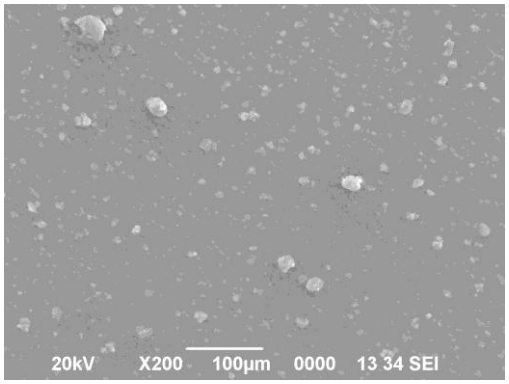

Figure 4.44: SEM picture of the cast film obtained from acetone dispersions of encapsulated ZnO nanoparticles (L/M:0.44) in the presence of PMMA-*stat*-PBA as matrix polymer.

The films pealed out in hot water were smooth and nearly transparent in appearance. SEM Picture of the free-standing composite film derived from the nanoparticle sample (with L/M:0.44) in Figure 4.44 shows fairly homogenous distribution of the stains of ZnO nanocrystallites. Such an observation can be ascribed to good film forming abilities of the polymer dispersions studied.

5. CONCLUSION

Outcomes of the experimental work described in this dissertation can be summarized as follows:

1- A new method is described for the synthesis of bromoethyl methacrylate monomer.

- A procedure is presented for the suspension polymerization yielding bromoethyl functional microspheres (125-422 micron range).
- Bromo ethyl functions were employed for surface initiated-ATRP of glycidyl methacrylate to give epoxy functional hairy grafts which are useful for further functionalization.
- The bromoethyl function on the surface were also employed as initiators for the ring opening polymerization of 2-methyl 2-oxazoline.
- Hydrolysis of oxazoline grafts yields linear poly(ethylene imine) brushes with the retention of the particle shapes.
- Considering chelating ability of poly(ethylene imine) brushes this material would be of interest for as chelating polymers.

2- P(S-DVB) microspheres were prepared and their surfaces were functionalize with bromo acetyl groups serving as efficient initiation sites to generate PS-b-PGMA brushes by ATRP method.

- The enzyme, lipase, was immobilized on the microspheres via epoxy groups of the second block (498.5 U g^{-1}).
- The resulting enzyme was demonstrated to be reasonably fast in esterification of the substrate, ethyl acetate due to homogenious conditions provided by PS spacer chains.

3- DVB microspheres (1-3 nm range) prepared by precipitation polymerization method was functionalized with azido groups via hydrobromination of residual double bonds and following substitution with NaN_3.

- A mixture of alkyne terminated polymers, PEG and PMMA or P*t*BA were anchored to azide functional microspheres via click chemistry methodology using copper as catalyst.
- The resulting microspheres bearing hydrophobic and hydrophilic blocks were demonstrated to have reversible protein binding abilities.

4- A general method was developed for surface modification and encapsulation of preexisting SiO_2 and TiO_2 nanopowders.

- This was achieved by adsorbtion of highly adhesive and self curable polyester, poly(2-hydroxy propylenemaleate) and followed curing of the surface adsorbed polyester at 180 ^oC for short term.
- The residual hydroxy groups on the surface of encapsulated nanoparticles were employed as initiation for ring opening polymerization of ε-Caprolactone.
- The resulting core-crosslinked nanoparticles with poly(ε-Caprolactone) brushes were used for preparing nearly transparent free-standing films by using poly(MMA-stat-BA) copolymer as dispersing medium.

5- A ligand exchange method was developed for size-controlled synthesis of ZnO nanoparticles using zinc-tetramine complexes as a precursor.

- In this protocol dodecylamine ligand was gradually exchanged with ammonia at room temperature in alcoho- water mixtures.
- TEM images and analysis (DLS,TGA) of the nanoparticles revealed that the particle size is inversely proportional to L/M molar ratio.
- Unexpectedly XRD of the nanoparticles revealed completely crystalline wurtzite structure for ZnO.
- The ZnO nanoparticles so obtained were reacted with poly(MMA-*b*-GMA) in toluene solution resulted in core-crosslinked structures with linear PMMA shells.

- Neither the core-shell nanoparticles nor premature nanoparticles did show florescence emission above 500 nm, most probably due to deactivation of the excited states by N-H and O-H groups.
- The resulting core-shell nanoparticles were demonstrated to give homogenous films by solvent casting from acetone solutions of poly(MMA-*stat*-BA) copolymer.

Although surface initiated polymerization of various monomers from planar and spherical surface was described before, Herein we described generation of robust brushes linked to the surfaces with non-hydrolysible linkages. This behaviour will expand the use of hairy graft polymers as reagent or catalyst carrier.

The newly developed ligand exchange methodology was demonstrated to provide size controlled synthesis of ZnO nanoparticle. However, this methodology seems to be generally applicable for preparing other nanoparticles of metal and metal oxides. Entrapment of the nanoparticles via reaction of cordinated amino groups with epoxy groups of the PGMA block is an important contribution which will find extensive use for preparing various core-crosslinked structures.

REFERENCES

[1] **Xu, F.J., Neoh, K.G., and Kang, E.T.**, 2009, Bioactive surfaces and biomaterials via atom transfer radical polymerization*, Progress in Polymer Science*, **34,** 719-761.

[2] **Willner, I. and Willner, B.**, 2002, Functional nanoparticle architectures for sensoric, optoelectronic, and bioelectronic applications*, Pure and Applied Chemistry*, **74,** 1773-1783.

[3] **Angot, S., Ayres, N., Bon, S.A.F., and Haddleton, D.M.**, 2001, Living radical polymerization immobilized on wang resins: Synthesis and harvest of narrow polydispersity poly(methacrylate)s*, Macromolecules*, **34,** 768-774.

[4] **Brady, D. and Jordaan, J.**, 2009, Advances in enzyme immobilisation*, Biotechnology Letters*, **31,** 1639-1650.

[5] **Huelseweh, B., Ehricht, R., and Marschall, H.J.**, 2006, A simple and rapid protein array based method for the simultaneous detection of biowarfare agents*, Proteomics*, **6,** 2972-2981.

[6] **Paul, D.R. and Robeson, L.M.**, 2008, Polymer nanotechnology: Nanocomposites*, Polymer*, **49,** 3187-3204.

[7] **De Rogatis, L., Cargnello, M., Gombac, V., Lorenzut, B., Montini, T., and Fornasiero, P.**, 2010, Embedded phases: A way to active and stable catalysts*, Chemsuschem*, **3,** 24-42.

[8] **Bicak, N., Gazi, M., Galli, G., and Chiellini, E.**, 2006, Polystyrene microspheres having epoxy functional dangling chains linked by hydrolytically stable bonds via atrp*, Journal of Polymer Science Part a-Polymer Chemistry*, **44,** 6708-6716.

[9] **Gazi, M., Galli, G., and Bicak, N.**, 2008, The rapid boron uptake by multi-hydroxyl functional hairy polymers*, Separation and Purification Technology*, **62,** 484-488.

[10] **Arica, M.Y. and Bayramoglu, G.**, 2006, Invertase reversibly immobilized onto polyethylenimine-grafted poly(gma-mma) beads for sucrose hydrolysis*, Journal of Molecular Catalysis B-Enzymatic*, **38,** 131-138.

[11] **Bhattacharya, A. and Misra, B.N.**, 2004, Grafting: A versatile means to modify polymers - techniques, factors and applications, *Progress in Polymer Science*, **29,** 767-814.

[12] **Jordan, R., Graf, K., Riegler, H., and Unger, K.K.**, 1996, Polymer-supported alkyl monolayers on silica: Synthesis and self-assembly of terminal functionalized poly(n-propionylethylenimine)s, *Chemical Communications*, 1025-1026.

[13] **Wang, J.S. and Matyjaszewski, K.**, 1995, Controlled living radical polymerization - atom-transfer radical polymerization in the presence of transition-metal complexes, *Journal of the American Chemical Society*, **117,** 5614-5615.

[14] **Percec, V. and Barboiu, B.**, 1995, Living radical polymerization of styrene initiated by arenesulfonyl chlorides and cu-i(bpy)(n)cl, *Macromolecules*, **28,** 7970-7972.

[15] **von Werne, T. and Patten, T.E.**, 1999, Preparation of structurally well-defined polymer-nanoparticle hybrids with controlled/living radical polymerizations, *Journal of the American Chemical Society*, **121,** 7409-7410.

[16] **Pyun, J., Kowalewski, T., and Matyjaszewski, K.**, 2003, Synthesis of polymer brushes using atom transfer radical polymerization, *Macromolecular Rapid Communications*, **24,** 1043-1059.

[17] **Li, D.J., Jones, G.L., Dunlap, J.R., Hua, F.J., and Zhao, B.**, 2006, Thermosensitive hairy hybrid nanoparticles synthesized by surface-initiated atom transfer radical polymerization, *Langmuir*, **22,** 3344-3351.

[18] **Gill, C.S., Venkatasubbaiah, K., Phan, N.T.S., Weck, M., and Jones, C.W.**, 2008, Enhanced cooperativity through design: Pendant co-iii-salen polymer brush catalysts for the hydrolytic kinetic resolution of epichlorohydrin (salen = n,n '-bis(salicylidene)ethylenediamine dianion), *Chemistry-a European Journal*, **14,** 7306-7313.

[19] **Raghuraman, G.K., Dhamodharan, R., Prucker, O., and Ruhe, J.**, 2008, A robust method for the immobilization of polymer molecules on sio2 surfaces, *Macromolecules*, **41,** 873-878.

[20] **Min, K., Hu, J.H., Wang, C.C., and Elaissari, A.**, 2002, Surface modification of polystyrene latex particles via atom transfer radical polymerization, *Journal of Polymer Science Part a-Polymer Chemistry*, **40,** 892-900.

[21] **Yu, W.H., Kang, E.T., and Neoh, K.G.**, 2004, Controlled grafting of well-defined epoxide polymers on hydrogen-terminated silicon substrates by surface-initiated atrp at ambient temperature, *Langmuir*, **20,** 8294-8300.

[22] **Zheng, G.D. and Stover, H.D.H.**, 2002, Grafting of polystyrene from narrow disperse polymer particles by surface-initiated atom transfer radical polymerization, *Macromolecules*, **35,** 6828-6834.

[23] **Zheng, G.D. and Stover, H.D.H.**, 2003, Formation and morphology of methacrylic polymers and block copolymers tethered on polymer microspheres, *Macromolecules*, **36,** 1808-1814.

[24] **Li, K. and Stover, H.D.H.**, 1993, Synthesis of monodisperse poly(divinylbenzene) microspheres, *Journal of Polymer Science Part a-Polymer Chemistry*, **31,** 3257-3263.

[25] **Wang, Y. and Herron, N.**, 1991, Nanometer-sized semiconductor clusters - materials synthesis, quantum size effects, and photophysical properties, *Journal of Physical Chemistry*, **95,** 525-532.

[26] **See, K.H., Mullins, M.E., Mills, O.P., and Heiden, P.A.**, 2005, A reactive core-shell nanoparticle approach to prepare hybrid nanocomposites: Effects of processing variables, *Nanotechnology*, **16,** 1950-1959.

[27] **Liu, P. and Su, Z.X.**, 2006, Preparation and characterization of pmma/zno nanocomposites via in-situ polymerization method, *Journal of Macromolecular Science-Physics*, **B45,** 131-138.

[28] **Demir, M.M., Memesa, M., Castignolles, P., and Wegner, G.**, 2006, Pmma/zinc oxide nanocomposites prepared by in-situ bulk polymerization, *Macromolecular Rapid Communications*, **27,** 763-770.

[29] **Russell, T.P.**, 2002, Surface-responsive materials, *Science*, **297,** 964-967.

[30] **Kickelbick, G.**, 2003, Concepts for the incorporation of inorganic building blocks into organic polymers on a nanoscale, *Progress in Polymer Science*, **28,** 83-114.

[31] **Abboud, M., Turner, M., Duguet, E., and Fontanille, M.**, 1997, Pmma-based composite materials with reactive ceramic fillers .1. Chemical modification and characterisation of ceramic particles, *Journal of Materials Chemistry*, **7,** 1527-1532.

[32] **Xia, J.H. and Matyjaszewski, K.**, 1997, Controlled/"living" radical polymerization. Atom transfer radical polymerization using multidentate amine ligands, *Macromolecules*, **30,** 7697-7700.

[33] **Husseman, M., Malmstrom, E.E., McNamara, M., Mate, M., Mecerreyes, D., Benoit, D.G., Hedrick, J.L., Mansky, P., Huang, E., Russell, T.P., and Hawker, C.J.**, 1999, Controlled synthesis of polymer brushes by "living" free radical polymerization techniques, *Macromolecules*, **32,** 1424-1431.

[34] **Barner, L., Davis, T.P., Stenzel, M.H., and Barner-Kowollik, C.**, 2007, Complex macromolecular architectures by reversible addition fragmentation chain transfer chemistry: Theory and practice, *Macromolecular Rapid Communications*, **28,** 539-559.

[35] **Carrot, G., Rutot-Houze, D., Pottier, A., Degee, P., Hilborn, J., and Dubois, P.**, 2002, Surface-initiated ring-opening polymerization: A versatile method for nanoparticle ordering, *Macromolecules*, **35,** 8400-8404.

[36] **Bailly, B., Donnenwirth, A.C., Bartholome, C., Beyou, E., and Bourgeat-Lami, E.**, 2006, Silica-polystyrene nanocomposite particles synthesized by nitroxide-mediated polymerization and their encapsulation through miniemulsion polymerization, *Journal of Nanomaterials*.

[37] **Burda, C., Chen, X.B., Narayanan, R., and El-Sayed, M.A.**, 2005, Chemistry and properties of nanocrystals of different shapes, *Chemical Reviews*, **105,** 1025-1102.

[38] **Sunkara, H.B., Jethmalani, J.M., and Ford, W.T.**, 1994, Composite of colloidal crystals of silica in poly(methyl methacrylate), *Chemistry of Materials*, **6,** 362-364.

[39] **Kubota, H. and Ogiwara, Y.**, 1980, Cellulose peroxides derived from carbonylated cellulose and hydrogen-peroxide, *Journal of Applied Polymer Science*, **25,** 683-689.

[40] **Misra, B.N., Dogra, R., and Mehta, I.K.**, 1980, Grafting onto cellulose .5. Effect of complexing agents on fentons reagent (fe2+-h2o2)-initiated grafting of poly(ethyl acrylate), *Journal of Polymer Science Part a-Polymer Chemistry*, **18,** 749-752.

[41] **Moharana, S., Mishra, S.B., and Tripathy, S.S.**, 1990, Chemical modification of jute fibers .1. Permanganate-initiated graft-copolymerization methyl-methacrylate onto jute fibers, *Journal of Applied Polymer Science*, **40,** 345-357.

[42] **Misra, B.N., Kaur, I., and Dogra, R.**, 1979, Grafting onto wool .6. Effect of amines in ceric ion-initiated grafting of polyvinyl acetate), *Journal of Applied Polymer Science*, **24,** 1595-1602.

[43] **Jordan, R. and Ulman, A.**, 1998, Surface initiated living cationic polymerization of 2-oxazolines, *Journal of the American Chemical Society*, **120,** 243-247.

[44] **Zhao, B. and Brittain, W.J.**, 2000, Synthesis of polystyrene brushes on silicate substrates via carbocationic polymerization from self-assembled monolayers, *Macromolecules*, **33,** 342-348.

[45] **Jordan, R., Ulman, A., Kang, J.F., Rafailovich, M.H., and Sokolov, J.**, 1999, Surface-initiated anionic polymerization of styrene by means of self-assembled monolayers, *Journal of the American Chemical Society*, **121,** 1016-1022.

[46] **Husemann, M., Mecerreyes, D., Hawker, C.J., Hedrick, J.L., Shah, R., and Abbott, N.L.**, 1999, Surface-initiated polymerization for amplification of self-assembled monolayers patterned by microcontact printing, *Angewandte Chemie-International Edition*, **38,** 647-649.

[47] **Choi, I.S. and Langer, R.**, 2001, Surface-initiated polymerization of l-lactide: Coating of solid substrates with a biodegradable polymer, *Macromolecules*, **34,** 5361-5363.

[48] **Jaworek, T., Neher, D., Wegner, G., Wieringa, R.H., and Schouten, A.J.**, 1998, Electromechanical properties of an ultrathin layer of directionally aligned helical polypeptides, *Science*, **279,** 57-60.

[49] **Mingotaud, A.F., Reculusa, S., Mingotaud, C., Keller, P., Sykes, C., Duguet, E., and Ravaine, S.**, 2003, Ring-opening metathesis polymerization on well defined silica nanoparticles leading to hybrid core-shell particles, *Journal of Materials Chemistry*, **13,** 1920-1925.

[50] **Jordi, M.A. and Seery, T.A.P.**, 2005, Quantitative determination of the chemical composition of silica-poly(norbornene) nanocomposites, *Journal of the American Chemical Society*, **127,** 4416-4422.

[51] **Moon, J.H. and Swager, T.M.**, 2002, Poly(p-phenylene ethynylene) brushes, *Macromolecules*, **35,** 6086-6089.

[52] **Huang, X.Y. and Wirth, M.J.**, 1997, Surface-initiated radical polymerization on porous silica, *Analytical Chemistry*, **69,** 4577-4580.

[53] **Matyjaszewski, K., Shipp, D.A., Wang, J.L., Grimaud, T., and Patten, T.E.**, 1998, Utilizing halide exchange to improve control of atom transfer radical polymerization, *Macromolecules*, **31,** 6836-6840.

[54] **Carrot, G., Diamanti, S., Manuszak, M., Charleux, B., and Vairon, I.P.**, 2001, Atom transfer radical polymerization of n-butyl acrylate from silica nanoparticles, *Journal of Polymer Science Part a-Polymer Chemistry*, **39,** 4294-4301.

[55] **Wight, A.P. and Davis, M.E.**, 2002, Design and preparation of organic-inorganic hybrid catalysts, *Chemical Reviews*, **102,** 3589-3613.

[56] **Zheng, G.D. and Stover, H.D.H.**, 2002, Grafting of poly(alkyl (meth)acrylates) from swellable poly(dvb80-co-hema) microspheres by atom transfer radical polymerization, *Macromolecules*, **35,** 7612-7619.

[57] **Senkal, B.F. and Bicak, N.**, 2003, Grafting on crosslinked polymer beads by atrp from polymer supported n-chlorosulfonamides, *European Polymer Journal*, **39,** 327-331.

[58] **Matyjaszewski, K., Miller, P.J., Shukla, N., Immaraporn, B., Gelman, A., Luokala, B.B., Siclovan, T.M., Kickelbick, G., Vallant, T., Hoffmann, H., and Pakula, T.**, 1999, Polymers at interfaces: Using atom transfer radical polymerization in the controlled growth of homopolymers and block copolymers from silicon surfaces in the absence of untethered sacrificial initiator, *Macromolecules*, **32,** 8716-8724.

[59] **Sedjo, R.A., Mirous, B.K., and Brittain, W.J.**, 2000, Synthesis of polystyrene-block-poly(methyl methacrylate) brushes by reverse atom transfer radical polymerization, *Macromolecules*, **33,** 1492-1493.

[60] **Baum, M. and Brittain, W.J.**, 2002, Synthesis of polymer brushes on silicate substrates via reversible addition fragmentation chain transfer technique, *Macromolecules*, **35,** 610-615.

[61] **Rowe-Konopacki, M.D. and Boyes, S.G.**, 2007, Synthesis of surface initiated diblock copolymer brushes from flat silicon substrates utilizing the raft polymerization technique, *Macromolecules*, **40,** 879-888.

[62] **Li, C.Z. and Benicewicz, B.C.**, 2005, Synthesis of well-defined polymer brushes grafted onto silica nanoparticles via surface reversible addition-fragmentation chain transfer polymerization, *Macromolecules*, **38,** 5929-5936.

[63] **Bian, K.J. and Cunningham, M.F.**, 2005, Synthesis of polymeric microspheres from a merrifield resin by surface-initiated nitroxide-mediated radical polymerization, *Journal of Polymer Science Part a-Polymer Chemistry*, **43,** 2145-2154.

[64] **Matsuno, R., Yamamoto, K., Otsuka, H., and Takahara, A.**, 2004, Polystyrene- and poly(3-vinylpyridine)-grafted magnetite nanoparticles prepared through surface-initiated nitroxide-mediated radical polymerization, *Macromolecules*, **37,** 2203-2209.

[65] **Kobayashi, M., Matsuno, R., Otsuka, H., and Takahara, A.**, 2006, Precise surface structure control of inorganic solid and metal oxide nanoparticles through surface-initiated radical polymerization, *Science and Technology of Advanced Materials*, **7,** 617-628.

[66] **Zhao, X.D., Fan, X.H., Chen, X.F., Chai, C.P., and Zhou, Q.F.**, 2006, Surface modification of multiwalled carbon nanotubes via nitroxide-mediated radical polymerization, *Journal of Polymer Science Part a-Polymer Chemistry*, **44,** 4656-4667.

[67] **Zhao, X.D., Lin, W.R., Song, N.H., Chen, X.F., Fan, X.H., and Zhou, Q.F.**, 2006, Water soluble multi-walled carbon nanotubes prepared via nitroxide-mediated radical polymerization, *Journal of Materials Chemistry*, **16,** 4619-4625.

[68] **Andruzzi, L., Senaratne, W., Hexemer, A., Sheets, E.D., Ilic, B., Kramer, E.J., Baird, B., and Ober, C.K.**, 2005, Oligo(ethylene glycol) containing polymer brushes as bioselective surfaces, *Langmuir*, **21,** 2495-2504.

[69] **Otsu, T. and Yoshida, M.**, 1982, Role of initiator-transfer agent-terminator (iniferter) in radical polymerizations - polymer design by organic disulfides as iniferters, *Makromolekulare Chemie-Rapid Communications*, **3,** 127-132.

[70] **Kidoaki, S., Nakayama, Y., and Matsuda, T.**, 2001, Measurement of the interaction forces between proteins and iniferter-based graft-polymerized surfaces with an atomic force microscope in aqueous media, *Langmuir*, **17,** 1080-1087.

[71] **Kidoaki, S., Ohya, S., Nakayama, Y., and Matsuda, T.**, 2001, Thermoresponsive structural change of a poly(n-isopropylacrylamide) graft layer measured with an atomic force microscope, *Langmuir*, **17,** 2402-2407.

[72] **Matsuda, T., Kaneko, M., and Ge, S.R.**, 2003, Quasi-living surface graft polymerization with phosphorylcholine group(s) at the terminal end, *Biomaterials*, **24,** 4507-4515.

[73] **Matsuda, T. and Ohya, S.**, 2005, Photoiniferter-based thermoresponsive graft architecture with albumin covalently fixed at growing graft chain end, *Langmuir*, **21,** 9660-9665.

[74] **de Boer, B., Simon, H.K., Werts, M.P.L., van der Vegte, E.W., and Hadziioannou, G.**, 2000, "Living" free radical photopolymerization initiated from surface-grafted iniferter monolayers, *Macromolecules*, **33,** 349-356.

[75] **Cui, Y., Tao, C., Zheng, S.P., He, Q., Ai, S.F., and Li, J.B.**, 2005, Synthesis of thermosensitive pnipam-co-mbaa nanotubes by atom transfer radical polymerization within a porous membrane, *Macromolecular Rapid Communications*, **26,** 1552-1556.

[76] **Raghuraman, G.K., Ruhe, J., and Dhamodharan, R.**, 2008, Grafting of pmma brushes on titania nanoparticulate surface via surface-initiated conventional radical and "controlled" radical polymerization (atrp), *Journal of Nanoparticle Research*, **10,** 415-427.

[77] **Fan, X.W., Lin, L.J., Dalsin, J.L., and Messersmith, P.B.**, 2005, Biomimetic anchor for surface-initiated polymerization from metal substrates, *Journal of the American Chemical Society*, **127,** 15843-15847.

[78] **Lattuada, M. and Hatton, T.A.**, 2007, Functionalization of monodisperse magnetic nanoparticles, *Langmuir*, **23,** 2158-2168.

[79] **An, L.J., Li, Z.Q., Wang, Z., Zhang, J.H., and Yang, B.**, 2005, Bifunctional fe3o4/cds nanocomposites synthesized by surface-initiated atom transfer radical polymerization, *Chemistry Letters*, **34,** 652-653.

[80] **Yao, F., Fu, G.D., Zhao, J.P., Kang, E.T., and Neoh, K.G.**, 2008, Antibacterial effect of surface-functionalized polypropylene hollow fiber membrane from surface-initiated atom transfer radical polymerization, *Journal of Membrane Science*, **319,** 149-157.

[81] **Liu, Y.L., Luo, M.T., and Lai, J.Y.**, 2007, Poly(tefrafluoroethylene) film surface functionalization with 2-bromoisobutyryl bromide as initiator for surface-initiated atom-transfer radical polymerization, *Macromolecular Rapid Communications*, **28,** 329-333.

[82] **Barner, L., Zwaneveld, N., Perera, S., Pham, Y., and Davis, T.P.**, 2002, Reversible addition-fragmentation chain-transfer graft polymerization of styrene: Solid phases for organic and peptide synthesis, *Journal of Polymer Science Part a-Polymer Chemistry*, **40,** 4180-4192.

[83] **Kiani, K., Hill, D.J.T., Rasoul, F., Whittaker, M., and Rintoul, L.**, 2007, Raft mediated surface grafting of t-butyl acrylate onto an ethylene-propyl ene copolymer initiated by gamma radiation, *Journal of Polymer Science Part a-Polymer Chemistry*, **45,** 1074-1083.

[84] **Kolb, H.C., Finn, M.G., and Sharpless, K.B.**, 2001, Click chemistry: Diverse chemical function from a few good reactions, *Angewandte Chemie-International Edition*, **40,** 2004-+.

[85] **Huisgen, R.**, 1968, On mechanism of 1,3-dipolar cycloadditions . Areply, *Journal of Organic Chemistry*, **33,** 2291-2297.

[86] **Gothelf, K.V. and Jorgensen, K.A.**, 1998, Asymmetric 1,3-dipolar cycloaddition reactions, *Chemical Reviews*, **98,** 863-909.

[87] **Rostovtsev, V.V., Green, L.G., Fokin, V.V., and Sharpless, K.B.**, 2002, A stepwise huisgen cycloaddition process: Copper(i)-catalyzed regioselective "ligation" of azides and terminal alkynes, *Angewandte Chemie-International Edition*, **41,** 2596-2599.

[88] **Tornoe, C.W., Christensen, C., and Meldal, M.**, 2002, Peptidotriazoles on solid phase: [1,2,3]-triazoles by regiospecific copper(i)-catalyzed 1,3-dipolar cycloadditions of terminal alkynes to azides*, Journal of Organic Chemistry*, **67,** 3057-3064.

[89] **Appukkuttan, P., Dehaen, W., Fokin, V.V., and Van der Eycken, E.**, 2004, A microwave-assisted click chemistry synthesis of 1,4-disubstituted 1,2,3-triazoles via a copper(i)-catalyzed three-component reaction*, Organic Letters*, **6,** 4223-4225.

[90] **Woodward, R.B. and Hoffmann, R.**, 1965, Stereochemistry of electrocyclic reactions*, Journal of the American Chemical Society*, **87,** 395-397.

[91] **Fringuelli, F. and Taticchi, A.**, 2002. *The diels alder reaction : Selected practical methods*. Chichester, New York, Wiley.

[92] **Birney, D.M. and Houk, K.N.**, 1990, Transition structures of the lewis acid-catalyzed diels-alder reaction of butadiene with acrolein - the origins of selectivity*, Journal of the American Chemical Society*, **112,** 4127-4133.

[93] **Furlani, T.R. and Gao, J.L.**, 1996, Hydrophobic and hydrogen-bonding effects on the rate of diels-alder reactions in aqueous solution*, Journal of Organic Chemistry*, **61,** 5492-5497.

[94] **Kong, S. and Evanseck, J.D.**, 2000, Density functional theory study of aqueous-phase rate acceleration and endo/exo selectivity of the butadiene and acrolein diels-alder reaction*, Journal of the American Chemical Society*, **122,** 10418-10427.

[95] **Dondoni, A.**, 2008, The emergence of thiol-ene coupling as a click process for materials and bioorganic chemistry*, Angewandte Chemie-International Edition*, **47,** 8995-8997.

[96] **Hoyle, C.E. and Bowman, C.N.**, 2010, Thiol-ene click chemistry*, Angewandte Chemie-International Edition*, **49,** 1540-1573.

[97] **Morgan, C.R., Magnotta, F., and Ketley, A.D.**, 1977, Thiol-ene photo-curable polymers*, Journal of Polymer Science Part a-Polymer Chemistry*, **15,** 627-645.

[98] **Griesbau.K**, 1970, Problems and possibilities of free-radical addition of thiols to unsaturated compounds*, Angewandte Chemie-International Edition*, **9,** 273-287.

[99] **Mather, B.D., Viswanathan, K., Miller, K.M., and Long, T.E.**, 2006, Michael addition reactions in macromolecular design for emerging technologies*, Progress in Polymer Science*, **31,** 487-531.

[100] **Cai, W.P. and Zhang, L.D.**, 1997, Synthesis and structural and optical properties of mesoporous silica containing silver nanoparticles, *Journal of Physics-Condensed Matter*, **9,** 7257-7267.

[101] **Valentini, A., Carreno, N.L.V., Probst, L.F.D., Leite, E.R., and Longo, E.**, 2004, Synthesis of ni nanoparticles in microporous and mesoporous al and mg oxides, *Microporous and Mesoporous Materials*, **68,** 151-157.

[102] **Okuyama, K., Lenggoro, I.W., Tagami, N., Tamaki, S., and Tohge, N.**, 1997, Preparation of zns and cds fine particles with different particle sizes by a spray-pyrolysis method, *Journal of Materials Science*, **32,** 1229-1237.

[103] **Ebelmen, M.**, 1846, Sur les combinaisons des acides borique et silicique avec les ethers, *Ann. Chim. Phys.*, **16**.

[104] **Bischoff, B.L. and Anderson, M.A.**, 1995, Peptization process in the sol-gel preparation of porous anatase (tio2), *Chemistry of Materials*, **7,** 1772-1778.

[105] **Wu, Z.G., Zhao, Y.X., Xu, L.P., and Liu, D.S.**, 2003, Preparation of zirconia aerogel by heating of alcohol-aqueous salt solution, *Journal of Non-Crystalline Solids*, **330,** 274-277.

[106] **Niederberger, M., Bartl, M.H., and Stucky, G.D.**, 2002, Benzyl alcohol and titanium tetrachloride - a versatile reaction system for the nonaqueous and low-temperature preparation of crystalline and luminescent titania nanoparticles, *Chemistry of Materials*, **14,** 4364-4370.

[107] **Pechini, M.P.**, 1967, Method for preparing lead and alkaline earth titanates and niobates and coating method using the same to form a capacitor, **3,330,697**.

[108] **Zhang, L.Y. and Xue, D.S.**, 2002, Preparation and magnetic properties of pure coo nanoparticies, *Journal of Materials Science Letters*, **21,** 1931-1933.

[109] **Cushing, B.L., Kolesnichenko, V.L., and O'Connor, C.J.**, 2004, Recent advances in the liquid-phase syntheses of inorganic nanoparticles, *Chemical Reviews*, **104,** 3893-3946.

[110] **Liu, Y., Zhu, W., Tse, M.S., and Shen, S.Y.**, 1995, Study of a new alcohol gas sensor made from ultrafine sno2-fe2o3 powders, *Journal of Materials Science Letters*, **14,** 1185-1187.

[111] **Akhtar, M.K., Pratsinis, S.E., and Mastrangelo, S.V.R.**, 1994, Vapor-phase synthesis of al-doped titania powders, *Journal of Materials Research*, **9,** 1241-1249.

[112] **Zhu, W.Z. and Yan, M.**, 1998, Synthesis of nanometer-sized sic powders through chemical vapour deposition - i. Effect of reaction temperature*, Materials Chemistry and Physics*, **53,** 262-266.

[113] **Han, W.Q., Fan, S.S., Li, Q.Q., and Hu, Y.D.**, 1997, Synthesis of gallium nitride nanorods through a carbon nanotube-confined reaction*, Science*, **277,** 1287-1289.

[114] **Zhang, H.Z., Yu, D.P., Ding, Y., Bai, Z.G., Hang, Q.L., and Feng, S.Q.**, 1998, Dependence of the silicon nanowire diameter on ambient pressure*, Applied Physics Letters*, **73,** 3396-3398.

[115] **Gao, P.X., Ding, Y., and Wang, I.L.**, 2003, Crystallographic orientation-aligned zno nanorods grown by a tin catalyst*, Nano Letters*, **3,** 1315-1320.

[116] **Gillberg, G., Lehtinen, H., and Friberg, S.**, 1970, Nmr and ir investigation of conditions determining stability of microemulsions*, Journal of Colloid and Interface Science*, **33,** 40-&.

[117] **Lisiecki, I. and Pileni, M.P.**, 1993, Synthesis of copper metallic clusters using reverse micelles as microreactors*, Journal of the American Chemical Society*, **115,** 3887-3896.

[118] **Boutonnet, M., Kizling, J., and Stenius, P.**, 1982, The preparation of monodisperse colloidal metal particles from micro-emulsions*, Colloids and Surfaces*, **5,** 209-225.

[119] **Lin, X.M., Sorensen, C.M., Klabunde, K.J., and Hajipanayis, G.C.**, 1999, Control of cobalt nanoparticle size by the germ-growth method in inverse micelle system: Size-dependent magnetic properties*, Journal of Materials Research*, **14,** 1542-1547.

[120] **Glavee, G.N., Klabunde, K.J., Sorensen, C.M., and Hadjipanayis, G.C.**, 1993, Borohydride reduction of cobalt ions in water - chemistry leading to nanoscale metal, boride, or borate particles*, Langmuir*, **9,** 162-169.

[121] **Kato, Y., Sugimoto, S., Shinohara, K., Tezuka, N., Kagotani, T., and Inomata, K.**, 2002, Magnetic properties and microwave absorption properties of polymer-protected cobalt nanoparticles*, Materials Transactions*, **43,** 406-409.

[122] **Smith, T.W. and Wychick, D.**, 1980, Colloidal iron dispersions prepared via the polymer-catalyzed decomposition of iron pentacarbonyl*, Journal of Physical Chemistry*, **84,** 1621-1629.

[123] **Borse, P.H., Kankate, L.S., Dassenoy, F., Vogel, W., Urban, J., and Kulkarni, S.K.**, 2002, Synthesis and investigations of rutile phase nanoparticles of tio2*, Journal of Materials Science-Materials in Electronics*, **13,** 553-559.

[124] **Cheng, H.M., Ma, J.M., Zhao, Z.G., and Qi, L.M.**, 1995, Hydrothermal preparation of uniform nanosize rutile and anatase particles, *Chemistry of Materials*, **7,** 663-671.

[125] **Gautam, U.K., Rajamathi, M., Meldrum, F., Morgan, P.E.D., and Seshadri, R.**, 2001, A solvothermal route to capped cdse nanoparticles, *Chemical Communications*, 629-630.

[126] **Caruso, F.**, 2001, Nanoengineering of particle surfaces, *Advanced Materials*, **13,** 11-+.

[127] **Rolland, J.P., Maynor, B.W., Euliss, L.E., Exner, A.E., Denison, G.M., and DeSimone, J.M.**, 2005, Direct fabrication and harvesting of monodisperse, shape-specific nanobiomaterials, *Journal of the American Chemical Society*, **127,** 10096-10100.

[128] **Dalsin, J.L., Hu, B.H., Lee, B.P., and Messersmith, P.B.**, 2003, Mussel adhesive protein mimetic polymers for the preparation of nonfouling surfaces, *Journal of the American Chemical Society*, **125,** 4253-4258.

[129] **Thomas, J.R.**, 1966, Preparation and magnetic properties of colloidal cobalt particles, *J. Appl. Phys.*, **37,** 2914–2915.

[130] **Ott, L.S., Hornstein, B.J., and Finke, R.G.**, 2006, A test of the transition-metal nanocluster formation and stabilization ability of the most common polymeric stabilizer, poly(vinylpyrrolidone), as well as four other polymeric protectants, *Langmuir*, **22,** 9357-9367.

[131] **Klingelhofer, S., Heitz, W., Greiner, A., Oestreich, S., Forster, S., and Antonietti, M.**, 1997, Preparation of palladium colloids in block copolymer micelles and their use for the catalysis of the heck reaction, *Journal of the American Chemical Society*, **119,** 10116-10120.

[132] **Platonova, O.A., Bronstein, L.M., Solodovnikov, S.P., Yanovskaya, I.M., Obolonkova, E.S., Valetsky, P.M., Wenz, E., and Antonietti, M.**, 1997, Cobalt nanoparticles in block copolymer micelles: Preparation and properties, *Colloid and Polymer Science*, **275,** 426-431.

[133] **Ahmed, S.R. and Kofinas, P.**, 2002, Controlled room temperature synthesis of cofe2o4 nanoparticles through a block copolymer nanoreactor route, *Macromolecules*, **35,** 3338-3341.

[134] **Rabelo, D., Lima, E.C.D., Reis, A.C., Nunes, W.C., Novak, M.A., Garg, V.K., Oliveira, A.C., and Morais, P.C.**, 2001, Preparation of magnetite nanoparticles in mesoporous copolymer template, *Nano Letters*, **1,** 105-108.

[135] **Barbey, R., Lavanant, L., Paripovic, D., Schuwer, N., Sugnaux, C., Tugulu, S., and Klok, H.A.**, 2009, Polymer brushes via surface-initiated controlled radical polymerization: Synthesis, characterization, properties, and applications, *Chemical Reviews*, **109,** 5437-5527.

[136] **Parvole, J., Laruelle, G., Khoukh, A., and Billon, L.**, 2005, Surface initiated polymerization of poly(butyl acrylate) by nitroxide mediated polymerization: First comparative polymerization of a bimolecular and a unimolecular initiator-grafted silica particles, *Macromolecular Chemistry and Physics*, **206,** 372-382.

[137] **Furniss, B.H.H., A.J. Rogers,V. Smith, P.W.G. Tatchell, A.R.** , 1978, Vogel's textbook of practical organic chemistry, longman inc. 4th edition, new york, us.

[138] **Acar, M.H. and Bicak, N.**, 2003, Synthesis of hexylated triethylenetetramine: New ligand for homogeneous atom transfer radical polymerization, *Journal of Polymer Science Part a-Polymer Chemistry*, **41,** 1677-1680.

[139] **Gunes, D., Karagoz, B., and Bicak, N.**, 2009, Synthesis of methacrylate-based functional monomers via boron ester acidolysis and their polymerization, *Designed Monomers and Polymers*, **12,** 445-454.

[140] **Bicak, N., Senkal, B.F., and Yarbas, T.**, 1998, Crosslinked poly(styrenesulfonamide) with iminoacetic acid chelating groups for hard-water treatment, *Macromolecular Chemistry and Physics*, **199,** 2731-2735.

[141] **Basset, J.D., R.C. Jeffery, G.H.** , 1978, Vogel's textbook of quantitative inorganic chemistry, ed. Mendham, j. Longman, fourth edition, london.

[142] **Bradford, M.M.**, 1976, Rapid and sensitive method for quantitation of microgram quantities of protein utilizing principle of protein-dye binding, *Analytical Biochemistry*, **72,** 248-254.

[143] **Bayramoglu, G., Kaya, B., and Arica, M.Y.**, 2005, Immobilization of candida rugosa lipase onto spacer-arm attached poly(gma-hema-egdma) microspheres, *Food Chemistry*, **92,** 261-268.

[144] **Lime, F. and Irgum, K.**, 2009, Hydrobromination of residual vinyl groups on divinylbenzene polymer particles followed by atom transfer radical surface graft polymerization, *Journal of Polymer Science Part a-Polymer Chemistry*, **47,** 1259-1265.

[145] **Battersby, B.J. and Trau, M.**, 2002, Novel miniaturized systems in high-throughput screening, *Trends in Biotechnology*, **20,** 167-173.

[146] **Goradia, D., Cooney, J., Hodnett, B.K., and Magner, E.**, 2005, The adsorption characteristics, activity and stability of trypsin onto mesoporous silicates, *Journal of Molecular Catalysis B-Enzymatic*, **32,** 231-239.

[147] **Odaci, D., Timur, S., Pazarlioglu, N., Montereali, M.R., Vastarella, W., Pilloton, R., and Telefoncu, A.**, 2007, Determination of phenolic acids using trametes versicolor laccase, *Talanta*, **71,** 312-317.

[148] **Yalcinkaya, E.E. and Guler, C.**, 2010, Electrokinetic properties of acid-activated montmorillonite dispersions, *Separation Science and Technology*, **45,** 635-642.

[149] **Saka, E.E. and Guler, C.**, 2006, The effects of electrolyte concentration, ion species and ph on the zeta potential and electrokinetic charge density of montmorillonite, *Clay Minerals*, **41,** 853-861.

[150] **Bicak, N., Karagoz, B., and Tunca, U.**, 2003, Self-curable polyester by a reaction of glycidol with maleic anhydride, *Journal of Polymer Science Part a-Polymer Chemistry*, **41,** 2549-2555.

[151] **Bicak, N., Gazi, M., and Senkal, B.F.**, 2005, Polymer supported amino bis-(cis-propan 2,3 diol) functions for removal of trace boron from water, *Reactive & Functional Polymers*, **65,** 143-148.

[152] **Zheng, G.D. and Stover, H.D.H.**, 2003, Grafting of poly(epsilon-caprolactone) and poly(epsilon-caprolactone-block-(dimethylamino)ethyl methacrylate) from polymer microspheres by ring-opening polymerization and atrp, *Macromolecules*, **36,** 7439-7445.

[153] **Cheng, Z.P., Zhu, X.L., Shi, Z.L., Neoh, K.G., and Kang, E.T.**, 2005, Polymer microspheres with permanent antibacterial surface from surface-initiated atom transfer radical polymerization, *Industrial & Engineering Chemistry Research*, **44,** 7098-7104.

[154] **Xu, F.J., Yuan, Z.L., Kang, E.T., and Neoh, K.G.**, 2004, Branched fluoropolymer-si hybrids via surface-initiated atrp of pentafluorostyrene on hydrogen-terminated si(100) surfaces, *Langmuir*, **20,** 8200-8208.

[155] **Aoi, K. and Okada, M.**, 1996, Polymerization of oxazolines, *Progress in Polymer Science*, **21,** 151-208.

[156] **Jeong, J.H., Song, S.H., Lim, D.W., Lee, H., and Park, T.G.**, 2001, DNA transfection using linear poly(ethylenimine) prepared by controlled acid hydrolysis of poly(2-ethyl-2-oxazoline), *Journal of Controlled Release*, **73,** 391-399.

[157] **Arica, M.Y. and Bayramoglu, G.**, 2004, Reversible immobilization of tyrosinase onto polyethyleneimine-grafted and cu(ii) chelated poly(hema-co-gma) reactive membranes, *Journal of Molecular Catalysis B-Enzymatic*, **27,** 255-265.

[158] **Nagai, D., Fujii, A., Ochiai, B., Sudo, A., and Endo, T.**, 2008, Solid-supported synthesis of well-defined amphiphilic block copolymer from methacrylates, *Journal of Polymer Science Part a-Polymer Chemistry*, **46,** 1990-1997.

[159] **Mizuki, T., Watanabe, N., Nagaoka, Y., Fukushima, T., Morimoto, H., Usami, R., and Maekawa, T.**, 2010, Activity of an enzyme immobilized on superparamagnetic particles in a rotational magnetic field, *Biochemical and Biophysical Research Communications*, **393,** 779-782.

[160] **Yong, Y., Bai, Y.X., Li, Y.F., Lin, L., Cui, Y.J., and Xia, C.G.**, 2008, Characterization of candida rugosa lipase immobilized onto magnetic microspheres with hydrophilicity, *Process Biochemistry*, **43,** 1179-1185.

[161] **Li, Y.G., F. Wei, W. Qu, J-B. Ma, G-H. Zhou, W-Q**, 2010, Pore size of macroporous polystyrene microspheres affects lipase immobilization *Journal of Molecular Catalysis B: Enzymatic*, **66,** 182-189.

[162] **Gupta, S., Kumar, Y., Singh, K., and Bhattacharya, A.**, 2010, Lipase immobilized on poly (vinyl alcohol) modified polysulfone membrane: Application in hydrolytic activities for olive oil, *Polymer Bulletin*, **64,** 141-158.

[163] **Kang, Y., He, J., Guo, X.D., Guo, X., and Song, Z.H.**, 2007, Influence of pore diameters on the immobilization of lipase in sba-15, *Industrial & Engineering Chemistry Research*, **46,** 4474-4479.

[164] **Ahmed, E.H., Raghavendra, T., and Madamwar, D.**, 2010, An alkaline lipase from organic solvent tolerant acinetobacter sp eh28: Application for ethyl caprylate synthesis, *Bioresource Technology*, **101,** 3628-3634.

[165] **Mahmood, I., Guo, C., Xia, H.S., Ma, J.H., Jiang, Y.Y., and Liu, H.Z.**, 2008, Lipase immobilization on oleic acid-pluronic (l-64) block copolymer coated magnetic nanoparticles, for hydrolysis at the oil/water interface, *Industrial & Engineering Chemistry Research*, **47,** 6379-6385.

[166] **Bayramoglu, G. and Arica, M.Y.**, 2008, Preparation of poly (glycidylmethacrylate-methylmethacrylate) magnetic beads: Application in lipase immobilization, *Journal of Molecular Catalysis B-Enzymatic*, **55,** 76-83.

[167] **Kartal, F., Akkaya, A., and Kilinc, A.**, 2009, Immobilization of porcine pancreatic lipase on glycidyl methacrylate grafted poly vinyl alcohol, *Journal of Molecular Catalysis B-Enzymatic*, **57,** 55-61.

[168] **Tutar, H., Yilmaz, E., Pehlivan, E., and Yilmaz, M.**, 2009, Immobilization of candida rugosa lipase on sporopollenin from lycopodium clavatum, *International Journal of Biological Macromolecules*, **45,** 315-320.

[169] **Dandavate, V., Keharia, H., and Madamwar, D.**, 2009, Ethyl isovalerate synthesis using candida rugosa lipase immobilized on silica nanoparticles prepared in nonionic reverse micelles, *Process Biochemistry*, **44,** 349-352.

[170] **Ye, P., Xu, Z.K., Che, A.F., Wu, J., and Seta, P.**, 2005, Chitosan-tethered poly(acrylonitrile-co-maleic acid) hollow fiber membrane for lipase immobilization, *Biomaterials*, **26,** 6394-6403.

[171] **Wolfson, A., Atyya, A., Dlugy, C., and Tavor, D.**, 2010, Glycerol triacetate as solvent and acyl donor in the production of isoamyl acetate with candida antarctica lipase b, *Bioprocess and Biosystems Engineering*, **33,** 363-366.

[172] **Rodrigues, R.C. and Fernandez-Lafuente, R.**, 2010, Lipase from rhizomucor miehei as an industrial biocatalyst in chemical process, *Journal of Molecular Catalysis B-Enzymatic*, **64,** 1-22.

[173] **Ozyilmaz, G. and Gezer, E.**, 2010, Production of aroma esters by immobilized candida rugosa and porcine pancreatic lipase into calcium alginate gel, *Journal of Molecular Catalysis B-Enzymatic*, **64,** 140-145.

[174] **Pires-Cabral, P., da Fonseca, M.M.R., and Ferreira-Dias, S.**, 2010, Esterification activity and operational stability of candida rugosa lipase immobilized in polyurethane foams in the production of ethyl butyrate, *Biochemical Engineering Journal*, **48,** 246-252.

[175] **Karra-Chaabouni, M., Ghamgui, H., Bezzine, S., Rekik, A., and Gargouri, Y.**, 2006, Production of flavour esters by immobilized staphylococcus simulans lipase in a solvent-free system, *Process Biochemistry*, **41,** 1692-1698.

[176] **Nyhus, A.K., Hagen, S., and Berge, A.**, 2000, Friedel-crafts reactions of pendant vinyl groups in macroporous monosized poly(meta-divinylbenzene) and poly(para-divinylbenzene) particles, *Journal of Polymer Science Part a-Polymer Chemistry*, **38,** 1366-1378.

[177] **Liu, B.L., Cao, S.S., Deng, X.B., Li, S.J., and Luo, R.**, 2006, Adsorption behavior of protein onto siloxane microspheres, *Applied Surface Science*, **252,** 7830-7836.

[178] **Cullen, S.P., Liu, X., Mandel, I.C., Himpsel, F.J., and Gopalan, P.**, 2008, Polymeric brushes as functional templates for immobilizing ribonuclease a: Study of binding kinetics and activity, *Langmuir*, **24,** 913-920.

[179] **Cao, L.**, 2005, Carrier-bound immobilized enzymes, wiley-vch, weinheim, germany.

[180] **Popat, K.C., Sharma, S., and Desai, T.A.**, 2004, Quantitative xps analysis of peg-modified silicon surfaces, *Journal of Physical Chemistry B*, **108,** 5185-5188.

[181] **Music, S., Popovic, S., Maljkovic, M., Furic, K., and Gajovic, A.**, 2002, Influence of synthesis procedure on the formation of ruo2, *Materials Letters*, **56,** 806-811.

[182] **Du, X.W., Fu, Y.S., Sun, J., Han, X., and Liu, J.**, 2006, Complete uv emission of zno nanoparticles in a pmma matrix, *Semiconductor Science and Technology*, **21,** 1202-1206.

[183] **Lu, N., Lu, X.D., Jin, X., and Lu, C.L.**, 2007, Preparation and characterization of uv-curable zno/polymer nanocomposite films, *Polymer International*, **56,** 138-143.

[184] **Hong, R.Y., Qian, J.Z., and Cao, J.X.**, 2006, Synthesis and characterization of pmma grafted zno nanoparticles, *Powder Technology*, **163,** 160-168.

CURRICULUM VITA

Candidate's full name: Bünyamin KARAGÖZ

Place and date of birth: Çankırı, 10/02/1977

Permanent Address: G-62 Sokak**,** No:34/3, 34457 Ayazağaköyü/Istanbul, Turkey

Universities and Colleges attended:

2003-2010 *Philosophy of Doctorate* (Polymer Science and Technology) Istanbul Technical University, Istanbul, Turkey.

2000-2003 *Master of Science* (Polymer Science and Technology), Istanbul Technical University, Istanbul, Turkey.

1996–2000 *Bachelor of Science* (Chemistry), Istanbul Technical University, Istanbul, Turkey.

1992-1996 Fatih Sultan Mehmet High School, Ankara, Turkey.

Publications:

- Preparation of Crosslinked Poly(2-bromoethyl methacrylate) Microspheres and Decoration of Their Surfaces with Functional Polymer Brushes. **Karagoz B**, Gunes D, Bicak N. *Macromolecular Chemistry and Physics* 211, 1999–2007 **(2010)**.
- Novel strategy for tailoring of SiO_2 and TiO_2 nanoparticle surfaces with poly(epsilon-caprolactone). **Karagoz B**, Galli G, Durmaz H, Hizal G, Tunca U, Bicak N. *Colloid and Polymer Science* 288, 535-542 (**2010**).
- Modification of Poly(divinylbenzene) Microspheres by Hydrobromination-Click Chemistry Protocol and Their Protein Adsorption Properties. Durmaz YY, **Karagoz B**, Bicak N, Demirkol DO, Yalcinkaya EE, Timur S, Yagci Y. *Macromolecular Bioscience* (accepted) **(2010)**.

- Poly(glycidylmethacrylate)-polystyrene copolymer grafted nano-composite P(S-DVB) microspheres from surface initiated-atom transfer radical polymerization: Immobilization of lipase and application in esters synthesis. **Karagoz B**, Bayramoglu G, Altintas B, Bicak N, Arica MY. *Industrial and Engineering Chemistry Research 49,* 9655–9665 (**2010).**
- Room-temperature Ligand Exchange Process for Size Controlled Synthesis of Zinc Oxide Nanocrystallites and Generation of Core-Sell structures by post treatment with Glycidylmethacrylate Block Copolymers. **Karagoz B**, Bicak N. (in preparation) **(2010).**
- Surface Modification of Silica, Titania, and Zinc Oxide Micro Particles with Epoxidized Soybean Oil for Preparation of Polystyrene Composite Films. Alemdar N, **Karagoz B**, Erciyes AT, Bicak N. *Journal of Applied Polymer Science* 116, 165-171(**2010**).
- Functionalization of Poly(divinylbenzene) Microspheres by Combination of Hydrobromination and Click Chemistry Processes: A Model Study. **Karagoz B**, Durmaz YY, Gacal BN, Yagci Y, Bicak N. *Designed Monomers and Polymers* 12, 511-522 (**2009**).
- Synthesis of Methacrylate-Based Functional Monomers via Boron Ester Acidolysis and Their Polymerization. Gunes D, **Karagoz B**, Bicak N. *Designed Monomers and Polymers* 12, 445-454 (**2009**).
- Synthesis of block copolymers by combination of ATRP and photoiniferter processes. Durmaz YY, **Karagoz B**, Bicak N, Yagci Y. *Polymer International* 57, 1182-1187 (**2008**).
- Novel photocurable polyethers with methacrylate pendant groups. **Karagoz B**, Bicak N. *European Polymer Journal* 44, 106-112 (**2008**).
- A method for polyaniline coatings on solid polystyrene surfaces and electroless copper deposition. Girginer B, **Karagoz B**, Urgen M, Bicak N. *Surface & Coatings Technology* 202, 4176-4182 (**2008**).
- A new photoiniferter/RAFT agent for ambient temperature rapid and well-controlled radical polymerization. Tasdelen MA, Durmaz YY, **Karagoz B**, Bicak N, Yagci Y. *Journal of Polymer Science Part A-Polymer Chemistry* 46, 3387-3395 (**2008**).
- Copper patterned polystyrene panels by reducing of surface bound Cu (II)-sulfonyl hydrazide complex. Bicak N, **Karagoz B**. *Surface & Coatings* 202, 1581-1587 (**2008**).
- Phenacylpyridinium oxalate as a novel water-soluble photoinitiator for free radical polymerization. Tasdelen MA, **Karagoz B**, Bicak N, Yagci Y. *Polymer Bulletin* 59, 759-766 (**2008**).
- Merrifield-like resin beads by acid catalyzed incorporation of benzyl chloride into dehydrochlorinated PVC. Bicak N, **Karagoz B**. *European Polymer Journal* 43, 4719-4725 (**2007**).

- A method for polymethymetacrylate coating via self-curable unsaturated polyester primer on metal and glass surfaces. Alemdar N, **Karagoz B**, Erciyes AT, Bicak N. *Progress In Organic Coatings* 60, 69-74 (**2007**).
- Polymerization of aniline by copper-catalyzed air oxidation. Bicak N, **Karagoz B**. *Journal of Polymer Science Part A-Polymer Chemistry* 44, 6025-6031 (**2006**).
- New water-soluble polymer with allyl pendant groups. Bicak N, Gazi M, **Karagoz B**. *Designed Monomers and Polymers* 9, 193-200 (**2006**).
- Atom transfer graft copolymerization of 2-ethyl hexylacrylate from labile chlorines of poly(vinyl chloride) in an aqueous suspension. Bicak N, **Karagoz B**, Emre D. *Journal of Polymer Science Part A-Polymer Chemistry* 44, 1900-1907 (**2006**).
- Synthesis of new polyesters with methacrylate pendant groups. Bicak N, **Karagoz B**. *Polymer Bulletin* 56, 87-93 (**2006**).
- Self-curable polyester by a reaction of glycidol with maleic anhydride. Bicak N, **Karagoz B**, Tunca U. *Journal Of Polymer Science Part A-Polymer Chemistry* 41, 2549-2555 (**2003**).